NTNU

Norwegian University of
Science and Technology

Advanced Casing Design Model

Buckling of Casing in Washed Out Sections

Hanne Stensrød

Petroleum Geoscience and Engineering
Submission date: June 2016
Supervisor: Sigbjørn Sangesland, IPT
Co-supervisor: Bjørn A. Brechan, IPT

Norwegian University of Science and Technology
Department of Petroleum Engineering and Applied Geophysics

Abstract

Casing design for a well is based on an investigation of all possible loads the well can experience during its lifetime. A thesis model has been made in Excel based on the equations and assumptions given in literature; these are the same calculations the industry leading software (ILS) is supposedly based on. The well inputs in the thesis model and the ILS are the same, and several load cases are calculated in both models. However, not all the equations and assumptions in the ILS are known, which may be the reason why some of the results from the ILS are different from the thesis model results.

The results from the thesis model are compared to the output from the ILS, and not all the aspects of the models are the same. The differential pressures, axial loads, and the axial, collapse and burst safety factors are the same in both models, or so close that the difference is insignificant. However, the force due to buckling of the casing is stronger and occurs earlier in the ILS than in the thesis model, and the triaxial safety factor is almost always more pessimistic in the ILS. These issues are investigated further in this study.

The main focus of this study is some issues that are not addressed in the ILS. Among these are excessive hole enlargement (i.e. washout), poor cement job and misalignment of the casing. A washout may be a significant issue in some formations, and is therefore interesting to examine. As the washout increases the clearance between the casing and the formation, it may lead to significant buckling of the casing. If the cement job is a failure, i.e. little or no cement in the annulus, it is interesting to see how the axial load will behave and whether it has an impact on the casing design. This study also examines what happens if the cement job is a failure and a washout occurs. The last issue, misalignment of casing, checks what will happen if the casing is not in the middle of the hole as the ILS assumes, when the borehole is washed out.

These issues are investigated in comparison to the different axial loads, and the axial and triaxial safety factors as these aspects are directly affected by buckling of the casing. From these comparisons it is considered whether the issues will affect the casing design and should be implemented in the ILS. This study shows that the worst scenario is when the casing is misaligned and a washout occurs. In that case, the washout does not need to be large in comparison to the other cases to be significant in relation to the casing design.

Sammendrag

Fôringsrørdesignet i en brønn baseres på en undersøkelse av alle mulige laster som brønnen kan oppleve gjennom levetiden. En modell er laget i Excel basert på ligningene og antagelsene gitt i litteraturen; disse er de samme ligningene som skal være brukt i den industriledende programvaren. Dataene brukt til å modellere brønnen er de samme både i den nye modellen og i ILS, og flere lastscenarier er simulert i begge modellene. Ikke alle ligninger og antagelser gjort i ILS er kjent, noe som kan være grunnen til at ikke alle resultatene fra modellene er like.

Resultatene fra begge modellene sammenlignes, men det viser seg at ikke alle resultatene er like. Differensialtrykket, de aksielle lastene og de aksielle, kollaps og sprengnings-sikkerhetsfaktorene er helt like, eller så like at forskjellen er ubetydelig. Derimot opptrer buckling av fôringsrørene både tidligere og sterkere i ILS, og den triaksiale sikkerhetsfaktoren er nesten alltid mer pessimistisk i ILS. Disse problemene blir undersøkt nærmere i denne studien.

Hovedfokuset i denne studien er enkelte problemer som ikke tas hensyn til i ILS. Disse problemene er bl.a. utvidelse av borehullet (utvasking), dårlig sementeringsjobb og feiljusterte fôringsrør. En utvasking av borehullet kan være et stort problem i enkelte formasjoner, og er dermed interessant å undersøke. Ettersom en utvasking øker klaringen mellom fôringsrøret og formasjonen, kan det lede til betydelig buckling av fôringsrøret. Hvis sementjobben er en fiasko, er det interessant å undersøke hvordan den aksielle lasten vil oppføre seg, og om det vil ha en innvirkning på fôringsrørdesignet. Det undersøkes også hva som vil skje dersom sementjobben er en fiasko, samtidig som en utvasking oppstår. Til slutt undersøkes effekten av feiljusterte fôringsrør; hva vil hende dersom fôringsrøret ikke er i midten av borehullet som ILS antar, samtidig som det er en utvasking av borehullet.

Disse problemstillingene undersøkes i forhold til de forskjellige aksielle lastene, og de aksielle og triaksiale sikkerhetsfaktorene, ettersom disse blir direkte påvirket av buckling av fôringsrøret. Ut fra disse sammenligningene blir det vurdert hvorvidt problemene vil påvirke fôringsrørdesignet og dermed burde bli implementert i ILS. Denne studien viser at det verste scenariet er når en feiljustering av fôringsrøret sammenfaller med en utvasking av borehullet. I det tilfellet trenger ikke utvaskingen være særlig stor relativt til de andre tilfellene for å ha betydning i forhold til fôringsrørdesignet.

Acknowledgement

This thesis is carried out at the Department of Petroleum Engineering and Applied Geophysics at the Norwegian University of Science and Technology, and builds on the work done during the specialization project and the course “TPG4520- Drilling Engineering”.

I would like to thank my supervisor Professor Sigbjørn Sangesland for suggesting this interesting subject and giving valuable start-up help. A deep gratitude goes to my co-supervisor PhD student Bjørn Astor Brechan for all the guidance and advice.

Last but not least, a special thanks to all my fellow students for the interesting debates and coffee breaks!

Table of Contents

Table of Figures

List of Tables

1. Introduction

When the ILS was introduced, casing design suddenly became a lot simpler. It no longer required a lot of time and calculations, instead a program does all the calculations. A lot of trust is put into this software, as the casing design is based on the output from the program. Therefore the equations and assumptions used must make sense. This study looks into the literature to make a model based on the relevant equations and assumptions. A well is made with the same input to the thesis model as the input to the ILS, and several load cases are simulated in both models. The thesis model is then compared against the ILS.

The similarities between the models will be briefly stated. Any differences between the thesis model and the ILS is closely examined and discussed further. The thesis model is made to be as close to the ILS as possible, as the main focus of this study is to investigate some issues not covered by the ILS.

After the similiarities and differences are examined, the thesis model can be used to investigate the issues not covered by the ILS. The first of these issues is an excessive hole enlargement, which may be a serious problem in some formations. Another issue is whether a poor cement job in addition to a washout will affect the casing design. The ILS assumes that the casing is in the middle of the hole at all times, which is why the last issue the thesis model examines is what will happen when the casing is misaligned and the borehole is washed out.

All these issues are regarded in relation to the axial load, axial safety factor and triaxial safety factor, as these factors wil be affected by any increase in the radial clearance. If the thesis model gives the same results as the ILS for the other load cases investigated, the results from the thesis model in relation to these special cases should be close to the results the ILS would give if the software investigated these issues. From this it should be possible to determine whether it would be interesting and useful to examine these issues in the ILS.

2. Theory

This study investigates the effects an excessive hole enlargement, has on the casing design. The washout is also investigated in addition to a poor cement job and to a misalignment of casing. Hole enlargements are not focused on in the literature, they are barely mentioned in relation to drilling when encountering problems. There seems to be little or no mention of washouts in relation to casing design. However, washouts can occur in soft or unconsolidated formations, and they become more severe with time. Thus the effect of a washout is interesting to investigate relative to casing design.

A washout will affect the radial clearance between the casing and the borehole, and so it may initiate buckling. Buckling of the casing depends on several aspects other than the radial clearance, including these axial loads:

- Weight of Casing
- Piston Forces
- Ballooning Effects
- Temperature Effects
- Bending Stresses

These loads are presented in the following chapters, and are the axial loads used in the thesis model. The theory used to find the different safety factors is presented in Appendix A.1.

Several load cases are investigated in this study:

- Initial Conditions
- Pressure Test
- Lost Returns with Mud Drop
- Tubing Leak

The theory behind these load cases are given in chapter 2.2 and Appendix A.3.

2.1. Axial Loads

Axial loads are affected by several different factors; the most important are pressure, temperature and the weight of the casing (Bellarby, 2009, p.478). The axial loads can be tensile or compressive. In this study, the tensile loads are expressed as positive forces and the compressive as negative forces.

2.1.1. Weight of Casing

The air weight of the casing is the weight per foot of the casing, multiplied with the projected vertical length of the casing, as presented in eq.(1) (Aadnoy and Kaarstad, 2006, p.7). For the derivation of this equations, see Appendix A.2.1.

$$F_{air} = w(D_{TVD} - D) \tag{1}$$

where,

F_{air} = the air weight of the casing [lb]

w= the weight per foot of the casing [lb/ft]

D= depth at top of casing [ft]

D_{TVD}= true vertical depth at the base of the casing [ft]

2.1.2. Piston Forces

When considering the buoyancy effects, there are two different "schools of thought"; the Archimedes principle and the piston-force approach (Aadnoy, 2006, p.37). As this study investigates some issues by comparing them to the ILS, the thesis model uses the same buoyancy calculations as in the ILS; the piston-force approach. A more detailed investigation of the two different ways of calculating the buoyancy is made in Appendix A.2.2.

The piston-force approach calculates the buoyancy as the pressure exposed to a projected area. The hydrostatic force at the bottom of the casing is given by (Aadnoy, 2006, p.44):

$$F_{hydrostatic} = p_{i,b}A_i - p_{o,b}A_o \tag{2}$$

where,

$F_{hydrostatic}$= hydrostatic force at bottom of casing [lb]

$p_{i,b}$= internal pressure at bottom of casing [psi]

$p_{o,b}$= external pressure at bottom of casing [psi]

A_i= internal area of the casing [in^2]

A_o= external area of the casing [in^2]

The initial axial force at the top of the casing is the air weight of the casing along with the hydrostatic force at the bottom of the casing:

$$F_{a,i} = F_{hydrostatic} + F_{air} = p_{i,b}A_i - p_{o,b}A_o + w(D_{TVD} - D) \quad (3)$$

where,

$F_{a,i}$ = the initial axial force at the top of the casing [lb]

2.1.3. Ballooning Effects

Both axial strain and radial compressive strain is generated when a casing is loaded in axial tension (Bellarby, 2009, p.487). The axial and radial compressive strains are proportional to each other in the elastic region, as shown in the following equation:

$$\mu = -\frac{\text{Radial strain}}{\text{Axial strain}} \quad (4)$$

where,

μ= Poisson's ratio

For most steels the Poisson's ratio, also known as the material property, is approximately 0.3. This is the value used in the thesis model.

Ballooning effects are observed when pressure is applied to the casing or tubing as seen in Figure 2-1. With a fixed pipe, an axial tensile force is created from applied internal pressure, and an axial compressive force is generated from applied external pressure. Eq.(5) shows how the axial force resulting from ballooning effects is calculated:

$$F_{bal} = 2\mu(A_i\Delta p_i - A_o\Delta p_o) \quad (5)$$

where,

F_{bal} = force resulting from ballooning effects [lb]

Δp_i = change in internal pressure relative to initial conditions [psi]

Δp_o = change in external pressure relative to initial conditions [psi]

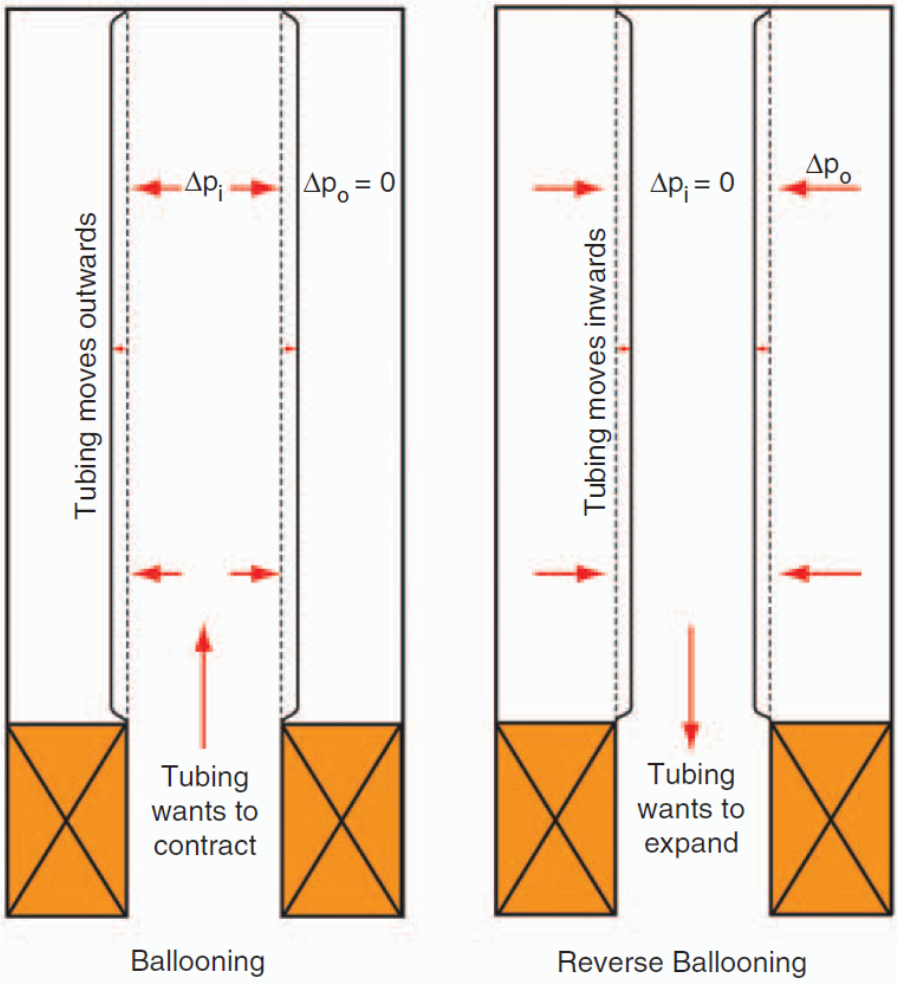

Figure 2-1 Ballooning effects (Bellarby, 2009, p.488)

If the casing is free to move, applied internal pressure will force the casing to shorten while applied external pressure will elongate the casing, according to Hooke's law. The following equation gives the length change due to ballooning:

$$\Delta L_{bal} = \frac{-2\mu L}{E(A_o - A_i)}(\Delta p_i A_i - \Delta p_o A_o) \tag{6}$$

where,

ΔL_{bal} = length change due to ballooning [ft]

E=Young's modulus [psi]

2.1.4. Temperature Effects

While drilling a new section below the casing shoe, or during the production operations, the casing temperature changes. During drilling, this is due to the drilling fluid being heated up as it moves down to the bottom of the hole, and then cooled off as it moves back up (Rahman and Chilingar, 1995, p.106). An increase or decrease in the surrounding temperature will result in an additional compressive or tensile stress when the casing is fixed at both ends. The force is compressive if the casing is heated, and tensile if the casing is cooled. If the casing is uniformly heated from temperature T_0 to T_1, the force is given by (Aadnoy, 2006, p.141):

$$F_T = -C_T E(T_1 - T_0)(A_o - A_i) = -C_T E \Delta T (A_o - A_i) \tag{7}$$

where,

F_T = force resulting from temperature change [lb]

C_T =coefficient of thermal expansion [°F^{-1}]

T_0 = initial temperature [°F]

T_1 = final temperature [°F]

ΔT = average change in temperature from the base case to the load case [°F]

The coefficient of thermal expansion used in the thesis model is 6*10^{-6} °F^{-1}. If the casing is free to move, the following equation gives the length change due to temperature change:

$$\Delta L_T = C_T \Delta T L \tag{8}$$

where,

ΔL_T = expansion or shortening of casing due to temperature change [ft]

2.1.5. Bending Stresses

Bending of the casing can occur because of drilling doglegs, or by buckling of the casing (Bellarby, 2009, p.490). The theory used to calculate the bending stresses is called beam theory. The outside of the casing is where the bending stresses are highest; the following equation shows how to calculate these stresses:

$$\sigma_b = \pm \frac{E d_n}{2R} \tag{9}$$

where,

σ_b = bending stress [psi]

d_n = nominal outer diameter [in]

R = radius of the bend [in]

The stresses are tensile on the outside of the bend, and compressive on the inside; hence the '±' sign. The dogleg severity is more commonly used to find the bend radius, and is usually given in degrees per 100 feet. Eq.(9) then becomes:

$$\sigma_b = \pm \frac{E d_n \pi \alpha}{360 \cdot 100 \cdot 12} \tag{10}$$

where,
α= the dogleg severity [°/100ft]

The bending loads caused by doglegs are local, unlike the previously mentioned axial loads. This means that the bending stresses are added to the existing axial stress profile at the point the bending stress occurs. To consider the worst-case scenario, the bending stresses are considered tensile when the axial stress is in tension, and compressive when the axial stress is in compression. This is shown in Figure 2-2.

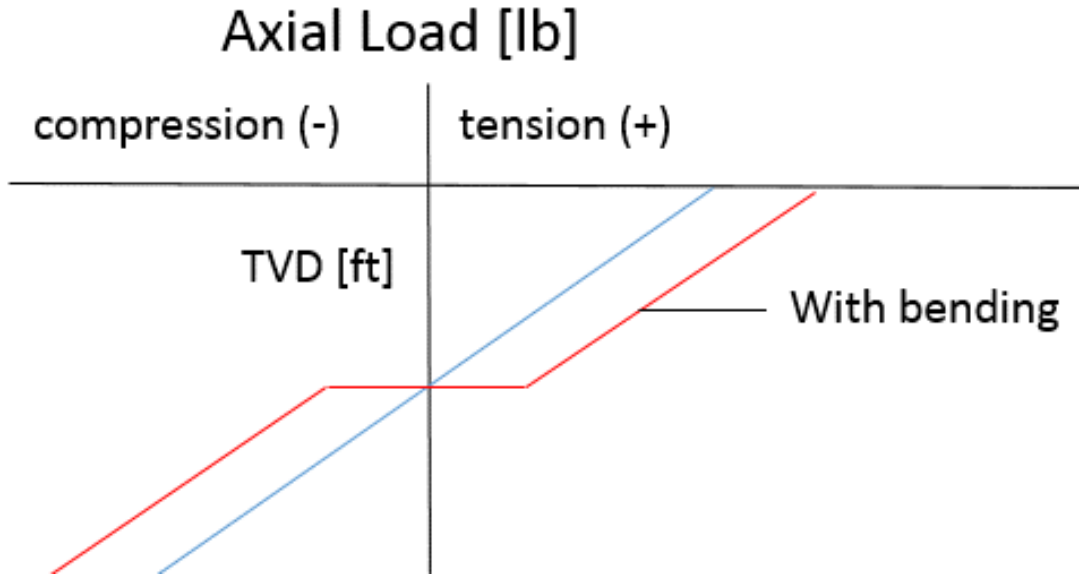

Figure 2-2 Axial loads with bending

2.1.6. Buckling Effects

In straight holes, the casing usually hangs straight down, while it often lies on the low side of the hole in deviated wells (Lake and Mitchell, 2006, p.303). The thermal or pressure-effects may produce compressive loads, which in turn may make the initial configuration unstable. Since the casing is confined within an open hole, it can deform into another stable configuration; this is called buckling of the casing.

There are two types of buckling. The first is sinusoidal or S-shaped buckling, also called lateral buckling, the left figure in Figure 2-3. The second type is called helical buckling, the right figure in Figure 2-3. Usually the helical buckling occurs in a vertical wellbore, while the sinusoidal buckling occurs in a deviated buckling. Helical buckling is the most severe mode. Usually buckling of casing is not significant as there is a small clearance between the casing and the formation, resulting in a small degree of buckling. However, in this study the clearance is increased due to washout and misalignment of casing, which gives significant results as seen in chapter 3.

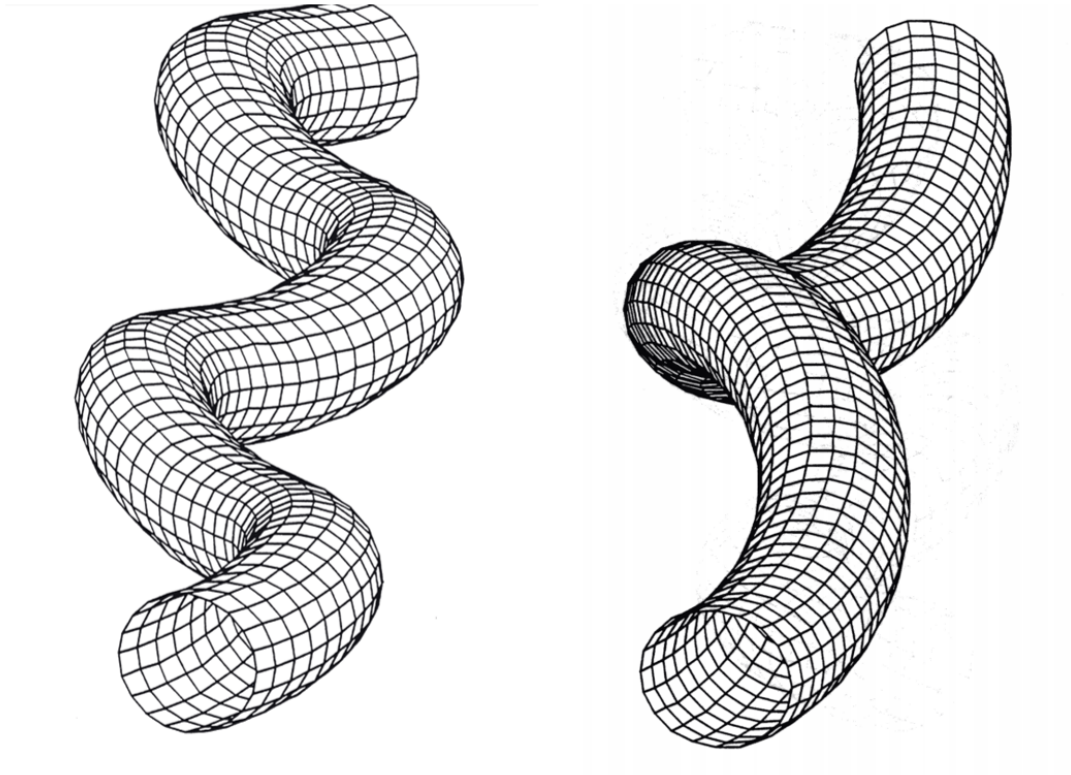

Figure 2-3 The left figure shows lateral buckling, while the right figure shows helical buckling (Mitchell, 2006, p.12)

Experiments with axial compression show that the presence of cement is important to be able to prevent buckling (Veeken et al., 1994). The absence of cement creates cavities behind the casing, allowing the casing to move and buckle. Another problem when considering casing buckling is washout and bad cement, or no cement in the washed out interval (Byrom, 2007, p.196). If there is heated circulating fluid or produced fluids in this interval, buckling can occur. These issue is furter examined in chapter 3.4.

It is important to prevent buckling, because it generates additional bending stresses that are not present in the initial conditions. These stresses can cause failure of the casing if the casing is initially close to yield. A permanent plastic deformation called “corkscrewing” occurs if the triaxial stress exceeds the yield strength of the material.

Buckling occurs if the buckling force is greater than a threshold force; the Paslay buckling force. The buckling force is defined as (Lake and Mitchell, 2006, p.304):

$$F_b = -F_a + p_i A_i - p_o A_o \tag{11}$$

where,
F_b = buckling force [lb]
F_a = axial force [lb]
p_i = internal pressure [psi]
p_o = external pressure [psi]

The axial force used in eq.(11) is the initial axial force given by eq.(3) along with the forces given by eq.(5) and eq.(7):

$$F_a = F_{a,i} + F_{bal} + F_T \tag{12}$$

Bending stresses are not included when calculating the buckling force. The Paslay buckling force is given as:

$$F_p = 2\sqrt{\frac{EIw_e \sin\theta}{r_c}} \tag{13}$$

where,

F_p = Paslay buckling force [lb]

w_e = effective (buoyed) weight per unit length [lb/in]

I = the moment of inertia [in^4]

θ = wellbore angle of inclination [radians]

r_c = radial annular clearance [in]

The moment of inertia is found by eq.(14), while the radial annular clearance is given by eq.(15):

$$I = \frac{\pi}{64}(d_n^4 - d_i^4) \tag{14}$$

$$r_c = \frac{OH - d_n}{2} \tag{15}$$

where,

d_i = internal diameter [in]

OH = openhole [in]

The relationship between the buckling force, the Paslay buckling force and the type of expected buckling is shown in Table 2-1.

Table 2-1 Buckling criteria (Lake and Mitchell, 2006, p.305)

Buckling Force Magnitude	Result
$\mathbf{F_b < F_p}$	No buckling
$\mathbf{F_p < F_b < \sqrt{2}F_p}$	Lateral (S-shaped) buckling
$\mathbf{\sqrt{2}F_p < F_b < 2\sqrt{2}F_p}$	Lateral or helical buckling
$\mathbf{2\sqrt{2}F_p < F_b}$	Helical buckling

If the internal pressure is increased, the buckling force will be affected in two ways (Lake and Mitchell, 2006, p.305). Firstly it increases the axial force, F_a, because of ballooning, which will decrease the buckling. Secondly the p_iA_i term is increased, which tends to increase buckling. This second effect is the largest and therefore most important, meaning that the overall effect of increased internal pressure is an increase in buckling. An increase in temperature will lead to a reduction in the axial tension (or increase in the compression). This

leads to an increase in buckling. The type and onset of buckling is a function of the hole angle.

The pitch of a helically buckled pipe is given by the following equation:

$$P_{hel} = \frac{2\pi}{\theta'} \tag{16}$$

where,
P_{hel} = pitch of helically buckled pipe [in]
θ' = rate of change of helix angle with respect to pipe length [radians/ft]

Several important qualities such as pipe curvature, bending moment, bending stress and casing length change are proportional to the square of θ'. If θ' is zero, the pipe is straight, hence a nonzero θ' means that the pipe is curving.
For lateral buckling the maximum value of θ' can be found by

$$\theta'_{\max} = \frac{1.1227}{\sqrt{2EI}} F_b^{0.04} (F_b - F_p)^{0.46} \tag{17}$$

The maximum value of θ' for helical buckling is given by:

$$\theta' = \sqrt{\frac{F_b}{2EI}} \tag{18}$$

The equation for the dogleg curvature for a helix is given by:

$$\kappa = r_c (\theta')^2 \tag{19}$$

where,
κ = dogleg curvature [radians/in]

The previous equation assumes that θ'' is negligible. To convert from radians per inch to degrees per 100ft, multiply by 68,755. This dogleg together with eq.(10) may be used to find the bending stress caused by buckling.

Another more direct way to find the bending stress caused by buckling is to use the following equations, where eq.(20) is for lateral buckling and eq.(21) is for helical buckling:

$$\sigma_b = 0.3151 \frac{d_n r_c}{I} F_b^{0.08} (F_b - F_p)^{0.92} \tag{20}$$

$$\sigma_b = 0.2500 \frac{d_n r_c}{I} F_b \tag{21}$$

2.2. Tubing Leak

The thesis model simulates several load cases; the initial conditions, pressure test of the casing, lost returns with mud drop and tubing leak. However, the main focus of this study is on the issues washout, misalignment of casing and poor cement. These issues are only investigated in tubing leak in the thesis model, as this is the only load case where buckling occurs. Therefore only this load case is presented in this chapter. The rest of the load cases simulated in the thesis model are explained in Appendix A.3.

This is a burst load case which is applicable in both production and injection operations, and represents a high surface pressure at top of the completion fluid in the production annulus due to a tubing leak near the wellhead (Economides et al., 1998, p.194). The worst-case scenario is a surface pressure based on a gas gradient that extends upwards from the reservoir pressure at the perforations. The internal pressure is calculated from:

$$p(z) = p_{res} - \gamma_g z_{res} + \gamma_{pf} z \qquad z < z_p \tag{22}$$

where,

p_{res} = reservoir pressure [psi]

z_{res} = true vertical depth of the reservoir [ft]

γ_g = gas gradient [psi/ft]

z_p = true vertical depth of packer [ft]

γ_{pf} = packer fluid gradient [psi/ft]

z = true vertical depth [ft]

Below the packer the casing will experience a different pressure, resulting from the produced fluid gradient subtracted from the reservoir pressure, as seen in Figure 2-4:

$$p(z) = p_{res} - \gamma_g z \qquad z > z_p \tag{23}$$

This difference below the packer can be neglected for simplicity, by extending the completion fluid (packer fluid) gradient down to the casing shoe. The difference is neglected in both the ILS and the thesis model.

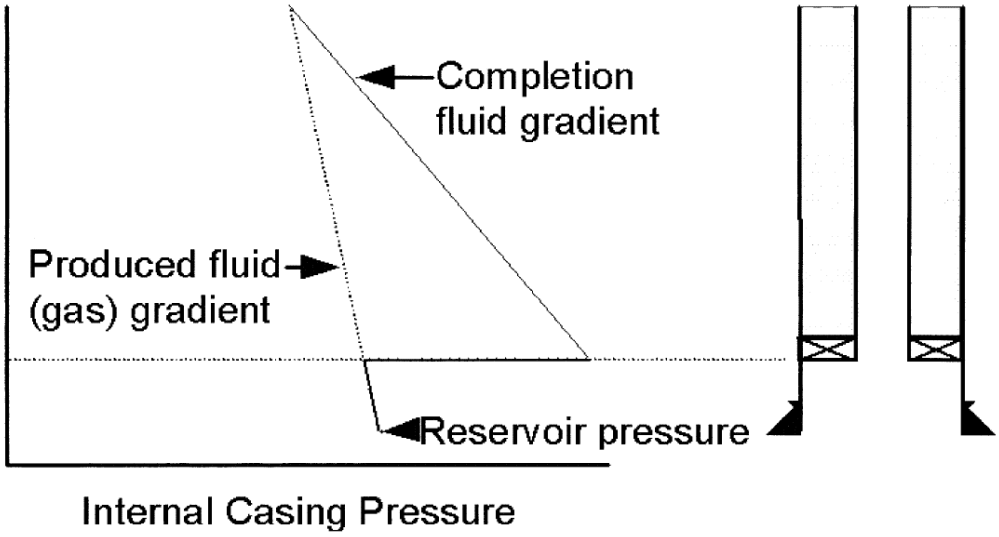

Figure 2-4 Internal pressure during a tubing leak (Landmark, 2008, p.36)

The external pressure is based on deteriorated mud down to TOC, as this load may happen long after drilling and it is likely that the mud will be deteriorated. Below TOC the external pressure is based on the pore pressure. This represents the worst-case scenario.

2.3. Misalignment of Casing

When calculating the different load cases, it seems like the ILS assumes that the casing is positioned in the middle of the hole at all times. This study investigates among other matters how the axial load is affected if the casing is misaligned. The radial clearance is changed if the casing is no longer in the middle of the bore hole, and is therefore not calculated with eq.(15). Instead, the radial clearance is assumed to be given by the following equation:

$$r_c = OH - d_n \tag{24}$$

When using eq.(24) for the radial clearance, the casing is assumed to be located close to the wall instead of in the middle as seen in the following figure. Also shown in the figure is misalignment of casing along with a washout, which is the case investigated further in this study as it is the most interesting. These changes affect the buckling of the casing, thereby changing the axial load and affecting the axial and triaxial safety factor.

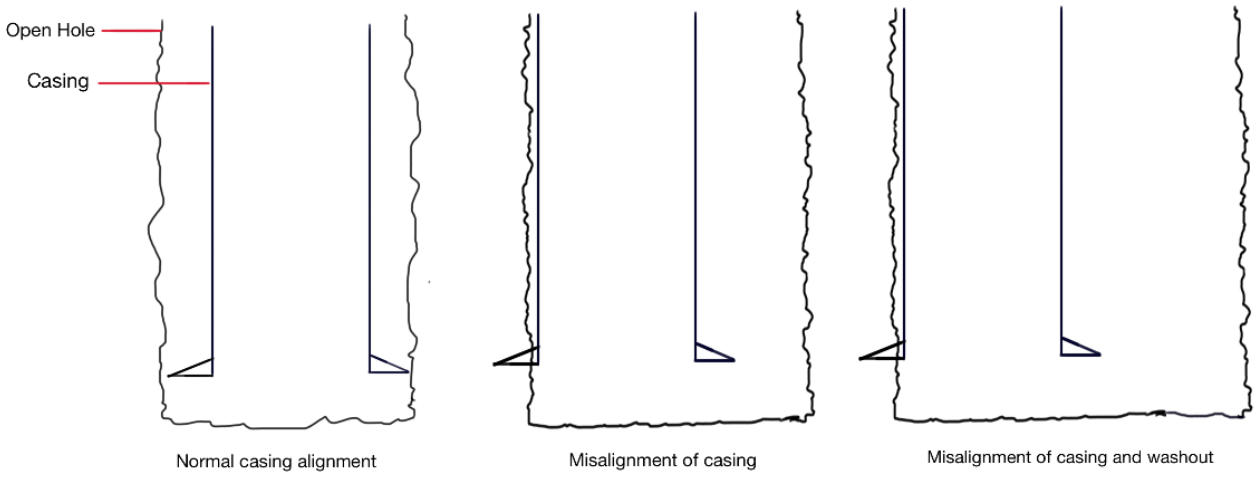

3. Results

A model with the most significant load cases and the initial conditions of a well is built in Excel based on the theory and equations from the literature as given in chapter 2 and Appendix A. The loads simulated are: initial conditions, pressure test, lost returns with mud drop and tubing leak. Tubing leak is only simulated in the production casing as this is the only casing this load case affects, while the rest are simulated for all casings. The properties of the casings for the reference well simulated in the ILS and the thesis model are presented in Table 3-1.

Table 3-1 Casing properties for the well simulated in ILS and thesis model

Casing Name	OD [in]	TOC (TVD) [ft]	Base (TVD) [ft]	Hole Size [in]	Weight [ppf]	Grade
Surface	20	1,072.8	2,624.7	26	169	K-55
Intermediate	13 3/8	5,795.3	7,054.1	17 1/2	77	P-110
Production	9 5/8	12,148.9	12,861.5	12 1/4	53.5	Q-125

The thesis model is then compared to the output from the ILS. Most of the output from the two models match and is presented for all the load cases investigated in all the casing sizes in Appendix B. The anomalies and interesting features is presented in this chapter, along with some new features the ILS does not consider. These new features include the effects of a washout, misalignment of casing and poor cement.

Only the casing strength is considered in this thesis, not the connection strength. Hence the design factor for the connections has in some cases been adjusted so that the output from the ILS is purely based on the casing strength.

The temperatures used to calculate the temperature effects in the thesis model are obtained from the ILS. As these temperatures are used to calculate the temperature derated yield strength, in addition to the temperature effects on the axial load, the temperature should be calculated by the thesis model to make the model even more accurate. However, this is not done in this thesis model. The yield strength of the casing decreases slightly with the increasing casing temperature. Both the thesis model and the ILS uses a temperature derating

of 0.03% per °F increase from the temperature of 68 °F. In other words, the yield strength decreases with 0.03% per °F temperature increase when the casing temperature is above 68°F. The temperature derated yield strength is used to find the axial, burst, collapse and triaxial safety factors.

The differential pressure, the difference between the internal and external pressure, has been used to compare the pressures from the thesis model to the pressures from the ILS. The internal and external pressures in the different load cases are based on the equations in chapter 2.2 and Appendix A.3. As explained in Appendix B, the differential pressures for the different loads in the thesis model are consistent with the results from the ILS, only some minor differences exists. Table 3.2 shows the differential pressure at the bottom of the casing for all the casing sizes and all the load cases, and as seen in the table the differential pressures from the different load cases in the thesis model are close to the differential pressures from the ILS.

Table 3-2 Differential pressure at the bottom of the casing for all the casings and load cases

Differential pressure [psi]	**Initial conditions**		**Pressure test**		**Lost returns with mud drop**		**Tubing Leak**	
Casing	Thesis model	ILS	Thesis model	ILS	Thesis model	ILS	Thesis model	ILS
Surface	-584.6	-585.3	1,488.2	1,488.2	-393.8	-393.6	N/A	N/A
Intermediate	-251.6	-251.9	5,124.7	5,094.7	-2,911.8	-2,915.5	N/A	N/A
Production	-61.7	-61.8	13,509	13,515	-3,790.6	-3,795.2	8,586	8,638

As mentioned in chapter 2.1.2 and examined closer in Appendix A.2.2, there are two different ways of calculating the buoyancy force. The ILS uses the piston force approach, which is why the same approach is used in this model as the two models are compared. In the initial conditions, the axial load is entirely based on eq.(3), which is the air weight of the casing along with the hydrostatic force at the bottom of the casing. The bending stresses are found with eq.(10). In the surface casing the bending stresses would be zero as the DLS is zero at this point, however, since variations in inclination and azimuth occur nearly continuous even though the hole section is designed to be straight, the DLS is assumed to be higher. The DLS-data used to calculate the bending stresses is based on the given DLS in the planned well path

along with the DLS override-data given in NTNU Governing Documentation (Brechan, 2014, p.10). In the other load cases, the axial load is based on the axial load from the initial conditions in addition to ballooning, temperature and buckling effects due to changes in the pressures and temperature. The ballooning force is calculated differently depending on whether the section is cemented or not. This matter is discussed further in Appendix B.3.3.6. In the cemented section it is assumed that the axial load has not changed from the initial conditions, and buckling is thus calculated with the initial axial load in the cemented parts. Appendix B shows that the axial loads in the different load cases from the thesis model are consistent with the output in the ILS, apart from some minor discrepancies. Table 3-3 shows the axial load with bending at the top of the casing for all the casings and load cases, and it is clear that the axial loads from the thesis model are consistent with the axial loads from the ILS.

Table 3-3 Axial load with bending at the top of the casing for all the casings and load cases

Axial load [10^3 lb]	**Initial conditions**		**Pressure test**		**Lost returns with mud drop**		**Tubing Leak**	
Casing	Thesis model	ILS	Thesis model	ILS	Thesis model	ILS	Thesis model	ILS
Surface	128.1	127.7	364.9	364.5	-168.0	-170.1	N/A	N/A
Intermediate	359.4	359.2	671.2	671.0	213.6	207.5	N/A	N/A
Production	495.3	495.1	832.9	832.7	411.1	409.4	821.0	823.8

The axial safety factor (SF) is calculated for each load case to investigate whether the casing grade is strong enough in regard to the axial load. This safety factor is found by dividing the tension force, given in eq.(39) in Appendix A.1.3, with the absolute value of the axial load with bending throughout the section. The yield strength used to find the tension force is the temperature derated yield strength, calculated as previously explained. The axial safety factors from the thesis model are exactly like the safety factors from the ILS, as explained in Appendix B, and shown in Table 3-4 for the top of the casing.

Table 3-4 Axial SF at the top of the casing for all the casings and load cases

Axial SF	Initial conditions		Pressure test		Lost returns with mud drop		Tubing Leak	
Casing	Thesis model	ILS	Thesis model	ILS	Thesis model	ILS	Thesis model	ILS
Surface	21.02	21.09	7.38	7.39	16.03	15.83	N/A	N/A
Intermediate	6.78	6.79	3.63	3.64	11.41	11.76	N/A	N/A
Production	3.92	3.93	2.33	2.34	4.73	4.75	2.37	2.36

To find out whether the casing grade is strong enough to withstand a substantial internal pressure, the burst strength given in eq.(25) in Appendix A.1.1 is calculated throughout the section with the temperature derated yield strength. Then the burst pressure, the internal pressure minus the external pressure, is calculated and the burst safety factor is found by dividing the burst strength by the burst pressure. The burst safety factor is calculated for the pressure test and tubing leak cases, and as shown in Appendix B the burst safety factors in the thesis model correspond to the output from the ILS. Table 3-5 shows the burst SF at the top of the casing; it is clear that the thesis model gives the same SF as the ILS.

Table 3-5 Burst SF at the top of the casing for all the casings and burst load cases

Burst SF	Pressure test		Tubing Leak	
Casing	Thesis model	ILS	Thesis model	ILS
Surface	2.63	2.63	N/A	N/A
Intermediate	1.80	1.80	N/A	N/A
Production	1.26	1.26	1.48	1.47

The collapse safety factor is much more complex than the burst safety factor, it is based on the theory and equations in Appendix A.1.2 and A.1.4. All the collapse safety factors are based on the effective yield strength as there is an axial load in all these cases. In addition, this effective yield strength is based on the temperature derated yield strength. The safety factor is found by dividing the resulting collapse pressure by the equivalent external pressure given in eq.(41). All the results from the thesis model concerning the collapse safety factor

match the ouptut from the ILS perfectly as shown in Table 3-6 for the top of the casing, and for the entire casing string in Appendix B.

Table 3-6 Collapse SF at the top of the casing for all the casings and collapse load cases

Axial SF	Initial conditions		Lost returns with mud drop	
Casing	Thesis model	ILS	Thesis model	ILS
Surface	64.2	64.1	5.20	5.21
Intermediate	61.77	61.72	5.14	5.13
Production	87.52	87.43	10.08	10.08

The triaxial safety factors are based on the equations given in Appendix A.1.5, and it is assumed that the ILS output is also based on these. However, there are some differences between the models, that is further discussed in chapter 3.1.

3.1. Triaxial Safety Factor

As mentioned previously, there are some differences between the models concerning the triaxial factor. The calculations in the thesis model are based on the same equations that are given in the manual for the ILS (Landmark, 2001), however there may be some assumptions that are not stated in this manual. The thesis model uses the same equations for all the load cases, given in Appendix A.1.5. There are four calculations to find the Von Mises-stress, of which the most significant stress is used for further calculations. The theory for the different load cases is given in chapter 2.2 and Appendix A.3.

Figure 3-1 displays the triaxial safety factor in the initial conditions for the production casing. This is the only load case where the thesis model matches the ILS perfectly.

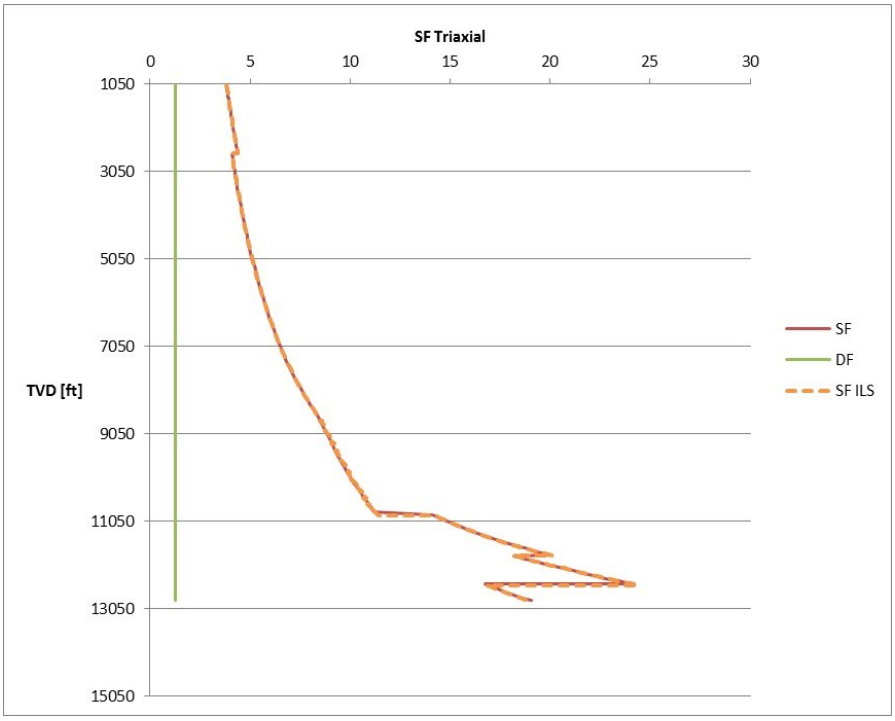

Figure 3-1 Triaxial SF for the initial conditions in the production casing

The figure below shows the triaxial safety factor for the pressure test in the production casing. As seen, the shape of both the safety factors is the same, although the thesis model is more optimistic with a higher SF. However, the triaxial safety factor is calculated in exactly the same way as in the initial conditions where both the models match. The reason why the safety factors do not match in this case is unknown, the reason may be that the ILS has some assumptions that are not given, or that there is a mistake in one of the models.

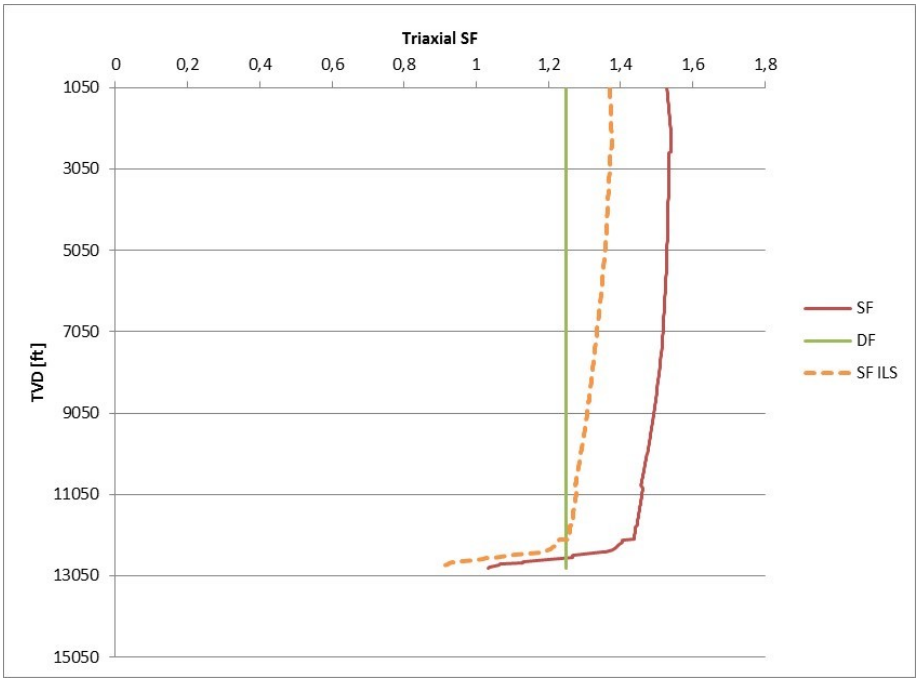

Figure 3-2 Triaxial SF for the pressure test of the production casing

For the lost returns with mud drop load case, the triaxial safety factors do not match either. However, in this case the shapes are the same but the distance between the safety factors is not constant as in the previous case. Because the triaxial safety factors of the thesis model are not consistent with the ILS, it is difficult to make decisions concerning the casing design based on the triaxial safety factor, as there seems to be a mistake in one of the models. This should be at the back of the mind when making decisions.

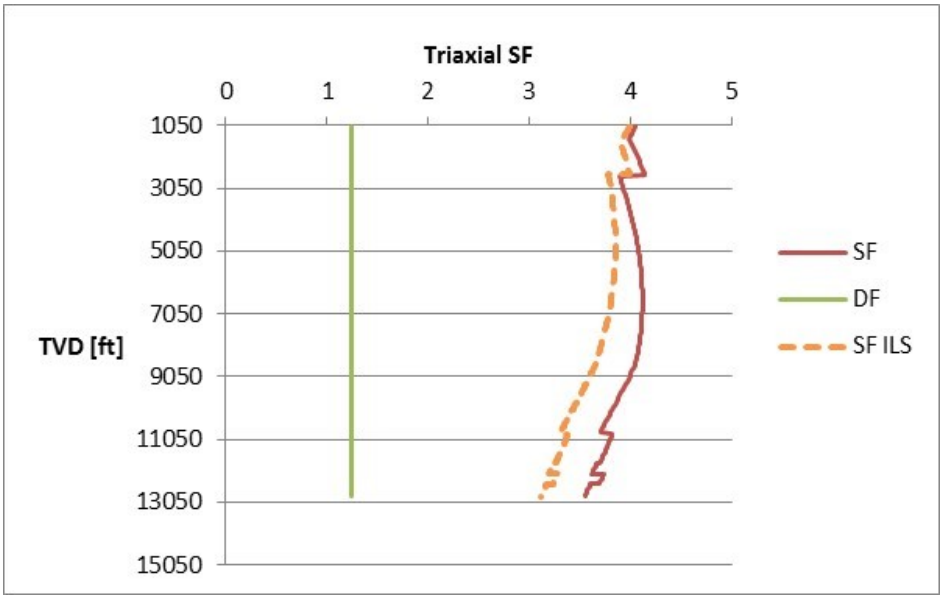

Figure 3-3 Triaxial SF for the lost returns with mud drop load case in the production casing

3.2. Buckling of Casing

The only load case examined in the thesis model in which buckling occurs is tubing leak. This load occurs during injection or production as described in chapter 2.2, thus affecting only the production casing. In the ILS, there is an option to include the capstan effect. This is not accounted for in the thesis model, and so this effect is not included in the ILS either to make it easier to compare. However, the issues addressed in this thesis should also be investigated with the capstan effect included.

The following figure shows the axial load for the tubing leak in both the thesis model and the ILS. As seen, the axial load without bending is the same for both models, however when including bending there is a difference directly above TOC. In the axial load from the ILS, buckling occurs around 10,200ft, while it occurs around 11,400ft in the thesis model. The buckling is also more significant in the ILS. Why the models differs in relation to the size and

onset of buckling is unknown, there may be some assumptions in the ILS that are unpublished.

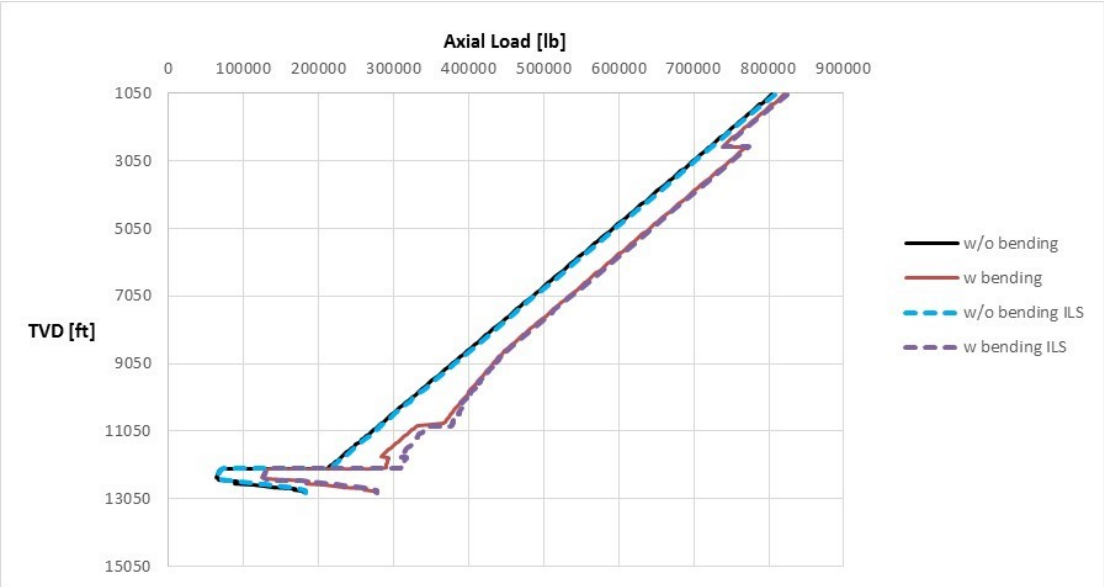

Figure 3-4 The axial load of the production casing during the tubing leak load case

This distinction in the axial load due to a difference in buckling-induced bending force leads to a difference in the axial safety factor as seen in Figure 3-5. In this case it does not affect the casing design, as the safety factor is well above the design factor, however it may be significant in another case.

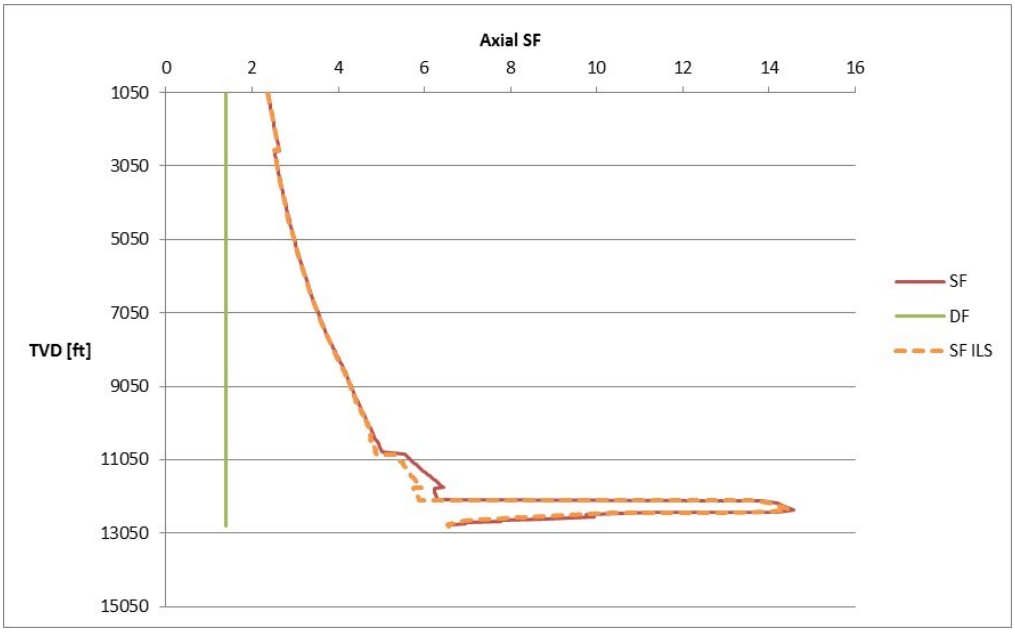

Figure 3-5 The axial SF for the production casing during the tubing leak load case

Concerning the triaxial safety factor, it is difficult to determine the influence of the buckling effect as the thesis model and the ILS does not match. However, it seems like in this case the

difference in axial load due to buckling is not significant enough to matter when considering the triaxial safety factor, as the shape is the same for the two models.

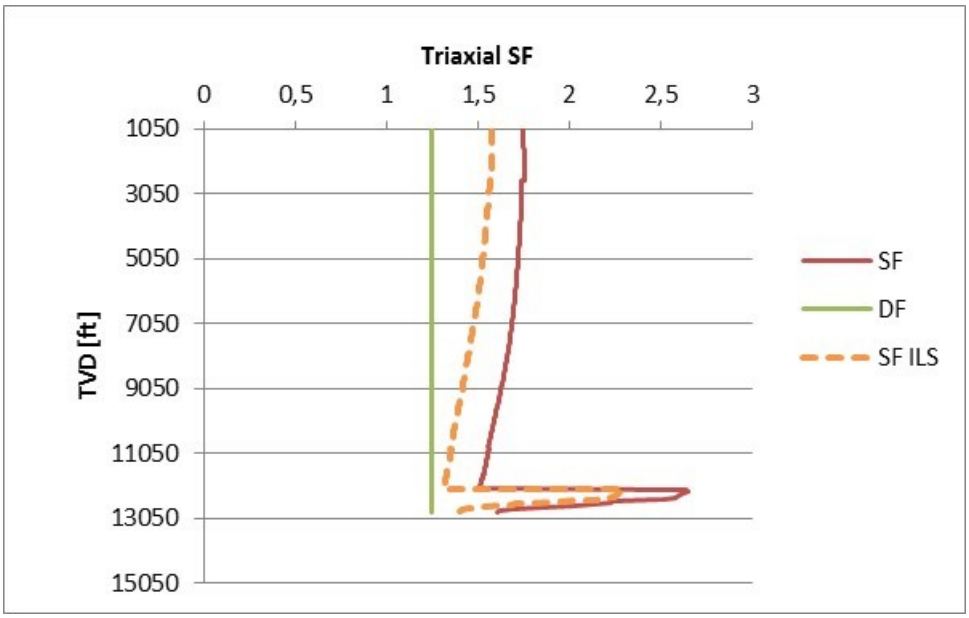

Figure 3-6 The triaxial safety factor for the production casing during the tubing leak load case

3.3. The Effect of Excessive Hole Enlargement on Casing Design

The ILS assumes that the borehole is stable and no excessive hole enlargements occur. This is investigated further, as any washout could have a significant impact on the axial load, because of buckling occuring due to a more significant radial clearance. The washout is examined in regard to the tubing leak load case as this is the only load case investigated where buckling occurs, however the issue should be investigated in other load cases as well, especially drilling loads. It would also be interesting to compare real data where a washout has occurred during tubing leak to the results from the thesis model. The differential pressure during the washout is assumed to be the same as during the tubing leak, however the issue should also be examined with a more realistic pressure for washout.

As the ILS does not have a load case for washout, the results from the thesis model are compared to the results from the ILS for the normal tubing leak load case. Since the pressures are the same for the washout as for the tubing leak, the burst safety factor is not affected and therefore not examined further.

To find the size a washout needs to be to influence the casing design, the OH-diameter in the radial clearance is adjusted until the triaxial SF is below the triaxial DF. When the OH-

diameter is 30 inches, the radial clearance is 10.1875 inches and the triaxial SF is below the DF. The axial load in Figure 3-7 is the axial load calculated with this OH-diameter.

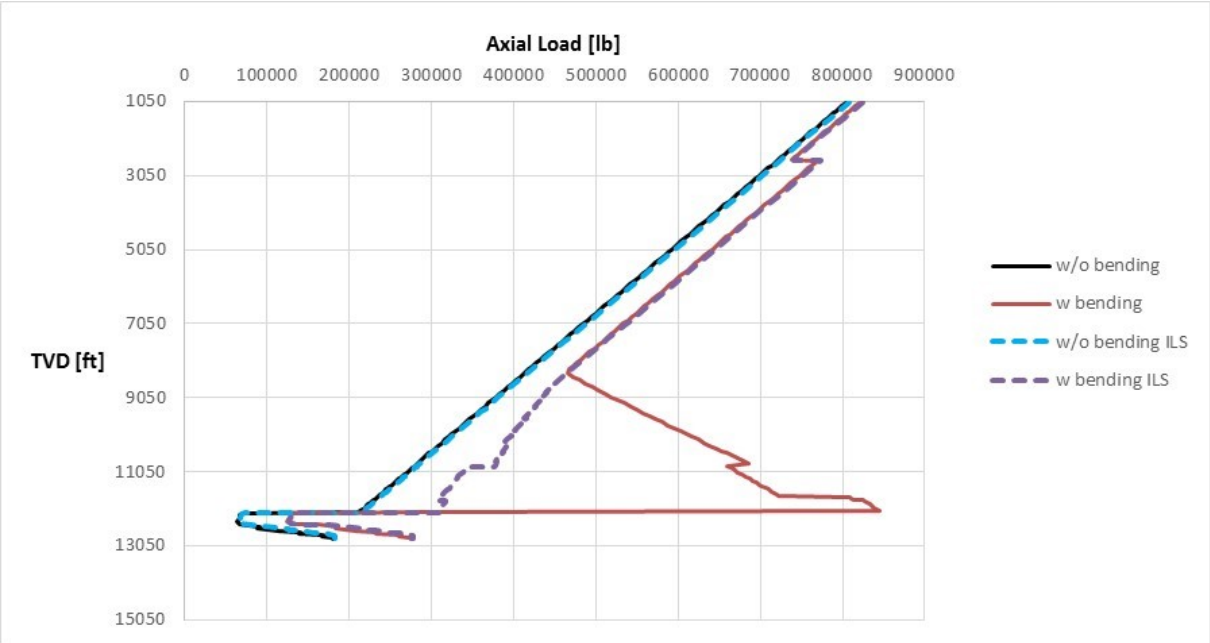

Figure 3-7 The axial load of the production casing during the tubing leak load case with washout

With this new radial clearance of 10.1875 inches, the axial SF is still above the axial DF as seen in the figure below.

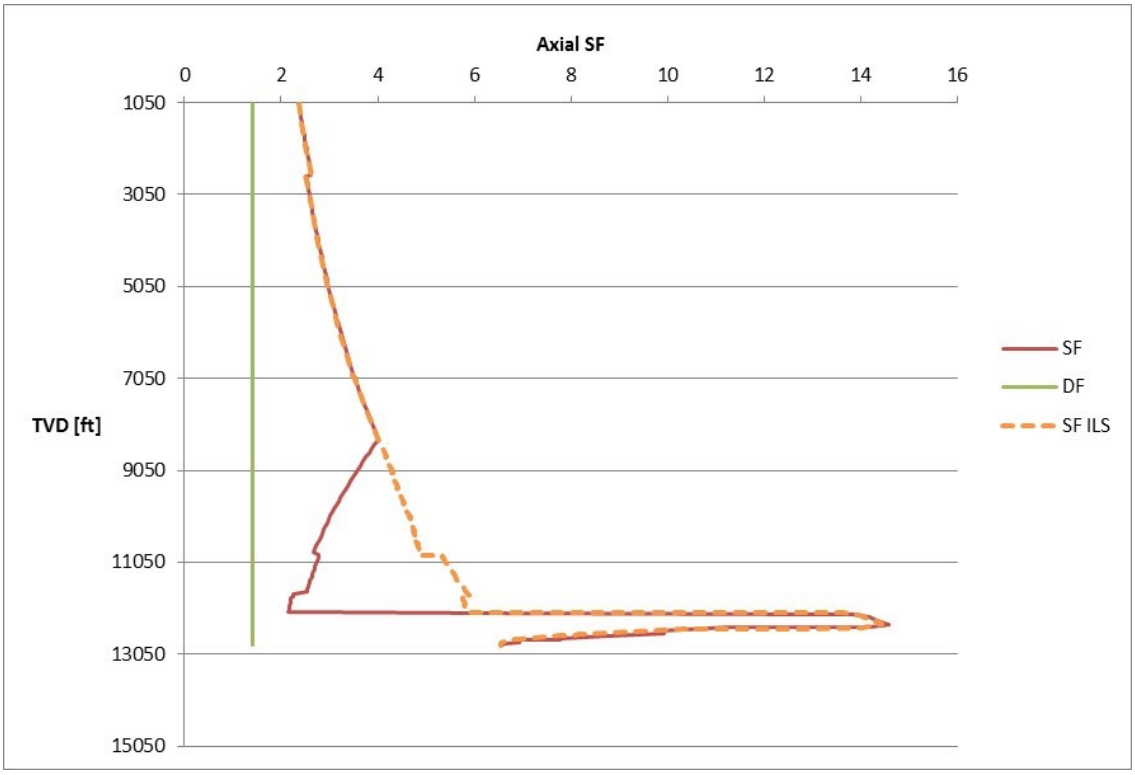

Figure 3-8 The axial SF for the production casing during the tubing leak load case with washout

This new radial clearance has an axial SF above the axial DF, however the triaxial SF is below the triaxial DF as depicted in Figure 3-9. In addition, the thesis model has had a more optimistic triaxial SF than the ILS throughout the load cases as discussed in chapter 3.1, and the buckling is stronger in the ILS; hence the washout may be even smaller and cause troubles earlier than the thesis model predicts.

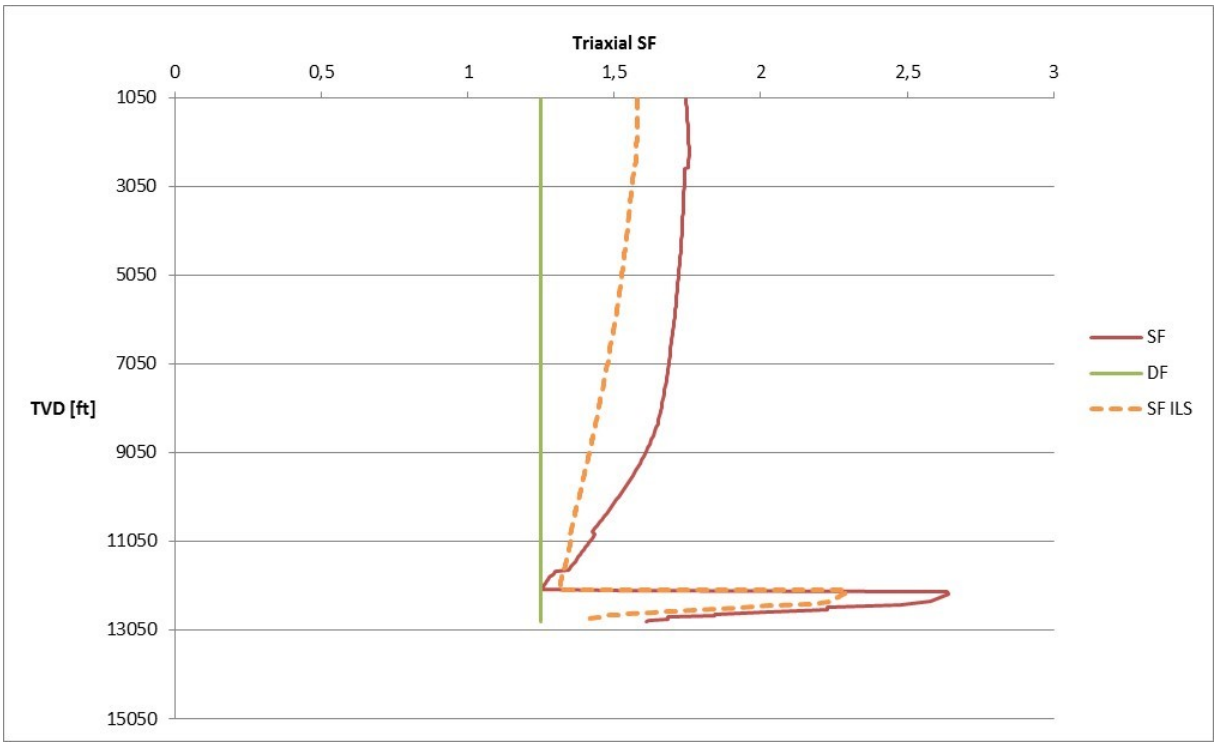

Figure 3-9 The triaxial SF for the production casing during the tubing leak load case with washout

3.4. The Effect of Excessive Hole Enlargement when Combined with Poor Cement

As mentioned earlier in chapter 3, it is assumed that in a cemented section the axial load stays the same as the initial load since the section is fixed and thus will not move. This means that the buckling is calculated with the initial axial load in these sections. However, this assumes that the cement job is perfect, which may not always be the case. This chapter investigates if buckling will occur in the load case tubing leak if the cement job is a failure, and whether this will have an impact on the casing design. In addition it is investigated if a washout in the section where the cement was supposed to be affects the casing design.

The axial load when the cement job is a failure is presented in Figure 3-10. It is quite different below the depth supposed to be the TOC compared to the axial load for a perfect cement job, represented by the output from the ILS.

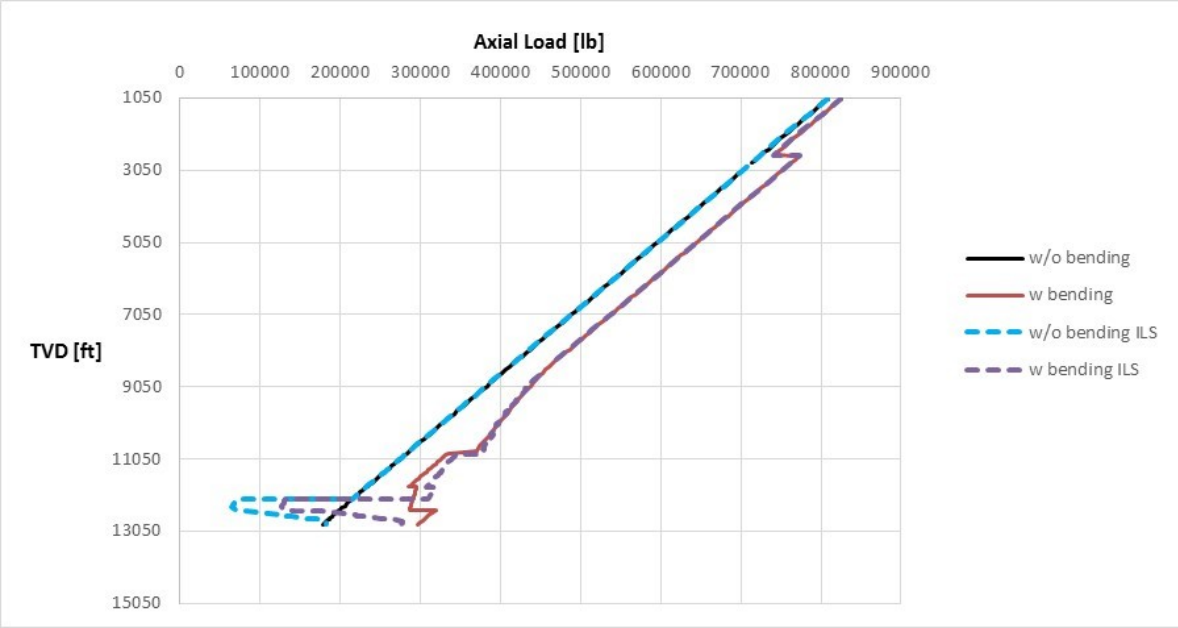

Figure 3-10 The axial load of the production casing during tubing leak load case with cement job failure

Figure 3-11 shows how the axial load will look like if there is a washout in addition to a poor cement job. The washout is with an OH-diameter of 30 inches, changing the axial load quite significantly.

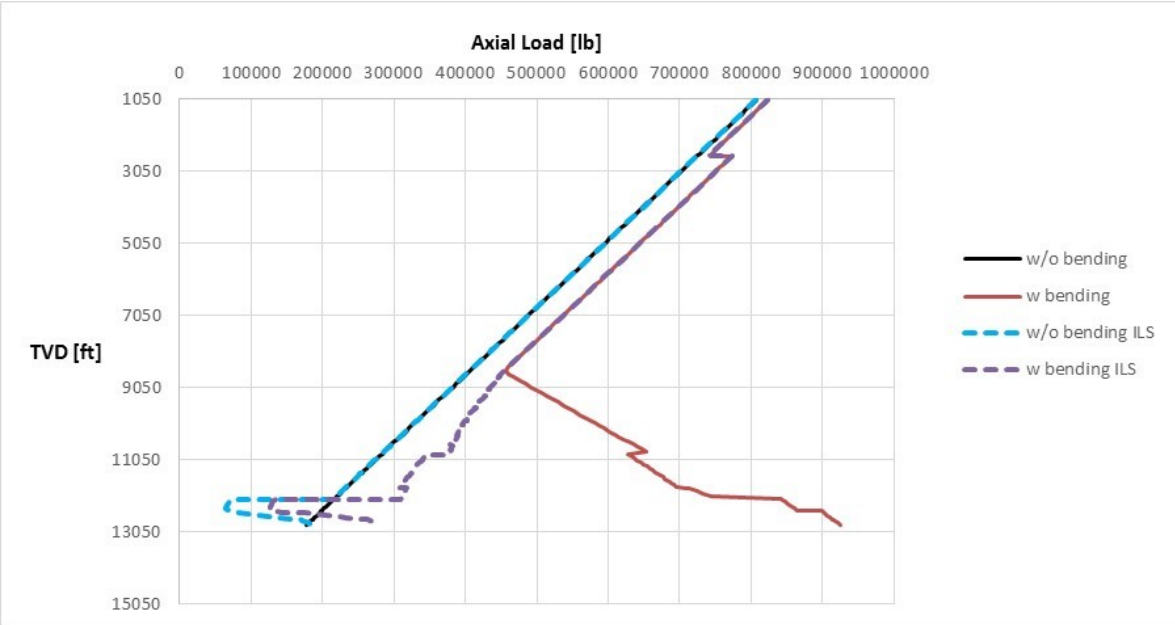

Figure 3-11 The axial load of the production casing during tubing leak load case with cement job failure and washout

The axial safety factor for the poor cement job is affected a lot below the supposed TOC as seen in the following figure, however the SF is still above the DF by a significant margin.

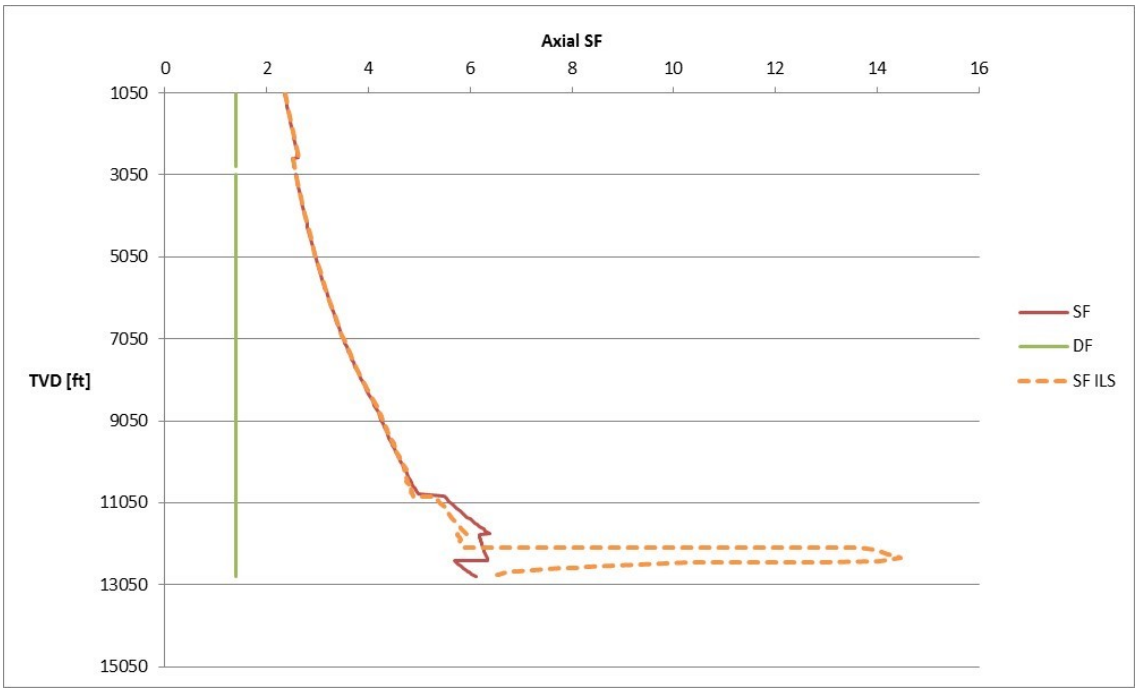

Figure 3-12 The axial SF for the production casing during tubing leak load case with cement job failure

When there is a washout in addition to a cement job failure, the axial SF changes quite significantly as seen in the following figure. However, the SF is still above the DF.

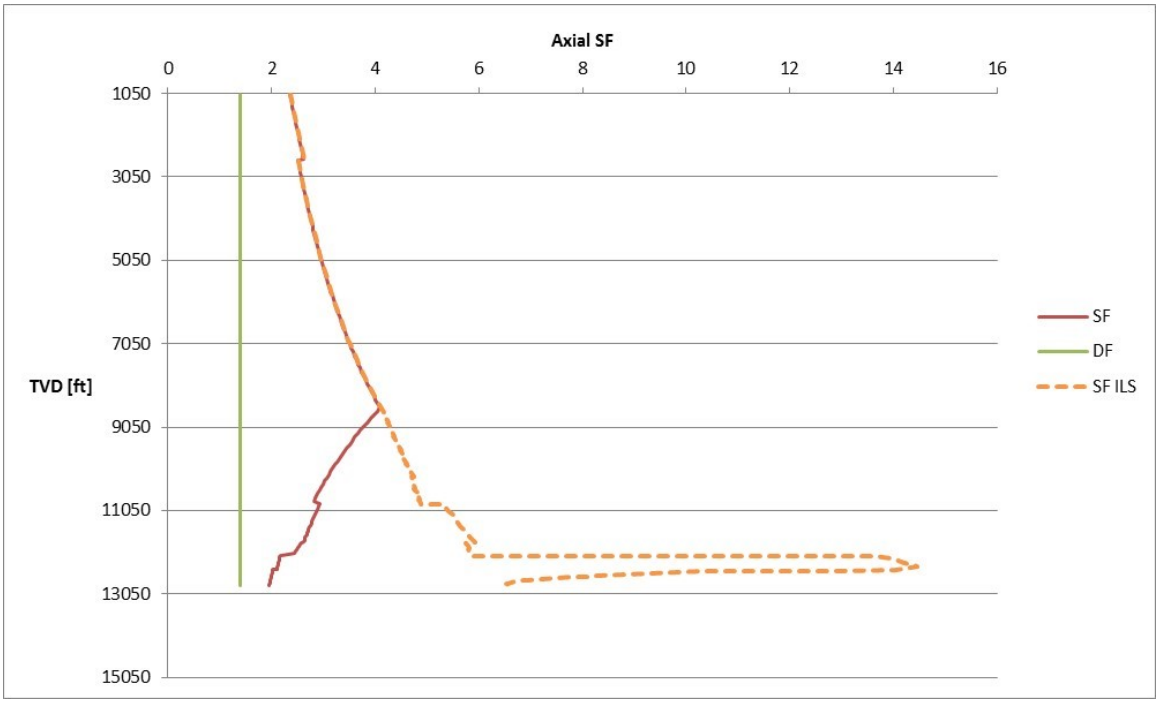

Figure 3-13 The axial SF for the production casing during tubing leak load case with cement job failure and washout

As for the axial SF, the triaxial SF is also altered significantly below the supposed TOC as depicted in Figure 3-14 when the cement job is a failure. However, the SF is still way above the DF, hence it will not affect the casing design in this load case if the cement job is a failure.

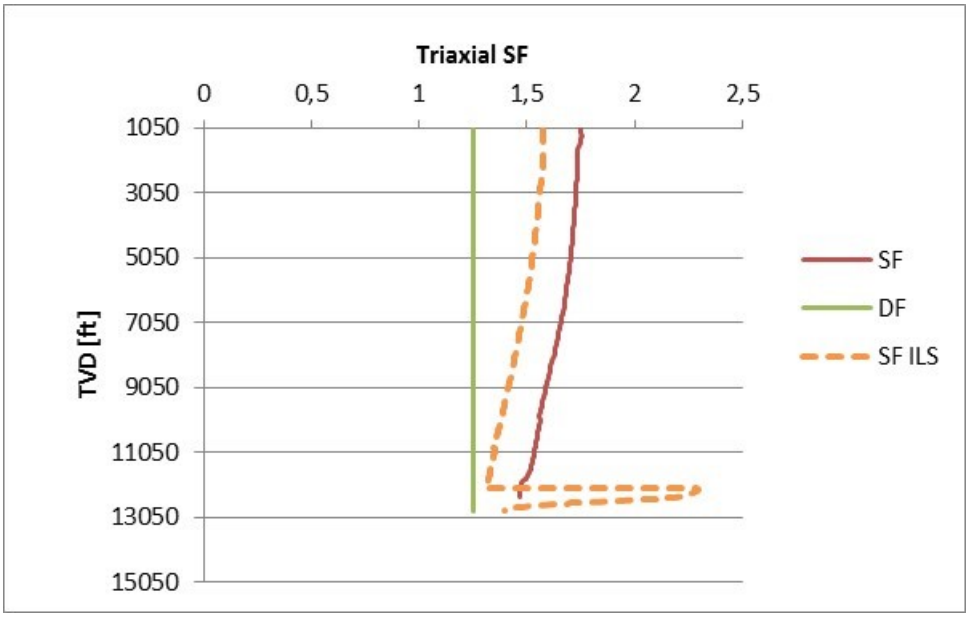

Figure 3-14 The triaxial SF for the production casing during tubing leak load case with cement job failure

In the case with poor cement and washout, the axial safety factor was above the design factor. However, the triaxial SF is below the DF when considering this case. The following figure shows how the SF crosses the DF below the depth where the TOC should be. The triaxial safety factor will cross the design factor at an even lower washout than 30inches. However, a misalignment of the casing in addition to a washout is more severe than a cement job failure in addition to a washout as wil be shown in the next chapter.

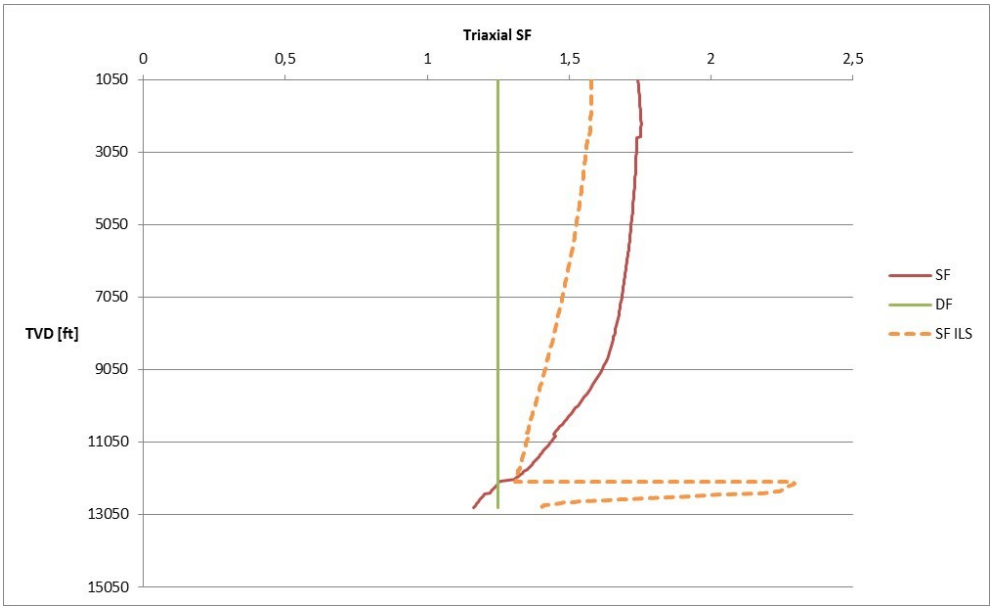

Figure 3-15 The triaxial SF for the production casing during tubing leak load case with cement job failure and washout

3.5. The Effect of Excessive Hole Enlargement and Misalignment of Casing

As mentioned in chapter 2.3, it seems like the ILS assumes that the casing is positioned in the middle of the hole at all times. Previously the effects of a washout were examined; in this chapter it is assumed that the casing is misaligned in addition to a washout. To account for the washout, the OH-diameter in the radial clearance is increased as before. To investigate the misalignment, the radial clearance is calculated with eq.(24).

Figure 3-16 shows the axial load when the OH-diameter in the radial clearance is changed from 12.25 inches to 28 inches. The radial clearance is also calculated so that the casing is close to the wall on one side. However, the results might be slightly exaggerated as the thesis model simplifies things by assuming that the casing is close to the washout wall all the way, which may be a bit unlikely. As seen from the figure below, this leads to significant buckling, changing the axial load a lot.

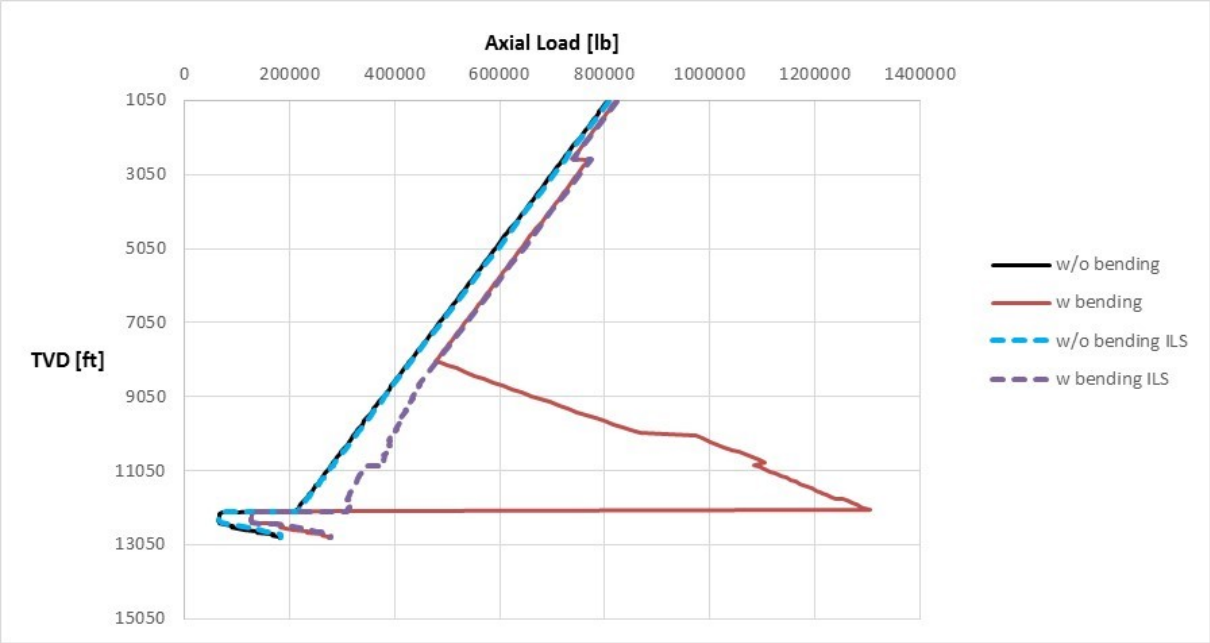

Figure 3-16 The axial load of the production casing during tubing leak load case with washout and misalignment of casing

The previous figure showed a washout with an OH-diameter of 28 inches. This is quite a significant washout, and so Figure 3-17 shows the axial load when the OH-diameter is 20 inches to see whether this will affect the casing design. As the OH-diameter is smaller in this case, the induced buckling is also smaller. However, a washout of from 12.25 inches to 20 inches is more likely than a washout to 28 inches.

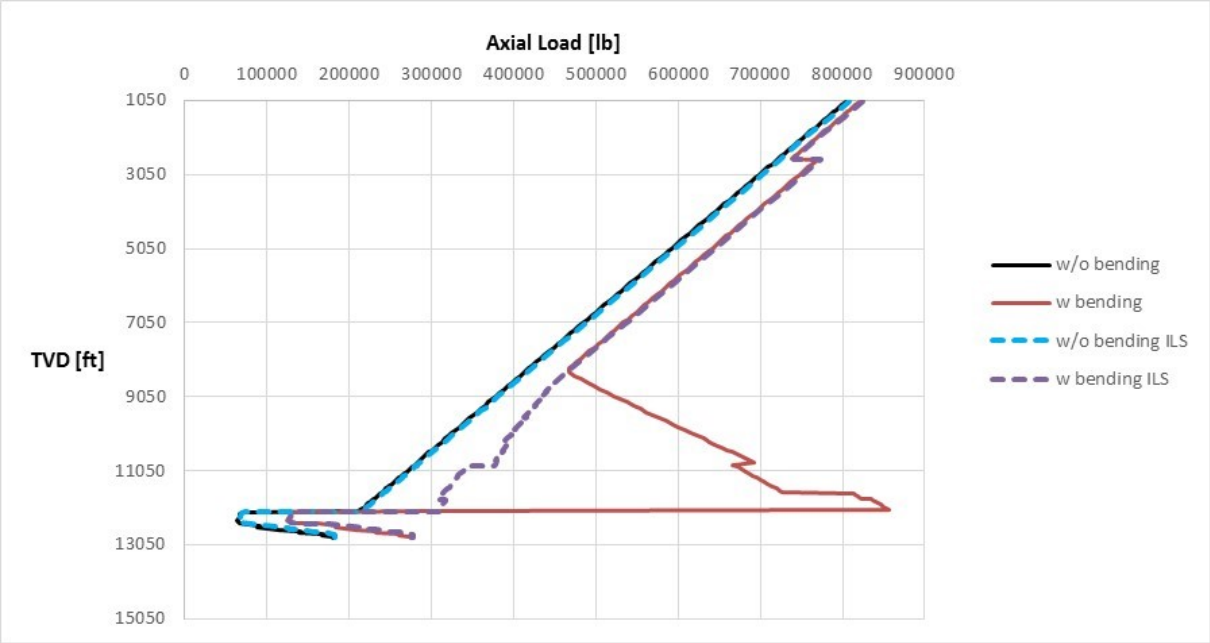

Figure 3-17 The axial load of the production casing during tubing leak load case with washout and misalignment of casing, with smaller radial clearance

As seen in Figure 3-18, the axial SF is lower than the DF. This figure corresponds to the axial load in Figure 3-16, with an OH-diameter of 28 inches.

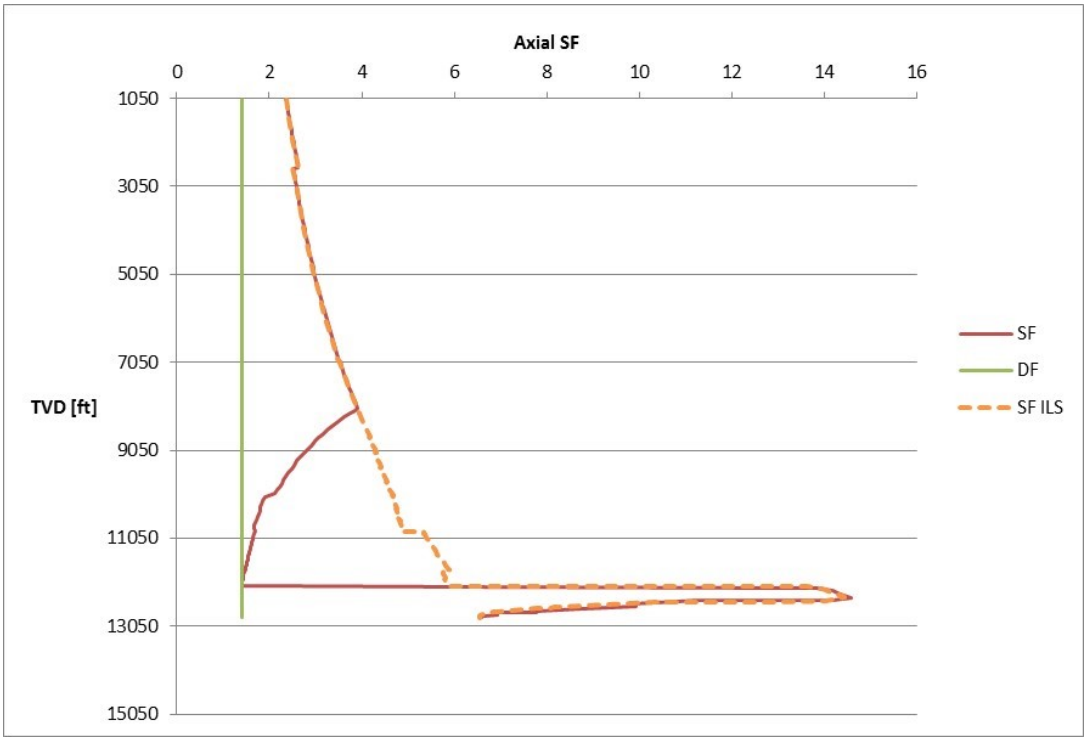

Figure 3-18 The axial SF for the production casing during tubing leak load case with washout and misalignment of casing

When the OH-diameter is 20inches, the axial SF is above the DF as seen in Figure 3-19. This axial SF corresponds to the axial load in Figure 3-17.

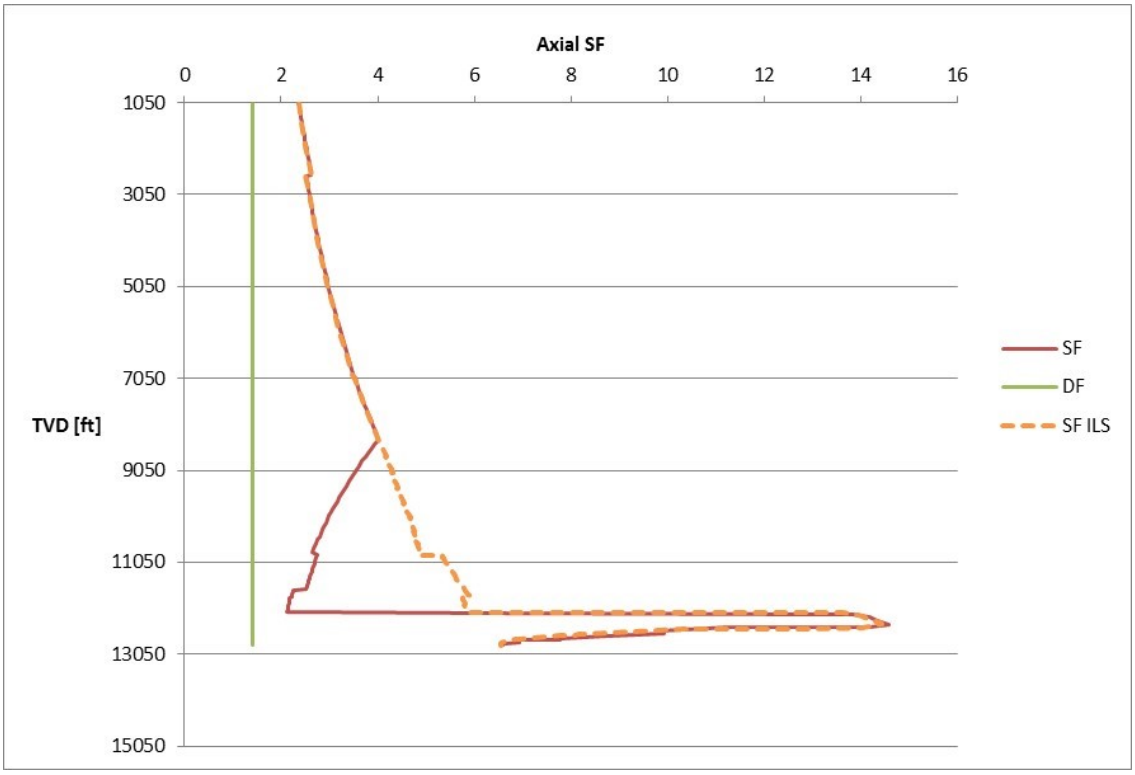

Figure 3-19 The axial SF for the production casing during tubing leak load case with washout and misalignment of casing, with smaller radial clearance

While the axial SF barely crosses the DF in Figure 3-18, the triaxial SF is clearly below the DF in Figure 3-20.

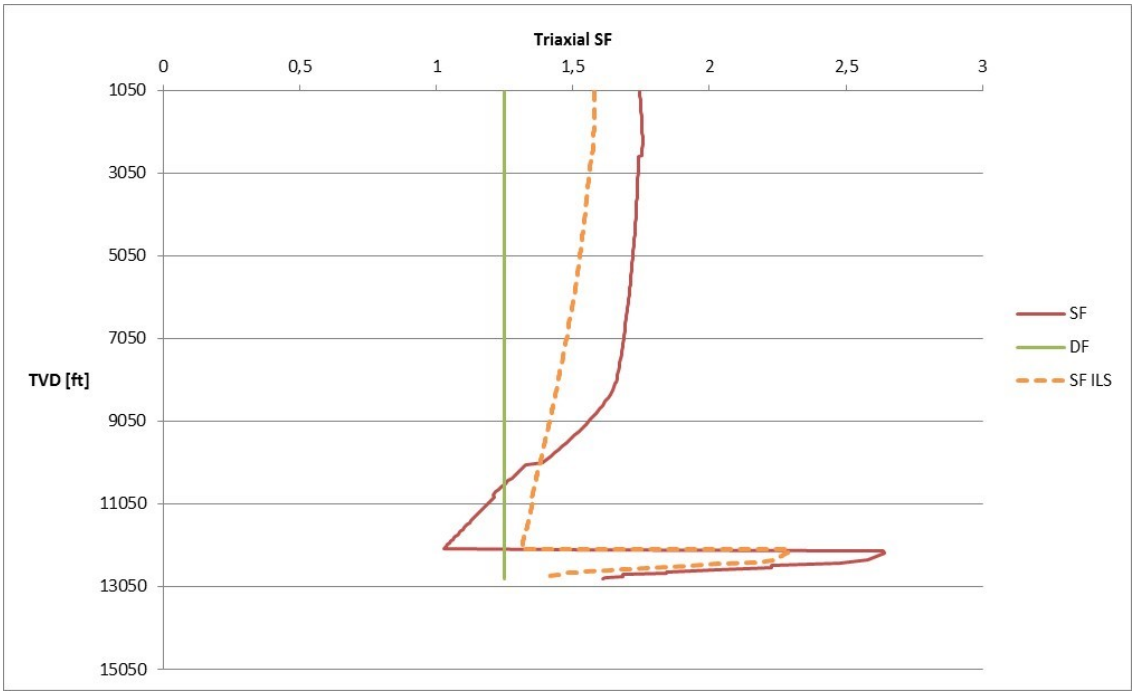

Figure 3-20 The triaxial SF for the production casing during tubing leak load case with washout and misalignment of casing

The triaxial safety factor corresponding to the axial load in Figure 3-17 is also below the DF as seen in the following figure; this will happen with a smaller washout than the other case and is therefore more likely. However, as explained in chapter 3.2, the ILS had a larger buckling force than the thesis model, which means that the triaxial SF may cross the DF at an even lower OH-diameter. In addition, as discussed in chapter 3.1, the triaxial SF from the ILS has been smaller than the triaxial SF from the thesis model throughout all the load cases. This means that if the ILS had calculated this scenario, an even smaller washout could have led to the triaxial SF being below the DF. As seen in the following figure, the triaxial safety factor for the ILS is already dangerously close to the design factor. If the ILS had investigated washout, the washout needed would probably be even smaller than 20 inches, and therefore even more likely.

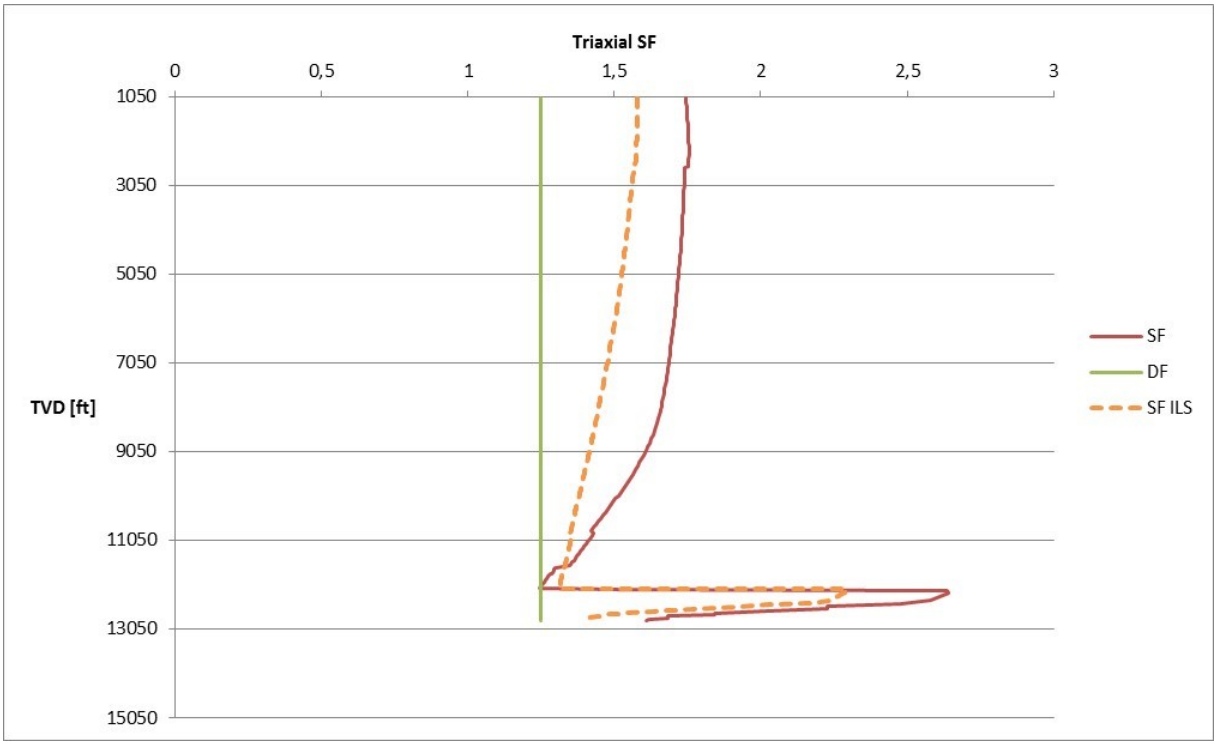

Figure 3-21 The axial SF for the production casing during tubing leak load case with washout and misalignment of casing, with smaller radial clearance

4. Discussion

Chapter 3 starts off discussing the similarities between the results from the thesis model and the output from the ILS. This includes the differential pressure, axial load, axial safety factor, collapse safety factor and burst safety factor. Further the chapter discusses the differences between the ouput from the models, including the triaxial safety factor and buckling. The calculations of all these aspects in the thesis model are done with the equations from the literature as given in chapter 2 and Appendix A. In addition to these similarities and differences, the chapter shows the impact of a washout, misalignment of the casing and poor cement.

The differential pressure is calculated from the external and internal pressure, and is almost exactly like the output from the ILS in all the load cases. This goes for the axial load, axial safety factor, collapse safety factor and burst safety factor as well. There are some small differences, but nothing significant. The axial loads are calculated the same way in the thesis model as the ILS, although there are some interesting details concerning the method of calculating the ballooning force, which are investigated further in Appendix B.3.3.6.

4.1. Triaxial Safety Factor

The triaxial safety factor in the thesis model differs somewhat from the ILS in nearly all the cases investigated, as discussed in chapter 3.1. The reason for this difference is unknown, as the equations in the ILS are unknown. However, the references for the triaxial safety factor that are given in the ILS are examined, and the same equations as in these references are used in the thesis model, meaning that the results should in theory match.

Since both the pressures and the axial loads with bending stresses are the same in both models for all the load cases as seen in Appendix B, the triaxial safety factors for both the models should also be the same as they are based on these pressures and axial loads. The ILS may use different assumptions than the thesis model, or there may be something wrong with either the thesis model or the ILS. As the output from the thesis model is generally more optimistic than the ILS, a casing design based on this could be less conservative.

The equations and assumptions behind the triaxial safety factor in the ILS should be investigated further as this in some cases has a significant impact on the casing design. When

examining washout and misalignment, this difference in the triaxial safety factor means that the washout diameter that is significant in relation to the triaxial safety factor may in fact be even smaller if the triaxial safety factor from the thesis model was equal to the ILS.

4.2. Buckling of Casing

In the ILS, there is an option called Capstan effect. This includes the contact forces with the wellbore, however this is not included in the thesis model as this model is somewhat simplified. Therefore this option is not included in the ILS either, so as to be able to compare the results. The different aspects examined in this thesis; washout, misalignment of casing and poor cement, should be examined with this effect included as well to see if the results are altered or not.

The buckling effect is calculated as shown in chapter 2.1.6, however there is a discrepancy between the results from the thesis model and the ILS concerning buckling. In the output from the ILS, buckling occurs earlier and stronger than in the thesis model. The reason for this is unknown, as the references used for calculating the buckling effect are the same. However, this should also be investigated further, as there may be something wrong with either the thesis model or the ILS.

4.3. Washout

Hole enlargements may be a big problem in some formations, especially shale. As examined in the thesis model, a significant washout will affect the axial load, axial safety factor and the triaxial safety factor because of buckling stresses created from the enlarged radial clearance. Chapter 3.3 examines the effects of a washout during a tubing leak case. Normally the borehole diameter is 12.25 inches in the production casing, however this chapter examines what happens if this is enlarged. When the new borehole diameter is 30 inches, the triaxial safety factor crosses the design factor as seen in Figure 3-9. A hole enlargement from 12.25 to 30 inches is a quite significant increase, and may be a bit unlikely. However, the triaxial safety factor from the ILS is quite close to the DF, and may cross the DF at a much smaller washout-diameter than the thesis model predicts. The ILS does not consider this issue, which may affect the casing design. In the thesis model, washout is investigated only in the load case tubing leak. However, it should be investigated in other load cases as well, especially during drilling. In addition, it would be interesting to compare real data from a washout during a tubing leak to the results from the thesis model.

4.4. Poor Cement

How the cement acts during the load cases after the initial conditions is debatable. The burst loads in the ILS uses the pore pressure below the TOC when calculating the external pressure. When this is the case, it is unsure whether the cement can be assumed to be a physical support to the casing.

The thesis model investigates whether there is buckling below TOC in the tubing leak load case if the cement job is a failure. When the cement job is poor, the induced buckling is not severe enough to cause the traixal safety factor to be too small as shown in chapter 3.4. However, if there is a washout with an OH-diameter of 30 inches in addition to the poor cement job, the buckling is severe enough to cause the triaxial safety factor to be below the triaxial design factor.

4.5. Misalignment of Casing

Another issue with the ILS is that it seems like the software assumes that the casing is in the middle of the hole at all times. This is unlikely, especially when the inclination increases. Chapter 3.5 shows that if the casing is misaligned, the washout need not be that large to affect the safety factors. Figure 3-21 shows the triaxial safety factor when the casing is misaligned, and a washout causes the borehole diameter to increase from 12.25 to 20 inches. This is a much more likely hole enlargement than the previously investigated 30 inches. As the thesis model simplifies by assuming that the casing is close to wall in all places, also in the washout zone, the results may be higher than what is likely. However, as mentioned in relation to a regular washout, the triaxial safety factor from the ILS is quite close to the design factor, and so the washout would have been smaller than 20 inches if the ILS investigated this issue. In addition the buckling force calculated by the ILS is more significant than the force calculated by the thesis model, meaning that the washout could be even smaller than estimated by the thesis model.

The ILS does not consider the issues of washout, poor cement and misalignment of casing; however, they may affect the casing design and thus they should be examined. As the equations are mainly the same, it would be easy to implement in the ILS. Washout and misalignment of the casing is only investigated in relation to the tubing leak load case, however it may be interesting to examine these issues in other load cases as well, especially drilling load.

5. Conclusion

The thesis model is used to compare the equations and assumptions given in literature to the output from the ILS. As stated in chapter 3 and shown in Appendix B, the axial loads, differential pressures, axial safety factors, collapse safety factors and burst safety factors calculated in the thesis model match the output from the ILS perfectly or nearly perfect in all the load cases. The only difference between the two models is concerning the buckling effect and the triaxial safety factor.

As shown in chapter 3.1, the triaxial safety factor from the thesis model does in some cases match the output from the ILS, however there is usually a discrepancy between the models. The triaxial safety factor is calculated the same way for all the load cases in the thesis model, and obviously the ILS calculates the same way in some cases, as the result is the same in those cases. However, there must be some assumptions in the ILS that is not known, as most of the results from the ILS concerning the triaxial SF differ from the thesis model.

Buckling of the casing is a serious issue, and is in the thesis model calculated as given in chapter 2.1.6. In the ILS there is an option to include the capstan effect, however this is not included in the thesis model, and therefore not in the ILS either to be able to compare the results. In spite of this, there is a difference in the buckling force in the example seen in chapter 3.2; the bending force due to buckling of the casing occurs earlier and stronger in the ILS than in the thesis model. The reason for this is not known, and should be investigated further.

The thesis model investigates an issue not examined in the ILS, the issue of washout of the borehole and misalignment of the casing. The impact of these issues is examined, and how significant the washout needs to be before it starts to affect the casing design. In the load case investigated, tubing leak in the production casing, an increase of the open hole diameter from 12.25 to 30 inches leads to the triaxial safety factor being below the triaxial design factor. Keeping in mind that the buckling in the ILS is stronger than in the thesis model, and that the triaxial safety factor is overall more pessimistic in the ILS, the washout could be smaller than 30 inches and still have an impact if the ILS examined this issue.

If the cement job is a failure, it is not a crisis in the case examined as discussed in chapter 3.4. However, if there is a washout in addition to the bad cement job, the result may have a severe impact. In this case, a washout modifying the OH-diameter to 30 inches results in a triaxial safety factor that is too small compared to the design factor.

As discussed in chapter 3.5, if the casing is misaligned the buckling gets more significant and the washout needed to affect the casing design is smaller. In the case examined, a misaligned casing, a washout of 20 inches makes the triaxial safety factor go below the triaxial design factor. This is more realistic than a washout of 30 inches.

The issues investigated in this study need quite a significant washout before the casing design is affected, as the smallest washout is from 12.25 to 20 inches, which may be unrealistic. However, as discussed previously, the washout may be smaller than this if the ILS investigated these issues, and therefore more realistic. This study shows that it would be interesting to examine these issues in more advanced software than the thesis model.

6. Further Work

- Build a model that consider the capstan effect as the ILS does, and investigate washout, poor cement and misalignment of casing in this new model.

- Examine whether the pressure during an eventual washout is changed, and what effect this has on the different safety factors.

- Investigate further the assumptions behind the triaxial safety factor, and find out why the ILS and the thesis model differ in regard to this.

- Examine the difference in the buckling effect between the models, and find the correct way to calculate buckling.

- The temperature of the casing in the different load cases should be investigated separately and compared to the ILS. The load cases, washout and misalignment of casing should be calculated again with these temperatures and compared to the results from this study.

- Investigate what effect a washout and misalignment of the casing would have on other load cases.

- Investigate real cases where washout has occurred, and whether there was buckling of the casing or not.

Nomenclature

A_i	internal area of the casing	[in^2]
A_o	external area of the casing	[in^2]
C_T	coefficient of thermal expansion	[$°F^{-1}$]
D	depth at top of casing	[ft]
d_i	inside diameter	[in]
DLS	dogleg severity	[°/100ft]
d_n	nominal outer diameter	[in]
D_{TVD}	true vertical depth at the base of the casing	[ft]
E	Young's modulus	[psi]
F_a	axial force	[lb]
$F_{a,arch}$	the axial force found by the principle of Archimedes	[lb]
$F_{a,i}$	the initial axial force at top of casing	[lb]
F_{air}	the air weight of the casing	[lb]
F_{ax}	the axial component of the weight of the casing	[lb]
F_b	buckling force	[lb]
F_{bal}	force resulting from ballooning effects	[lb]
F_{dev}	deviatoric force	[lb]
$F_{hydrostatic}$	hydrostatic force at bottom of casing	[lb]
$F_{hyd,av}$	average hydrostatic force	[lb]
F_n	the normal component of the weight of the casing	[lb]
F_p	Paslay buckling force	[lb]
F_T	force resulting from temperature change	[lb]
F_{ten}	tension force	[lb]
F_w	weight of casing	[lb]
F_1,F_2,F_3,F_4,F_5	empirical coefficients	
I	moment of inertia	[in^4]
L	length of casing	[ft]
OD	outer diameter	[in]
p_{br}	burst strength	[psi]
P_{cr}	collapse pressure	[psi]
p_e	equivalent external pressure	[psi]

p_f	pore pressure at lost-circulation zone depth	[psi]
P_{hel}	pitch of helically buckled pipe	[in]
p_i	internal pressure	[psi]
$p_{i,b}$	internal pressure at bottom of casing	[psi]
p_o	external pressure	[psi]
$p_{o,b}$	external pressure at bottom of casing	[psi]
p_{res}	reservoir pressure	[psi]
$p_{surface}$	test pressure at surface	[psi]
R	radius of the bend	[in]
r_c	radial annular clearance	[in]
r_i	inside radius of the pipe	[in]
r_o	outside radius of the pipe	[in]
t	nominal thickness	[in]
T_0	initial temperature	[°F]
T_1	final temperature	[°F]
w	the weight per foot of casing	[lb/ft]
w_e	effective (buoyed) weight per unit length	[lb/in]
Y	effective minimum yield strength	[psi]
z	true vertical depth	[ft]
z_{lc}	lost-circulation zone depth	[ft]
z_{md}	mud drop depth	[ft]
z_p	true vertical depth of packer	[ft]
z_{res}	true vertical depth of reservoir	[ft]
α	the inclination of the borehole	[°]
α	the dogleg severity	[°/100ft]
β	buoyancy factor	
ΔL_{bal}	length change due to ballooning	[psi]
ΔL_T	expansion or shortening of casing due to temperature change	[ft]
Δp_i	change in internal pressure relative to initial condition	[psi]
Δp_o	change in external pressure relative to initial condition	[psi]
ΔT	average change in temperature from base load to load case	[°F]
γ_m	mud gradient	[psi/ft]
γ_g	gas gradient	[psi/ft]
γ_{pf}	packer fluid gradient	[psi/ft]

γ_{sw}	saltwater gradient	[psi/ft]
κ	dogleg curvature	[radians/in]
μ	Poisson's ratio	
ρ_i	fluid density inside pipe	[ppg]
ρ_m	density of mud	[ppg]
ρ_o	fluid density outside pipe	[ppg]
ρ_p	density of pipe	[ppg]
σ_a	axial stress	[psi]
σ_b	bending stress	[psi]
σ_r	radial stress	[psi]
$\sigma_{r,i}$	radial stress at inner wall	[psi]
$\sigma_{r,o}$	radial stress at outer wall	[psi]
σ_t	tangential or hoop stress	[psi]
$\sigma_{t,i}$	tangential or hoop stress at inner wall	[psi]
$\sigma_{t,o}$	tangential or hoop stress at outer wall	[psi]
σ_{VME}	Huber-Hencky-Mises or triaxial stress	[psi]
σ_{yield}	minimum yield strength	[psi]
$(\sigma_{yield})_e$	effective minimum yield strength	[psi]
σ_z	axial stress	[psi]
θ	wellbore angle of inclination	[radians]
θ'	rate of change of helix angle with respect to pipe length	[radians/ft]

Abbreviations

DF	design factor
ILS	industry leading software
OH	openhole
SF	safety factor
TOC	top of cement
TVD	true vertical depth

References

API 1989. API bulletin. *Bulletin on formulas and calculations for casing, tubing, drill pipe and line pipe properties.* 5 ed. Washington: API.

BELLARBY, J. 2009. *Well Completion Design*, Amsterdam: Elsevier.

BOURGOYNE, A. T., JR., MILLHEIM, K. K., CHENEVERT, M. E. & YOUNG, F. S., JR. 1986. *Applied Drilling Engineering*, Richardson, TX, United States: Society of Petroleum Engineers.

BRECHAN, B. 2014. *NTNU Governing Documentation Casing Design*, Trondheim: NTNU.

BYROM, T. G. 2007. *Casing and Liners for Drilling and Completion*, Houston: Gulf Publishing Company.

ECONOMIDES, M. J., DUNN-NORMAN, S. & WATTERS, L. T. 1998. *Petroleum Well Construction*, Chichester: Wiley.

GOINS, W. C. 1980. 'Better understanding prevents tubular buckling problems'. *World Oil,* 190(2)**,** p. 101-105.

LAKE, L. W. & MITCHELL, R. F. 2006. *Petroleum Engineering Handbook, Volume 2: Drilling Engineering*, Richardson, TX, USA: Society of Petroleum Engineers.

LANDMARK 2001. *Wellcat Manual*, Houston, TX , USA: Landmark Graphics Corporation.

LANDMARK 2008. *StressCheck*, Houston, TX , USA: Landmark Graphics Corporation.

MITCHELL, R. F. 2006. 'Tubing Buckling- The State of the Art'. *SPE Annual Technial Conference and Exhibition.* San Antonio, Texas, USA: Society of Petroleum Engineers.

RABIA, H. 1987. *Fundamentals of Casing Design*, London: Graham & Trotman.

RAHMAN, S. S. & CHILINGAR, G. V. 1995. *Casing Design: Theory and Practice*, Amsterdam: Elsevier.

VEEKEN, C. A. M., WAHLEITNER, J. P. & KEEDY, C. R. 1994. 'Experimental modelling of casing deformation in a compacting reservoir'. *1994 Eurock SPE/ISRM Rock Mechanics in Petroleum Engineering Conference.* Delft, The Netherlands: Society of Petroleum Engineers, p.497-506.

AADNOY, B. S. 2006. *Mechanics of Drilling*, Aachen, Germany: Shaker Verlag.

AADNOY, B. S. 2010. *Modern Well Design*, Norway: Taylor & Francis.

AADNOY, B. S. & KAARSTAD, E. 2006. *Theory and Application of Buoyancy in Wells*.

Appendix A

This appendix shows the calculations and theory used in the thesis model related to casing strength, more detailed theory from chapter 2.1, and the rest of the load cases simulated in the models.

A.1 Casing Strength

The most significant load cases are investigated in relation to the burst, collapse, axial and triaxial strength of the casing.

A.1.1 Burst Strength

The maximum value of internal pressure required to cause the casing to yield is called burst strength (Rabia, 1987, p.41). The API burst rating, the minimum burst resistance of casing, is calculated by Barlow's formula:

$$p_{br} = 0.875 \frac{2\sigma_{yield} t}{d_n} \tag{25}$$

where,

p_{br} = burst strength [psi]

σ_{yield} = minimum yield strength [psi]

t = nominal thickness [in]

The factor 0.875 in eq.(25) is the wall thickness tolerance correction for API pipe (API, 1989). This factor makes sure that the pipe allows 12.5% variation in wall thickness due to manufacturing defects or casing wear (Rabia, 1987, p.42). The nominal thickness from eq.(25) is found by :

$$t = \frac{d_n - d_i}{2} \tag{26}$$

A.1.2 Collapse Strength

Collapse strength is defined as the maximum external pressure that is required to collapse the casing (Rabia, 1987, p.29). There are four different modes of collapse; yield-strength collapse, plastic collapse, transition collapse and elastic collapse. The slenderness ratio determines the type of collapse, and is defined as the ratio of the outer diameter to the wall thickness, d_n/t. In the following equations it is assumed that there is no internal pressure or axial stress (Bourgoyne et al., 1986, p.308).

The first step is to calculate the empirical coefficients in the following equations. The effective yield strength, $(\sigma_{yield})_e$, is equal to the minimum yield strength when the axial stress is zero, and is expressed as Y in this chapter to make the equations simpler.

$$F_1 = 2.8762 + 0.10679\times10^{-5}Y + 0.21301\times10^{-10}Y^2 - 0.53132\times10^{-16}Y^3 \tag{27}$$

$$F_2 = 0.026233 + 0.50609\times10^{-6}Y \tag{28}$$

$$F_3 = -465.93 + 0.030867Y - 0.10483\times10^{-7}Y^2 + 0.36989\times10^{-13}Y^3 \tag{29}$$

$$F_4 = \frac{46.95\times10^6(\frac{3F_2/F_1}{2+F_2/F_1})^3}{Y(\frac{3F_2/F_1}{2+F_2/F_1}-\frac{F_2}{F_1})(1-\frac{3F_2/F_1}{2+F_2/F_1})^2} \tag{30}$$

$$F_5 = F_4\frac{F_2}{F_1} \tag{31}$$

where,

$F_1, F_2, F_3, F_4, F_5 =$ empirical coefficients

$Y = (\sigma_{yield})_e =$ effective yield strength [psi]

The next step is to calculate the different slenderness ratios. Yield-strength collapse occurs only for the lower range of d_n/t values applicable for casings. The upper limit of yield-strength collapse is found by:

$$\frac{d_n}{t} = \frac{\sqrt{(F_1-2)^2 + 8(F_2+\frac{F_3}{Y})} + (F_1-2)}{2(F_2+\frac{F_3}{Y})} \tag{32}$$

Eq.(33) gives the lower limit of elastic collapse range:

$$\frac{d_n}{t} = \frac{2+F_2/F_1}{3F_2/F_1} \tag{33}$$

The upper limit of the plastic collapse range is also the lower limit of the transition collapse, and is given by:

$$\frac{d_n}{t} = \frac{Y(F_1 - F_4)}{F_3 + Y(F_2 - F_5)} \tag{34}$$

Now that all the empirical values and the different slenderness ratios are found, it is possible to calculate the collapse pressure rating. Comparing the correct slenderness ratio for the pipe to the ratios found from equations (32)-(34), the right collapse range is found and the right equation for collapse pressure rating can be used. The yield strength collapse rating is calculated with the following equation

$$P_{cr} = 2Y\frac{(d_n/t - 1)}{(d_n/t)^2} \tag{35}$$

where,

$P_{cr} =$ collapse pressure [psi]

Plastic collapse rating is given by:

$$P_{cr} = Y(\frac{F_1}{d_n/t} - F_2) - F_3 \tag{36}$$

The transition collapse region between the plastic and elastic collapse regions is found with the following equation:

$$P_{cr} = Y(\frac{F_4}{d_n/t} - F_5) \tag{37}$$

Which leaves only the elastic collapse rating, given by:

$$P_{cr} = \frac{46.95 \times 10^6}{(d_n/t)(d_n/t - 1)^2} \tag{38}$$

Yield Strength Collapse ↔ Plastic Collapse ↔ Transition Collapse ↔ Elastic Collapse

Figure A-1 The relationship between the different collapse types

A.1.3 Axial Strength

The axial tension limit rating for casing, or the pipe-body strength, is the minimum force expected to cause permanent deformation of the pipe (Bourgoyne et al., 1986, p.306). This pipe-body strength is used to determine the axial safety factor, and is given by:

$$F_{ten} = \frac{\pi}{4}\sigma_{yield}(d_n^2 - d_i^2) \tag{39}$$

where,

F_{ten} = tension force [lb]

A.1.4 Effects of Combined Stress

The equations given in chapter A.1.2 are valid only when both the internal pressure and axial stress is zero. However, axial tension or compression and bending stresses changes many of the casing performance properties (Bourgoyne et al., 1986, p.310). Thus the values for the performance properties must be corrected before they are used in casing design. If there is a significant axial stress, the following procedure is recommended by API for determining collapse pressure (API, 1989):

$$(\sigma_{yield})_e = \sigma_{yield}\left(\sqrt{1-\frac{3}{4}\left(\frac{\sigma_z}{\sigma_{yield}}\right)^2} - \frac{1}{2}\left(\frac{\sigma_z}{\sigma_{yield}}\right)\right) \tag{40}$$

where,

σ_z = axial stress [psi]

With this effective yield strength that takes into account the axial stress, the same approach as in chapter A.1.2 is used to find the corrected collapse pressure. If there is internal pressure present, the following equation is recommended by API to determine the equivalent external pressure (API, 1989)

$$p_e = p_o - \left(1-\frac{2}{d_n/t}\right)p_i \tag{41}$$

where,

p_e = equivalent external pressure [psi]

The equivalent external pressure along with the collapse pressure is used to find the collapse safety factor.

A.1.5 Triaxial Strength

The triaxial stress considers the combined effects of all the principal stresses in a general stress state; axial stress, radial stress and tangential stress, shown in Figure A-2. The triaxial stress is not a true stress; it is a theoretical value that compares a generalized three-dimensional stress state with a uniaxial failure criterion, the yield strength of the casing.

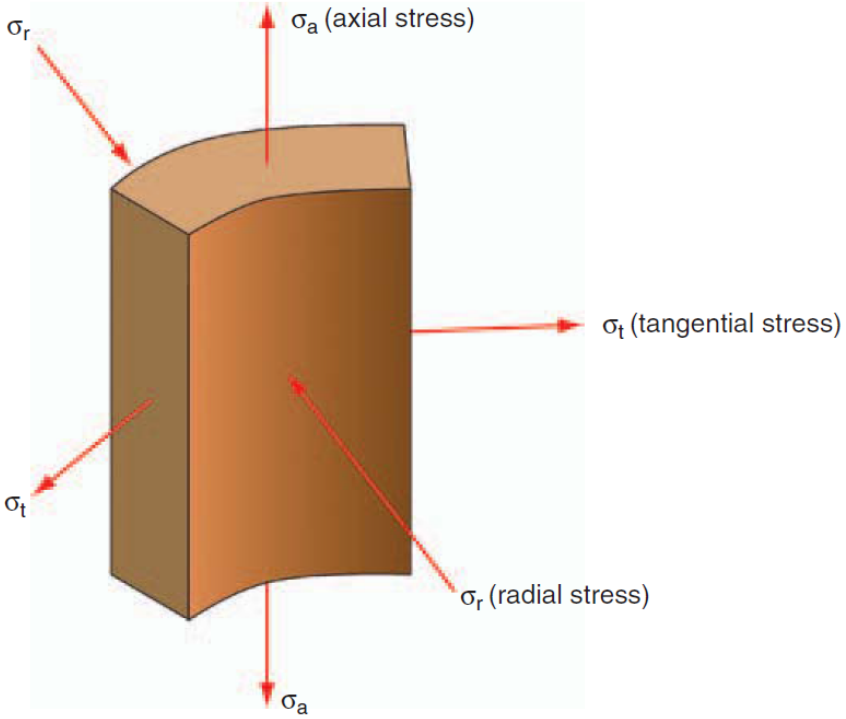

Figure A-2 Stress components of triaxial analysis (Bellarby, 2009, p.514)

The Huber-Hencky-Mises (abbreviated as Von Mises equivalent or VME) yield condition is the most widely used yield criterion. It is based on the maximum distortion energy theory. With the torque ignored, the yielding criterion becomes:

$$\sigma_{VME} = \frac{1}{\sqrt{2}}\sqrt{(\sigma_z - \sigma_t)^2 + (\sigma_t - \sigma_r)^2 + (\sigma_r - \sigma_z)^2} \tag{42}$$

where,

σ_{VME} = Huber-Hencky-Mises or triaxial stress [psi]

σ_t = tangential or hoop stress [psi]

σ_r = radial stress [psi]

When the VME stress exceeds the yield stress of the casing, yielding occurs. The axial stress is based on the air weight of casing, along with the stresses caused by bending, buckling, ballooning, thermal changes and buoyancy as explained in chapter 2.1. Classical elastic theory is used to determine the radial and tangential stress.

The radial stress can be expressed as (Bellarby, 2009, p.515):

$$\sigma_r = \frac{p_i A_i - p_o A_o}{A_o - A_i} - \frac{(p_i - p_o) A_i A_o}{(A_o - A_i) A} \tag{43}$$

At the inner wall, A is equal to A_i, which reduces the radial stress to:

$$\sigma_{r,i} = -p_i \tag{44}$$

Meanwhile at the outer wall A is equal to A_o, meaning that the radial stress is:

$$\sigma_{r,o} = -p_o \tag{45}$$

where,

$\sigma_{r,i}$ = radial stress at inner wall [psi]

$\sigma_{r,o}$ = radial stress at outer wall [psi]

The tangential stress is expressed as:

$$\sigma_t = \frac{p_i A_i - p_o A_o}{A_o - A_i} + \frac{(p_i - p_o) A_i A_o}{(A_o - A_i) A} \tag{46}$$

This expression is reduced to eq.(47) at the inner wall:

$$\sigma_{t,i} = \frac{p_i (A_i + A_o) - 2 p_o A_o}{A_o - A_i} \tag{47}$$

Whilst at the outer wall eq.(46) is reduced to:

$$\sigma_{t,o} = \frac{2 p_i A_i - p_o (A_i + A_o)}{A_o - A_i} \tag{48}$$

where,

$\sigma_{t,i}$ = tangential stress at inner wall [psi]

$\sigma_{t,o}$ = tangential stress at outer wall [psi]

The VME stress is highest at either the inside or the outside of the casing, and is calculated with the bending stresses in both compression and tension. This means that four calculations are needed to see which stress is the highest, as shown in Figure A-3. The highest of the four calculated stresses is then the peak VME stress, which is used to calculate the triaxial safety factor.

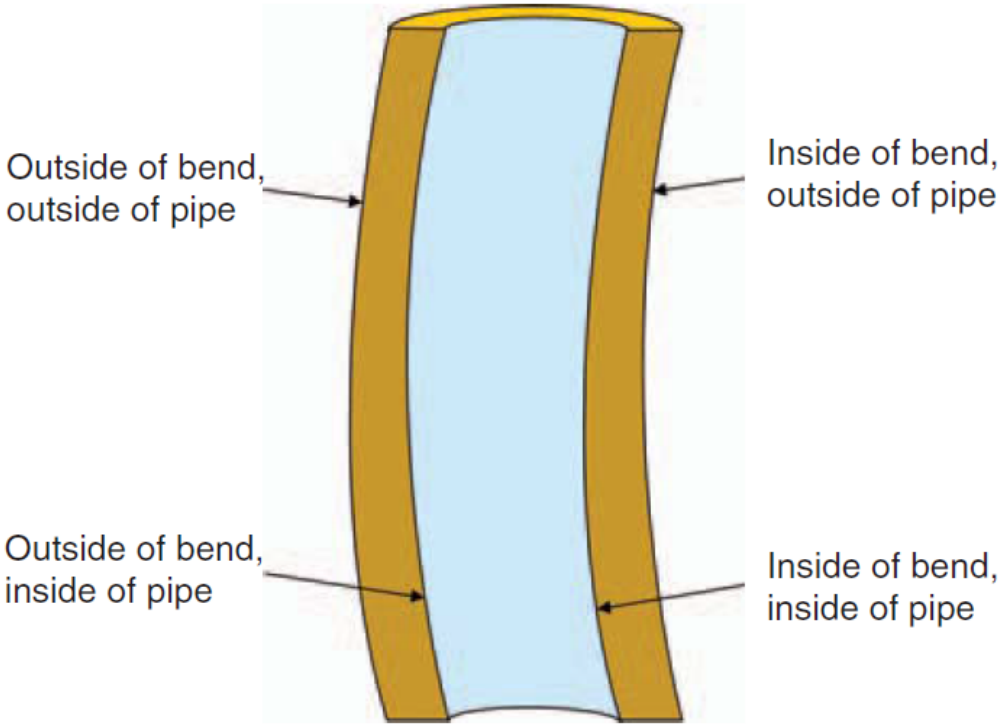

Figure A-3 Worst case stress locations (Bellarby, 2009, p.516)

The triaxial safety factor does not replace the burst, axial or collapse factor, but is a substitute. Collapse failure will often occur before the computed maximum triaxial stress reaches the yield strength, so triaxial stress should not be used as a collapse criterion (Landmark, 2001, p.709). However, in a thick-wall pipe yielding occurs before collapse.

A.1.6 Safety Factors and Design Factors

Safety factors (SF) are a method for comparing the rating of a pipe with the loads that the pipe can experience (Bellarby, 2009, p.520). When the safety factor is greater than 1, the rating is greater than the load. Safety factors are calculated for burst, axial, collapse and triaxial failures. The rating and load will be given as either stress or force, and the safety factor is calculated thus:

$$\mathrm{SF} = \frac{\text{rating}}{\text{load}} \tag{49}$$

The design factors (DF) are defined as the minimum allowable safety factors, and are always greater than 1 to account for the uncertainties concerning calculations, pipe behaviour, etc. Design factors vary from company to company, and from casing to connection to tubing. In this study the design factors used are shown in Table A-1 (Brechan, 2014, p.10).

Table A-1 Design factors

DF	Casing	
	Pipe	**Connection**
Burst	1,1	1,1
Tension	1,4	1,4
Compression	1,4	1,3
Collapse	1,1	N/A
Triaxial	1,25	N/A

A.2 Axial Loads

A.2.1 Derivation of the Weight of Casing

For a casing hanging free in a vertical well only fixed at the well head, the axial load is the weight of the casing (Bellarby, 2009, p.479). This means that there is no load at the bottom of the casing, and at the top the full weight of the casing is transferred to the well head. The casing weight is found by multiplying the weight per foot of the casing by the length of the casing.

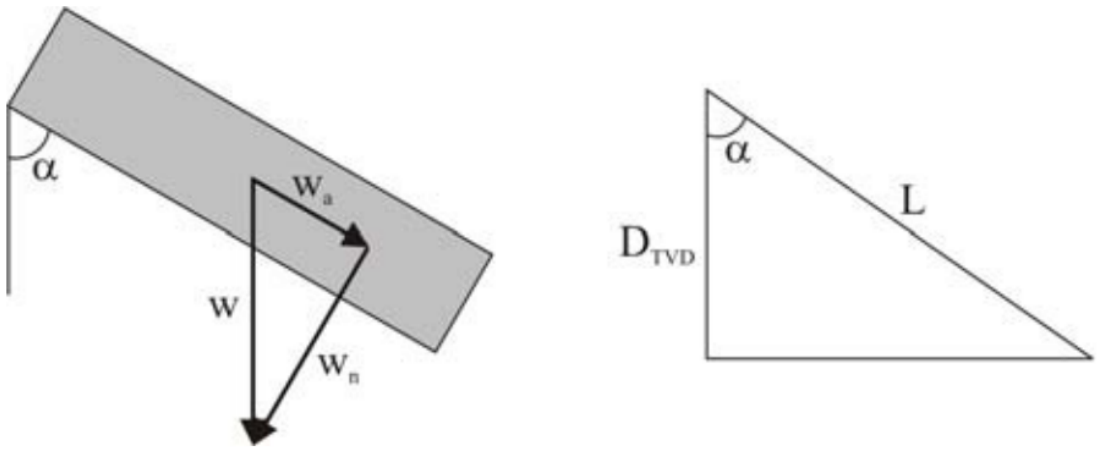

Figure A-4 Weight of pipe in inclined borehole (Aadnoy and Kaarstad, 2006, p.7)

Figure A-4 shows a casing resting on the low side in an inclined borehole (Aadnoy and Kaarstad, 2006, p.7). The weight of the casing is decomposed in an axial and a normal component as shown in the following equations:

$$F_w = wL \tag{50}$$

$$F_{ax} = F_w \cos\alpha = wL\cos\alpha \tag{51}$$

$$F_n = F_w \sin\alpha = wL\sin\alpha \tag{52}$$

where,

F_w = the weight of the casing [lb]

L = the length of the casing [ft]

F_{ax} = the axial component of the weight of the casing [lb]

F_n = the normal component of the weight of the casing [lb]

α = the inclination of the borehole [°]

From the geometry of the inclined pipe, the projected height becomes:

$$D_{TVD} = L\cos\alpha \tag{53}$$

By combining the former equations, an equation for the axial weight component can be found

$$F_{ax} = wD_{TVD} \tag{54}$$

This makes it easy to find the hook load in all wells, as this equation is valid for all well paths. It also means that deviated wells do not necessarily have higher axial stress than vertical wells to the same vertical depth.

A.2.2 Piston Forces and Buoyancy Effects

As mentioned in chapter 2.1.2, there are two "schools of thought" when it comes to calculating the buoyancy effects; the Archimedes principle and the piston-force approach. The buoyancy is often thought of as a force making a submerged object float. This is in part correct, however the way the buoyancy force is applied is often wrong (Goins, 1980, p.1). Goins (1980) performed an experiment to find out whether buoyancy is caused by the displaced fluid; or by the pressure exposed to a projected area.

As shown in Figure A-5, a beaker is fitted at the bottom with a rubber pad. A hollow steel cylinder is then bevelled on each end; internal on one end and external on the other. In "A" the cylinder is held in place with the external bevel down while the annulus is filled with mercury. This mercury applies a hydrostatic pressure to the end of the cylinder forcing the cylinder to rise and float when the cylinder is released. In "B" however, the cylinder is held in place with the internal bevel down while the annulus is filled with mercury. In this case the fluid pressure has no end area to act on, and therefore there is no axial force. This means that in "B" there is fluid displaced by air and steel, but no buoyancy. Hence Goins (1980)

demonstrated that the common concept that buoyancy is equal to the weight of fluid displaced is true only sometimes. For buoyancy forces to exist, there needs to be an exposed end or cross-sectional area to which hydrostatic pressure can be applied vertically.

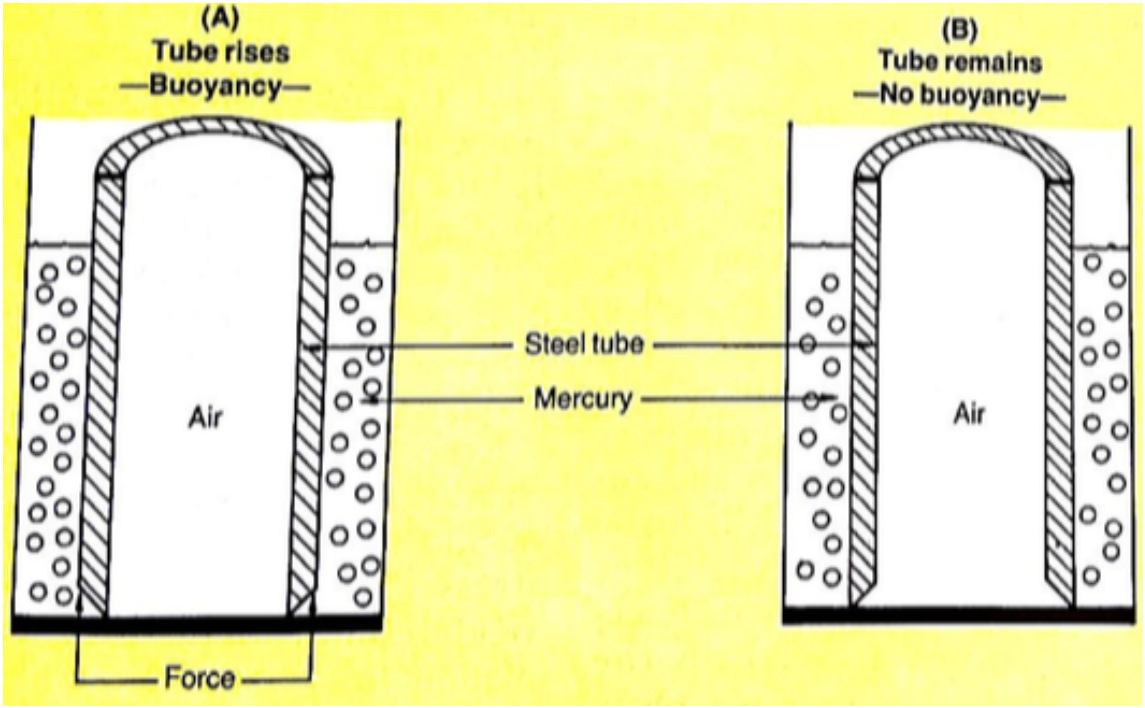

Figure A-5 Goins' experiment to show the effect of buoyancy (Goins, 1980, p.1)

A.2.2.1 The Principle of Archimedes

This principle is often used to explain why boats float, and is very simple. The simplest way to explain it is according to Aadnoy (2006, p.38) "when a body is submerged into a fluid, the buoyancy force equals the weight of the displaced fluid".

The effective or buoyed weight of a casing is obtained by multiplying the weight in air by the buoyancy factor:

$$\beta = \frac{\rho_p - \rho_m}{\rho_p} = 1 - \frac{\rho_m}{\rho_p} \tag{55}$$

where,

β= buoyancy factor

ρ_m= density of mud [ppg]

ρ_p= density of pipe [ppg]

Eq.(55) is only valid when the density of the fluid inside and outside the casing is the same. When there are different densities on the inside and the outside, the following equation is used (Aadnoy and Kaarstad, 2006, p.2):

$$\beta = 1 - \frac{\rho_o d_n^2 - \rho_i d_i^2}{\rho_p (d_n^2 - d_i^2)} \tag{56}$$

where,

ρ_0 = fluid density outside pipe [ppg]

ρ_i = fluid density inside pipe [ppg]

At the bottom the effective weight is zero. At the top of the casing the effective weight is:

$$F_{a,arch} = F_{air}\beta = w(D_{TVD} - D)(1 - \frac{\rho_o d_n^2 - \rho_i d_i^2}{\rho_p (d_n^2 - d_i^2)}) \tag{57}$$

where,

$F_{a,arch}$ = the axial force found by the principle of Archimedes [lb]

A.2.2.2 Piston Force

The piston-force approach is the calculation of the pressure exposed to a projected area. At the bottom of the casing the hydrostatic force is given by (Aadnoy, 2006, p.44):

$$F_{hydrostatic} = p_{i,b}A_i - p_{o,b}A_o \tag{58}$$

The axial force is then the hydrostatic force at bottom plus the air weight of the casing. This gives that the axial force at the top of casing is (Aadnoy, 2006, p.44):

$$F_a = F_{hydrostatic} + F_{air} = p_{i,b}A_i - p_{o,b}A_o + w(D_{TVD} - D) \tag{59}$$

This equation can be rewritten as:

$$F_a = 0.433(\rho_i D_{TVD} A_i - \rho_o D_{TVD} A_o + \rho_p (D_{TVD} - D)(A_o - A_i)) \tag{60}$$

where,

0.433 = a conversion factor $[\frac{\text{gal}}{\text{ft} \cdot \text{in}^2}]$

For surface load calculations, the piston force approach yields the same results as the Archimedes principle. However, for the rest of the casing the two methods give different results. The piston forces give the correct external loading on the string (Aadnoy, 2006, p.40), but should not be used in failure calculations as it neglects the three-dimensional state.

A.2.2.3 Deviatoric Forces

The loading in three dimensions can be calculated as follows:

$$\text{Total load} = \text{Hydrostatic load} + \text{Deviatoric load}$$

The deviatoric forces govern failure, and vary depending on the fluid densities inside and outside the pipe. The average hydrostatic force is (Aadnoy, 2006, p.42):

$$F_{hyd,av} = p_o A_o - p_i A_i \tag{61}$$

where,

$F_{hyd,av}$ = the average hydrostatic force [lb]

The deviatoric force at the bottom of the casing is then the total load given by the piston force approach subtracted the average hydrostatic force:

$$F_{dev} = F_{hydrostatic} - F_{hyd,av} = p_{i,b} A_i - p_{o,b} A_o + p_{o,b} A_o - p_{i,b} A_i = 0 \tag{62}$$

where,

F_{dev} = deviatoric force [lb]

The deviatoric force at the bottom of the casing is zero, the same as the Archimedes principle gives at this point.

At the top of the casing, combining eq.(60) and eq.(61) gives the deviatoric force:

$$F_{dev} = 0.433(\rho_i D_{TVD} A_i - \rho_o D_{TVD} A_o + \rho_p (D_{TVD} - D)(A_o - A_i) + (\rho_o A_o - \rho_i A_i) D) \tag{63}$$

Rewriting eq.(63):

$$F_{dev} = 0.433(\rho_p (D_{TVD} - D)(A_o - A_i) - (\rho_o A_o - \rho_i A_i)(D_{TVD} - D)) \tag{64}$$

As for the deviatoric force at the bottom of the casing, the deviatoric force at the top of the casing is the same as the principle of Archimedes yields. To show this, eq.(57) can be rewritten as:

$$F_{a,arch} = 0.433 \rho_p (D_{TVD} - D)(A_o - A_i)\left(1 - \frac{\rho_o A_o - \rho_i A_i}{\rho_p (A_o - A_i)}\right) \tag{65}$$

Solving this equation gives:

$$F_{dev} = 0.433(\rho_p (D_{TVD} - D)(A_o - A_i) - (\rho_o A_o - \rho_i A_i)(D_{TVD} - D)) \tag{66}$$

Which is the same result as the deviatoric force gives.

A.3 Load Cases

A.3.1 Pressure Test

Pressure testing of the casing is run after the casing is run and cemented, but before the float equipment is drilled out. This pressure is the highest burst pressure the well will experience, as it is based on the most significant burst load that may happen. A kick margin is added to the highest burst pressure from these loads; 15bar for casings and liners with a nominal OD of 16 ¾" and larger, and 35bar for casings and liners with a smaller nominal OD (Brechan, 2014, p.11). The pressure test is sometimes taken with 60% of the burst rating of the weakest grade of string in the casing (Rabia, 1987, p.81).

The internal pressure is based on the mud density and applied pressure at wellhead as shown in Figure A-6, and is found by (Economides et al., 1998, p.193):

$$p(z) = p_{surface} + \gamma_m z \tag{67}$$

where,

$p_{surface}$ = test pressure at surface [psi]

γ_m = mud gradient [psi/ft]

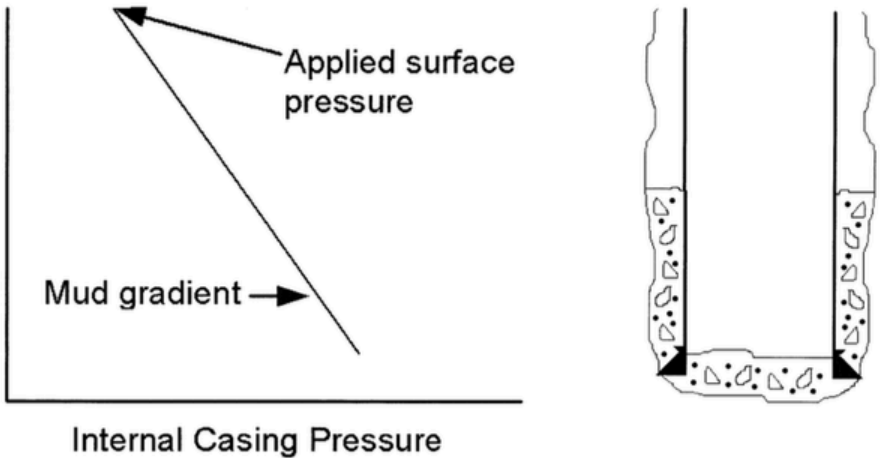

Figure A-6 Internal pressure during a pressure test (Landmark, 2008, p.35)

As the fluid used to pressure test is often the same as the fluid used when setting the casing, the differential pressure is usually a straight line down to TOC. The external pressure below TOC is the pore pressure since this gives the worst case. If the pore pressure is very low, and the pressure test very high, the differential pressure below TOC may become substantial, and the casing not strong enough. When the cement job is perfect, it seems likely that the cement will offer a physical support to the casing. However, it is normally not acceptable to assume

that, as there may be intervals where the cement is poor even though the cement job is perfect (Byrom, 2007, p.107).

A.3.2 Lost Returns with Mud Drop

When the mud hydrostatic column equilibrates with the pore pressure in a lost-circulation zone, the mud level drops, thus causing lost returns. When calculating the mud drop, the heaviest mud weight that will be used when drilling the next section, along with the depth where the pore pressure is at its lowest is usually used to find the greatest mud drop. To find the worst-case scenario, the cement job is assumed to be poor. Hence the external pressure is based entirely on the mud weight in which the casing was placed (Byrom, 2007, p.106).

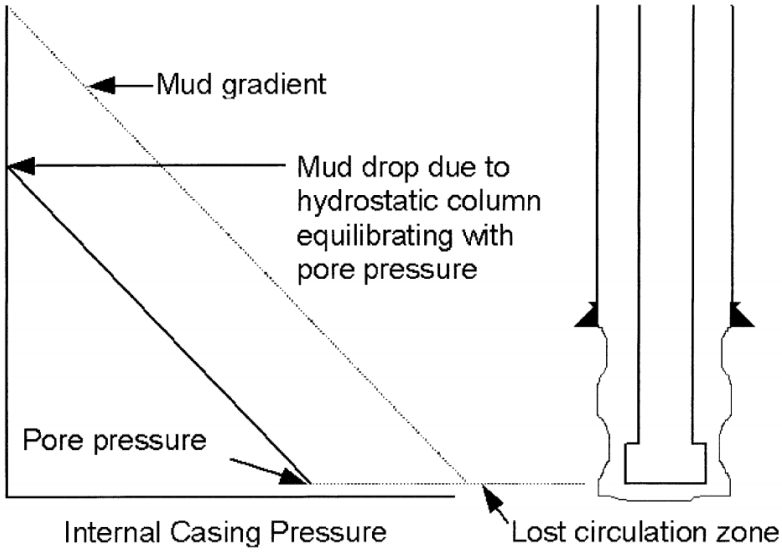

Figure A-7 Internal pressure during the load lost returns with mud drop (Landmark, 2008, p.39)

The following equations are used to find the mud drop level (Economides et al., 1998, p.193):

$$p(z) = 0 \qquad z < z_{md} \tag{68}$$

$$p(z) = p_f + \gamma_m (z - z_{lc}) \qquad z_{md} < z < z_{lc} \tag{69}$$

$$z_{md} = z_{lc} - \frac{p_f}{\gamma_m} \tag{70}$$

where,

z_{md} = mud drop depth [ft]

z_{lc} = lost-circulation zone depth [ft]

p_f = pore pressure [psi] at z_{lc}

When the pore pressure is unknown, the hydrostatic saltwater pressure may be used as a lower limit for the mud loss pressure, since pore pressures lower than this is seldom seen (Aadnoy, 2010, p.136). This means that if the pore pressure is unknown and mud loss occurs, the annulus level will stabilize when the bottomhole pressure is equal to the weight of a saltwater column to that depth. Eq.(70) is then altered to

$$z_{md} = z_{lc}(1 - \frac{\gamma_{sw}}{\gamma_m}) \tag{71}$$

where,

γ_{sw} = saltwater gradient [psi/ft]

Another option if the lithology and pore pressure is not well-known is to use the depth of the next casing seat as a conservative estimate for the lost-circulation zone depth (Bourgoyne et al., 1986, p.333).

A mud drop of more than 5,000ft caused by lost circulation during drilling is rarely experienced (Economides et al., 1998, p.193). Some operate with a mud drop level reduced to 250m (~820ft) if the field and formation is well known and there is experience from neighbour wells with insignificant lost circulation situations, or if low loss-zone permeability and refill capability can be documented (Brechan, 2014, p.23). Hence the mud drop may in some cases be smaller than calculated.

Appendix B

This appendix shows the results from the thesis model in detail, for the different load cases simulated in the different casings.

B.1 Initial Conditions

Initial conditions for casing are undisturbed temperatures and pressure right after the casing is landed and cemented. The axial load under initial conditions are defined as the air weight, or dry weight, of the casing along with the piston force working on the casing shoe. This means that in the initial conditions of all the casings, the axial load is given by eq.(59). As the surface casing is quite short, the temperature of the casing does not increase that much. The yield strength is derated only for temperatures over 68°F, so for the surface casing this is not a big issue as the temperature reaches 68°F around 2,300ft and the bottom of the casing is at 2,625ft. This means that the surface casing is affected by the temperature deration only towards the end, and not by much. Therefore, the difference in the safety factors due to temperature derated yield strength is shown for the intermediate casing where the difference is more significant.

B.1.1 Surface Casing

B.1.1.1 Differential Pressure

The differential pressure is the difference between the internal and external pressure, and is used to compare the pressures of the two different models. If the models differ when comparing the axial load or the safety factors, a difference in the differential pressure may be the answer as the pressures are used when calculating the rest.

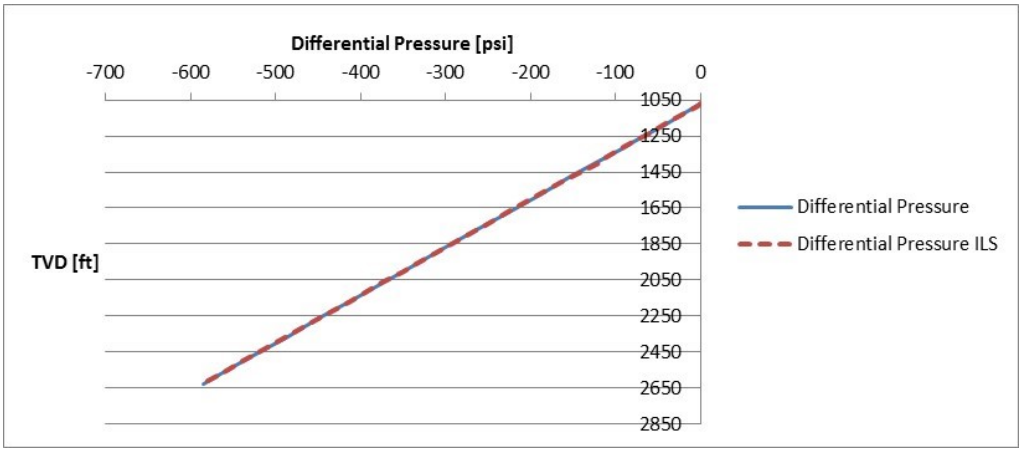

Figure B-1 Initial conditions surface casing differential pressure

B.1.1.2 Axial Load

As mentioned above, the axial load is calculated from eq.(59). The dogleg severity (DLS) is given to be zero in the surface casing by the well path, however the ILS operates with DLS override since variations in inclination or azimuth occur nearly continuous even though the hole section is designed to be straight. Therefore both the ILS and the thesis model calculate with the highest DLS from the well path and DLS override, which is why there are bending stresses in this section. As shown in Figure B-2, the thesis model and output from the ILS matches perfectly. The bending stresses are a result of the DLS override. As the axial load for the initial condition only depends on the weight of the casing, and the pressures at the bottom of the casing, the axial load is expected to be most significant at the top as this is where the weight is the most. The following figure shows that this is the case.

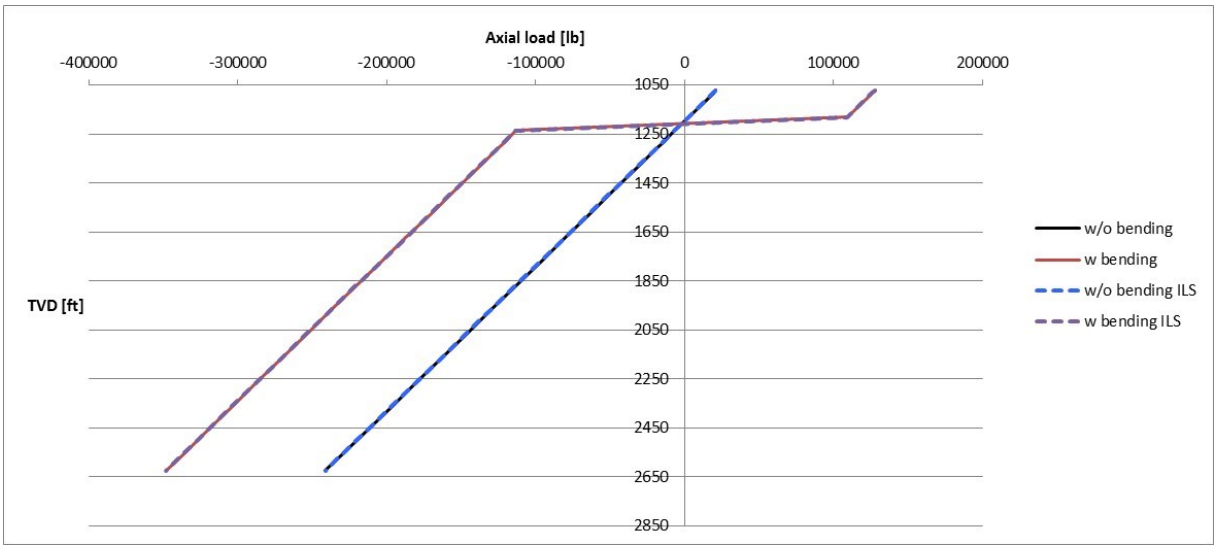

Figure B-2 Initial conditions surface casing axial load

B.1.1.3 Axial Safety Factor

The axial safety factor is found by dividing the tension force found with eq.(39) with the absolute value of the axial load (with bending) throughout the whole section. As the axial load with bending decreases, the axial SF increases. At around 1,180ft, the axial load with bending turns negative. However, the SF is found by the absolute value, and so as the axial load decreases on the negative side, the SF starts decreasing. The safety factor from the thesis model is compared with the one given by the ILS, and as Figure B-3 shows they are the same. The safety factors are also well above the design factor, which means that the chosen casing is strong enough for the initial conditions.

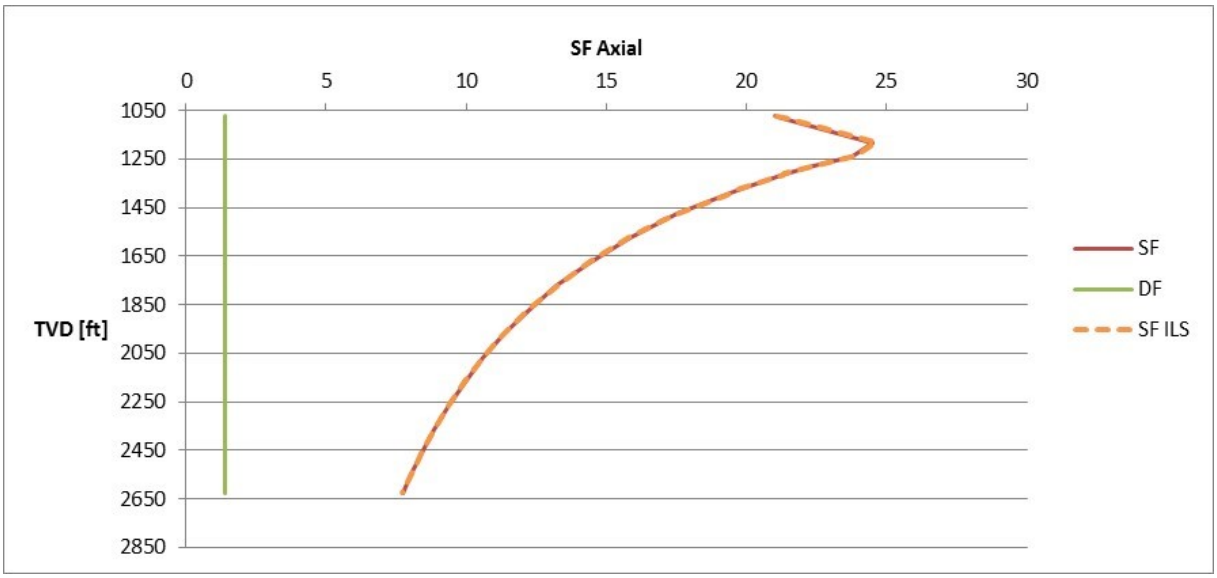

Figure B-3 Initial conditions surface casing axial SF

B.1.1.4 Collapse Safety Factor

Chapter A.1.2 along with chapter A.1.4 give the steps to calculate the collapse pressure. The collapse safety factor is given by the calculated collapse pressure divided by the equivalent external pressure at that point of the section. As shown in Figure B-4 the safety factor of the thesis model is equal to the output from the ILS. The SF is also above the DF, so the chosen casing is strong enough in comparison to the collapse pressure as well as in comparison to the initial condition.The temperature derated yield strength is used to find the effective yield strength, however this does not matter much in the surface casing as the temperature is not high.

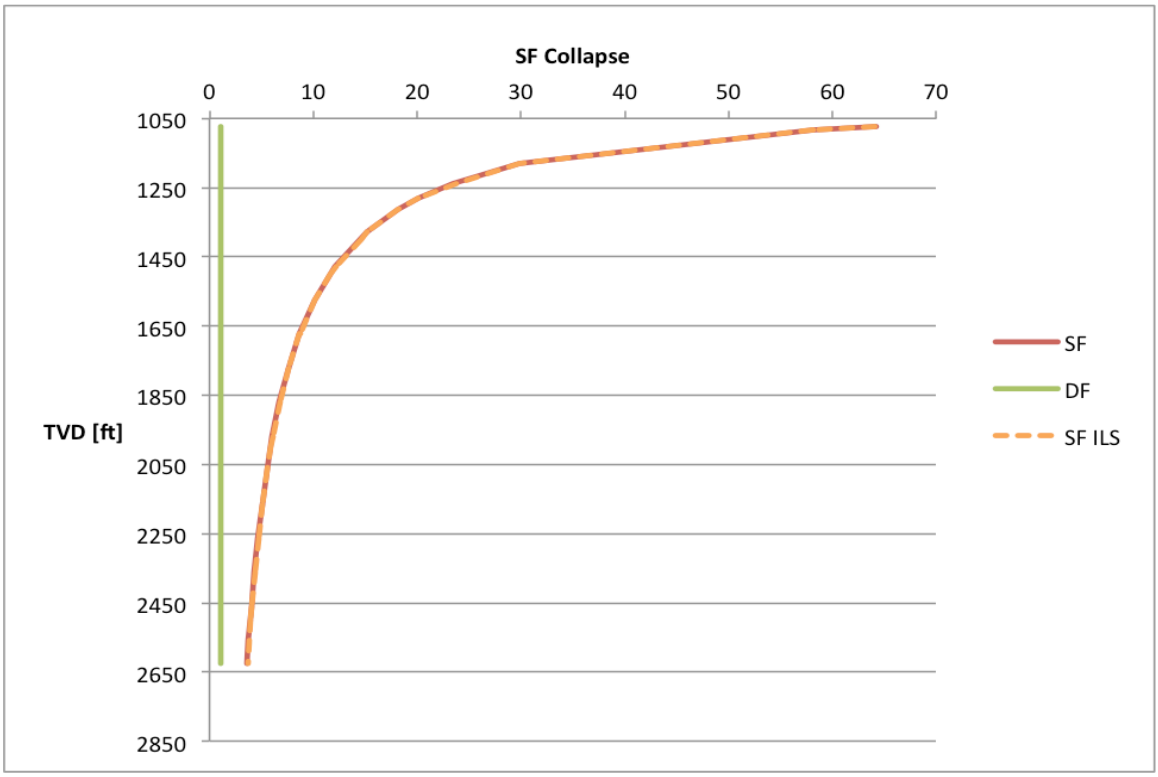

Figure B-4 Initial conditions surface casing collapse SF

B.1.1.5 Triaxial Safety Factor

As stated in chapter A.1.5, the VME stress is calculated in four different ways. The minimum yield strength of the casing divided by the highest of the calculated VME stresses is used to find the triaxial safety factor throughout the section. Figure B-5 shows the triaxial safety factor as calculated by the thesis model and the ILS. There is a slight difference, but both give a SF well above the DF. The reason for this difference us unknown, as both the models seemingly use the same equations. However, not all the equations and assumptions used in the ILS are known.

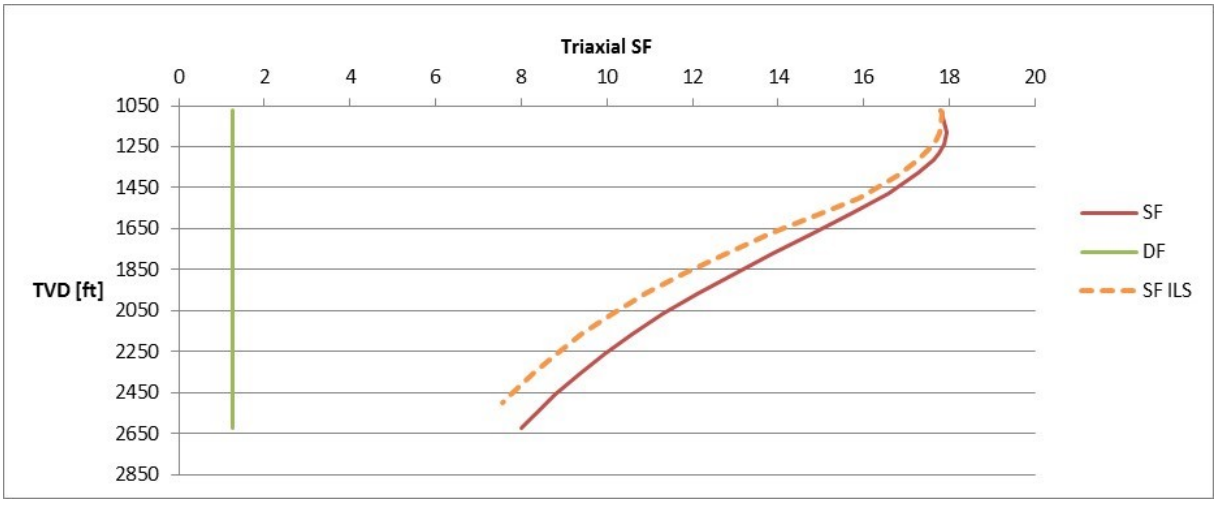

Figure B-5 Initial conditions surface casing triaxial SF

B.1.2 Intermediate Casing

B.1.2.1 Differential Pressure

The differential pressure is zero all the way down to TOC, as the fluid behind the casing is the same as the fluid inside the casing. Below TOC there is cement, with a much higher density. This gives a much higher external pressure than internal as seen by the differential pressure in Figure B-6. As evident in this figure, the thesis model and the ILS correspond neatly. The cement density used in both models is 1.9sg. It seems a bit unlikely that the initial conditions will have such a significant cement density, as the cement changes when it hardens. However, the thesis model use the same as the ILS to be able to compare the models, even though this may be a weakness with the ILS model.

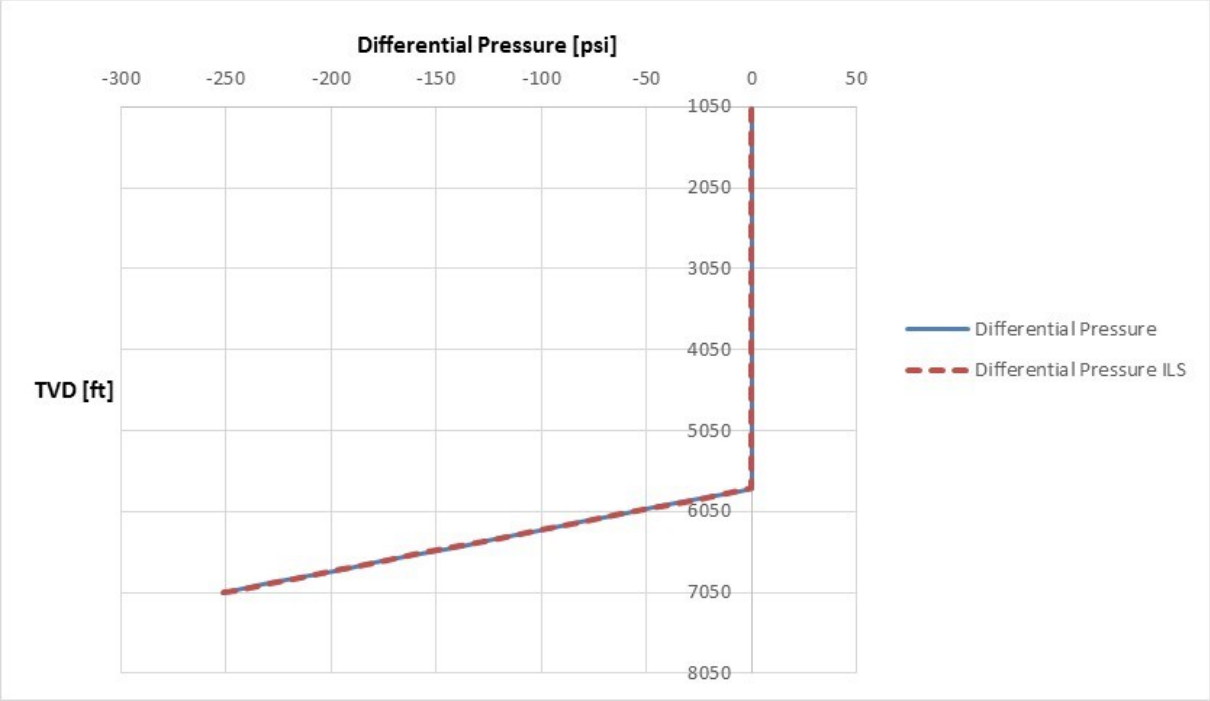

Figure B-6 Initial conditions intermediate casing differential pressure

B.1.2.2 Axial Load

The axial load for the intermediate casing is calculated the same way as in the surface casing. As for the surface casing, the output from the thesis model overlaps the output from the ILS as seen in Figure B-7. From the graph, it is clear that the bending stress increases around 2,650ft; this is due to an increase in the DLS from 0.5-1.5 °/100ft. The casing changes from tension to compression around 5,400ft.

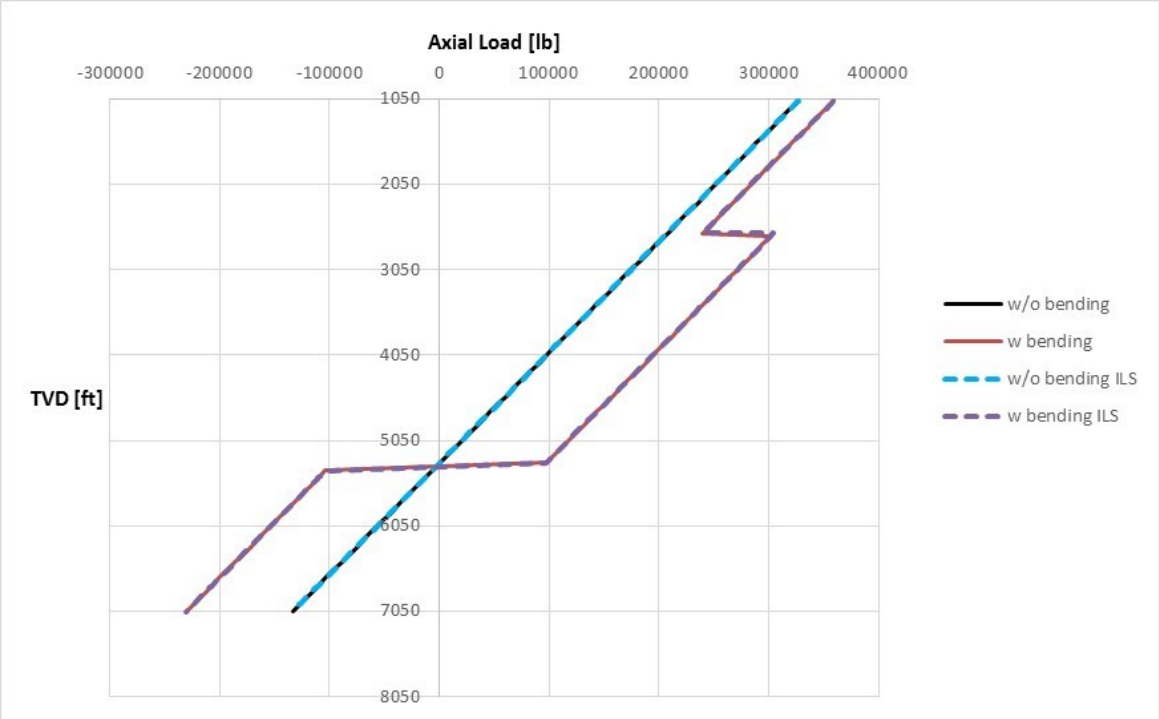

Figure B-7 Initial conditions intermediate casing axial load

B.1.2.3 Axial Safety Factor

The axial SF is found the same way as described for the surface casing. Figure B-8 indicates that the thesis model and the ILS agree on how to calculate the axial SF. The SF is well above the DF, indicating that the casing is well able to hold in the initial conditions. As seen from the graph, the sudden negative change in the SF around 2,650ft corresponds with the increase in the bending stress in Figure B-7. From this point the SF steadily increases as the axial load with bending decreases, until the axial load turns negative and so the SF decreases.

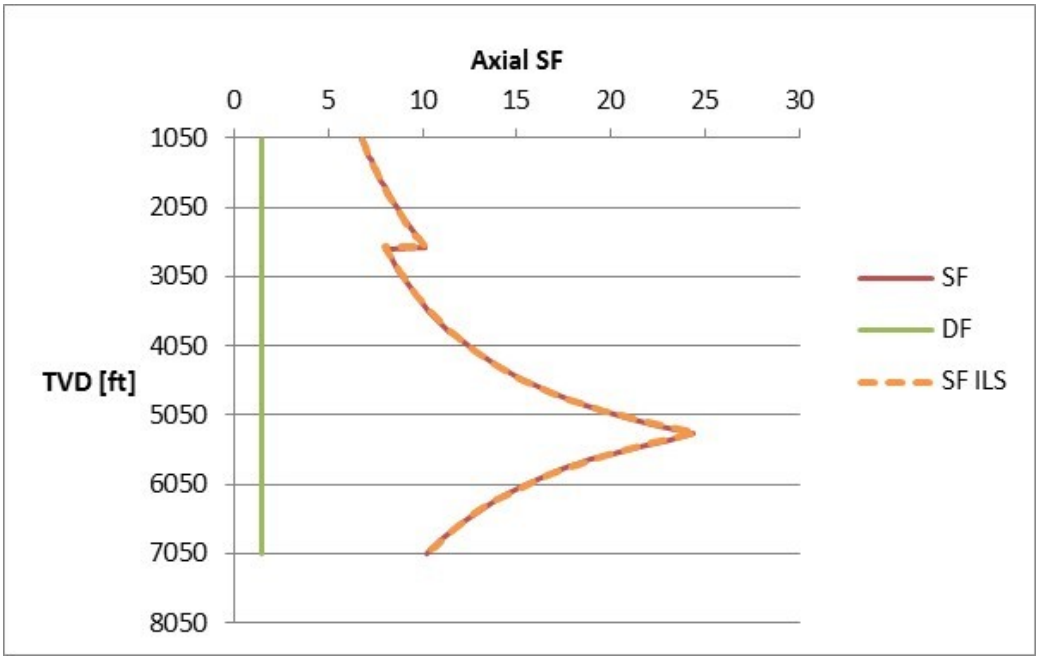

Figure B-8 Initial conditions intermediate casing axial SF

B.1.2.4 Collapse Safety Factor

The SF for collapse from the thesis model matches the SF from the ILS perfectly. The sudden kink seen around 5,795ft in Figure B-9 is due to changes in the external pressure due to the cement, as this is the TOC. However, the SF is still above the DF by a good margin.

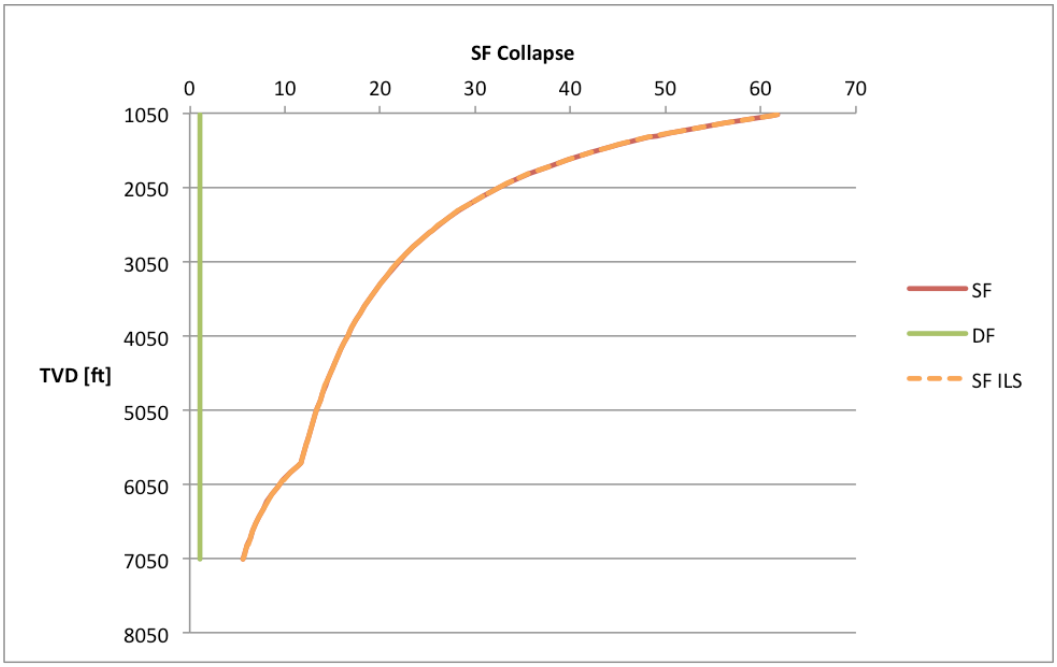

Figure B-9 Initial conditions intermediate casing collapse SF

B.1.2.5 Triaxial Safety Factor

The output from the thesis model for the triaxial SF is very close to the output from the ILS. All the way down to the TOC, the models are the same, but differ somewhat below. The reason for this discrepancy is unknown. Figure B-10 shows that the SF is well above the DF.

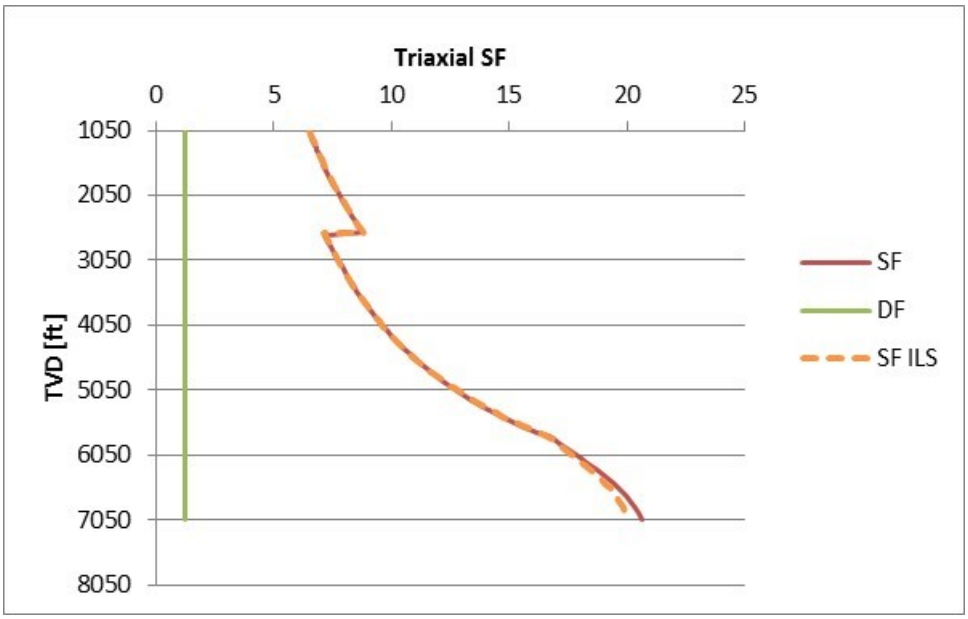

Figure B-10 Initial conditions intermediate casing triaxial SF

B.1.3 Production Casing

B.1.3.1 Differential Pressure

The differential pressure is zero down to TOC, 12,150ft, as evident in Figure B-11. The differential pressure from the thesis model is equal to the differential pressure from the ILS. Below the TOC the external pressure is based on the cement weight, which is why the differential pressure has such a steep drop as the cement weight is a lot higher than the mud weight.

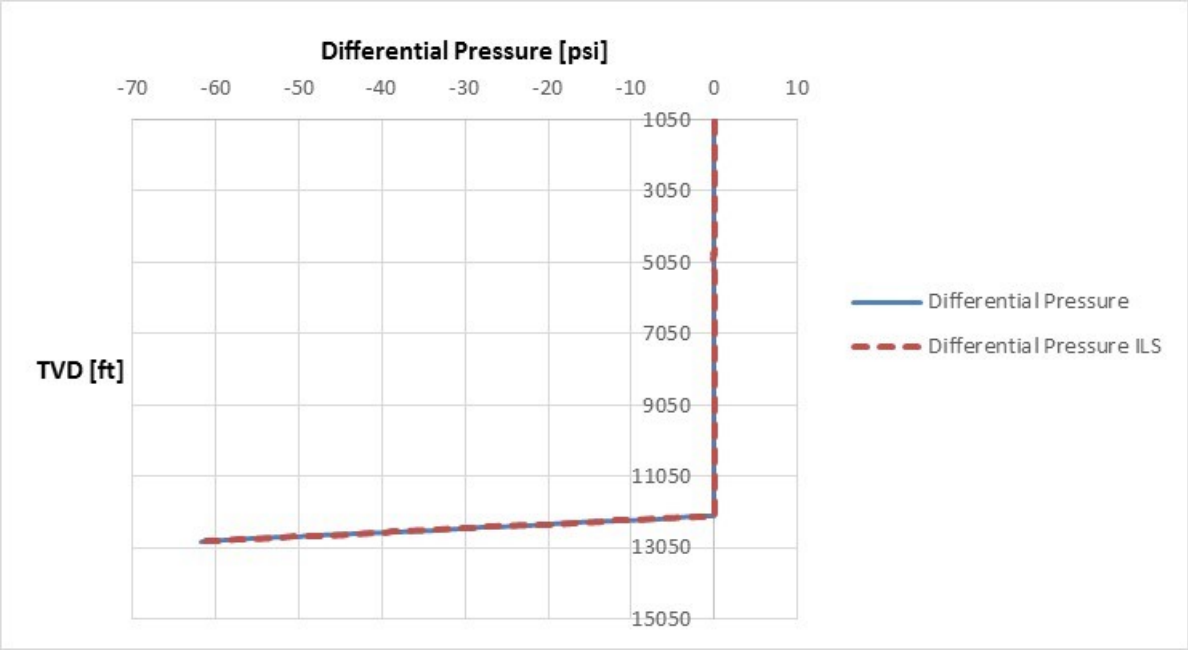

Figure B-11 Initial conditions production casing differential pressure

B.1.3.2 Axial Load

The axial load displayed in Figure B-12 is more complicated than for the surface or intermediate casing, but the thesis model follows the output from the ILS closely. The DLS goes from 0.5-1.5 °/100ft at about 2,650ft, and stays at 1.5°/100ft until 8,700ft. From this point to the bottom of the casing the DLS changes frequently, which is the reason for the many kinks in the graph for the bending stress. The casing string is in tension until around 10,000ft, from where it is in compression.

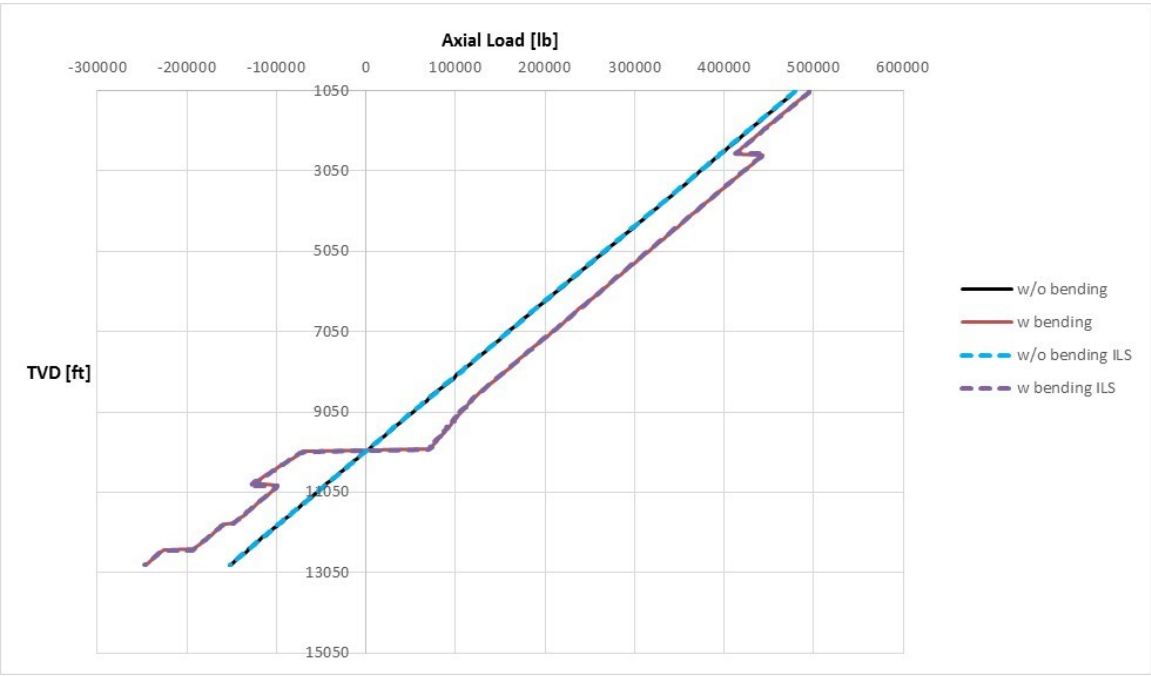

Figure B-12 Initial conditions production casing axial load

B.1.3.3 Axial Safety Factor

As the axial load, the axial SF is more complex than for the other casings. However, the output from the different models agrees, and the SF is well above the DF as seen in Figure B-13.

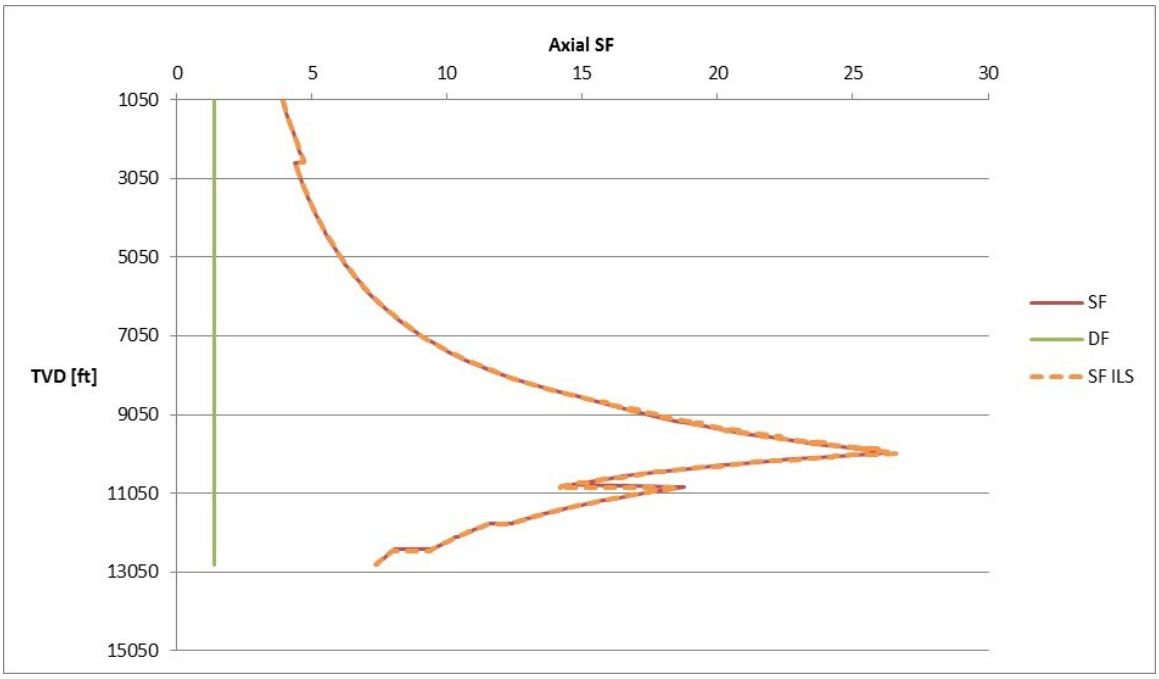

Figure B-13 Initial conditions production casing axial SF

B.1.3.4 Collapse Safety Factor

The collapse SF for both the models are equal, as shown in the following figure. They are also well above the DF, as the lowest SF is 6.9.

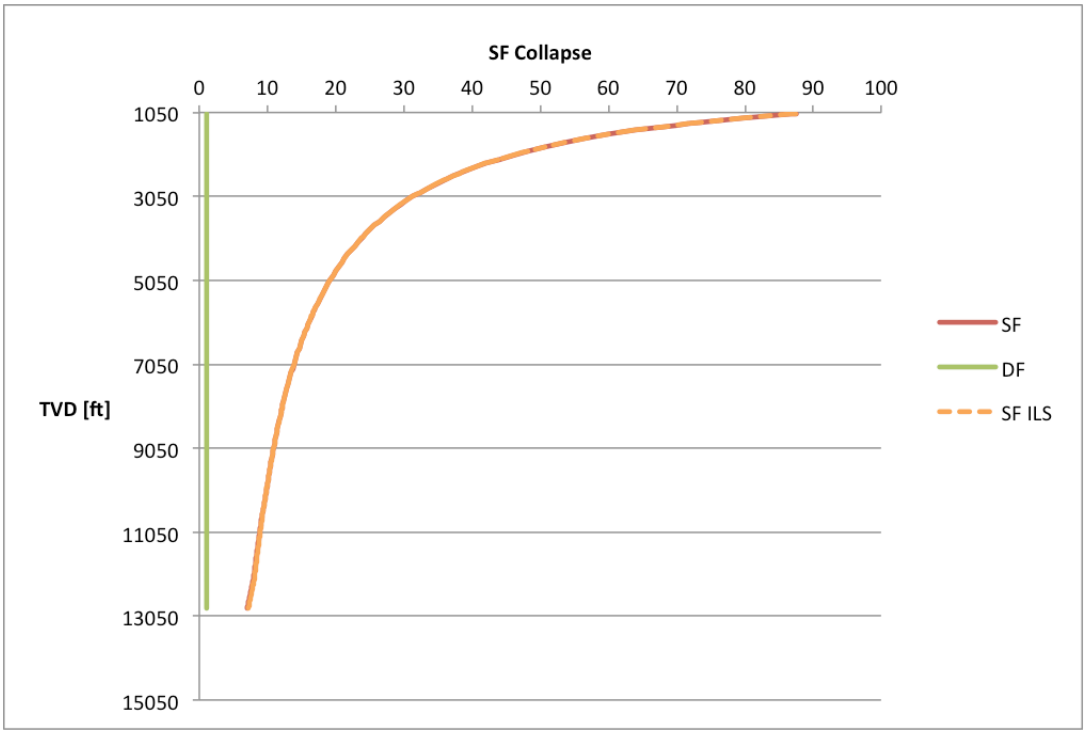

Figure B-14 Initial conditions production casing collapse SF

B.1.3.5 Triaxial Safety Factor

Figure B-15 shows that the two models match perfectly for the production casing, unlike the triaxial SF for surface and intermediate casing. The reason why the triaxial SF matches the ILS in this case and not the others is unknown, as the method for calculating the triaxial SF is the same in all cases. The SF is well above the DF in this case as well, with the lowest SF at the top of the casing where the axial load is the greatest.

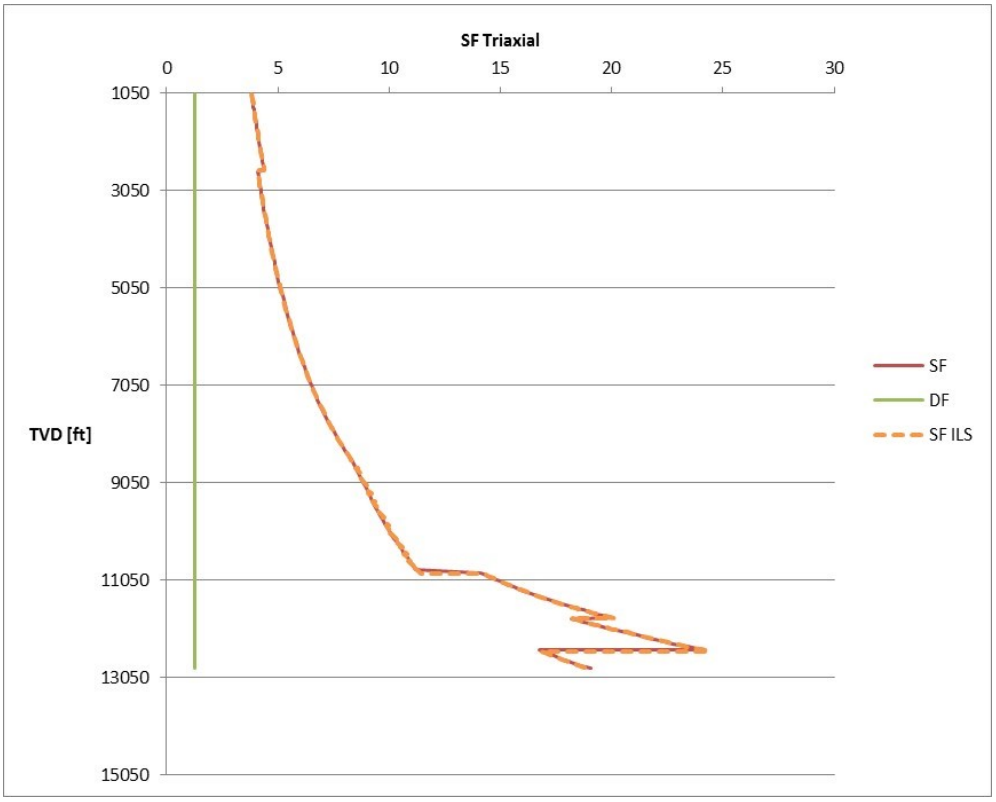

Figure B-15 Initial conditions production casing triaxial SF

B.2 Pressure Test

The pressure test is a burst load, meaning that the internal pressure will be much larger than the external. To find the worst-case scenario, the external pressure below TOC is set to the pore pressure, indicating that the pressure in the cement has equilibrated with the pore pressure in the formation. The external pressure above the TOC may be based on deteriorated mud, however as it is very unlikely that the mud is deteriorated already during the pressure test, the mud used in this load for both the ILS and the thesis model is not deteriorated. The internal pressure is based on the mud used to drill the section in addition to the added surface pressure. This means that the fluid behind the casing over TOC is the same as the fluid used to pressure test. The surface pressure is based on the most significant burst pressure the well will experience.

B.2.1 Surface Casing

B.2.1.1 Differential Pressure

The surface casing is cemented all the way to the top, which is why the external pressure is based on the pore pressure behind the whole section. This is the reason for the spike at the top of the casing seen in Figure B-16, as the pore pressure here is much lower than in the rest of the section. The pore pressure below this spike stays at the same "weight" as the mud inside

the casing, hence the only difference between the internal and external pressure, the differential pressure, is the surface pressure applied internally. There is a small difference in the differential pressure of the two models around the spike, which may be becomes the pore pressure used in the models differ. However, the difference is not large, and does not affect the outcome much.

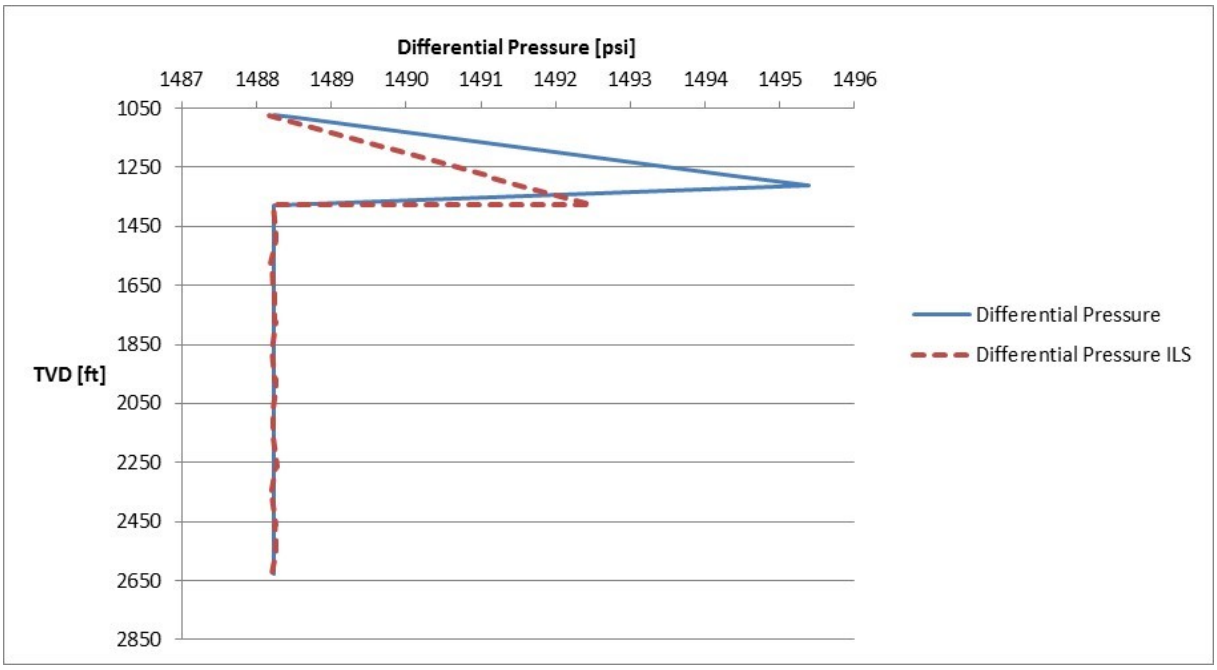

Figure B-16 Pressure test surface casing differential pressure

B.2.1.2 Axial Load

For the initial conditions, the axial load was based only on the air weight of the casing and the piston forces working on the casing shoe. During the pressure test however, the axial load is based on the axial load from the initial condition in addition to ballooning, temperature effects and buckling effects due to changes in pressure and temperature.

The ILS calculates the ballooning force two different ways depending on whether the section is cemented or not. In the uncemented section, the ballooning force is calculated with the average pressures of the whole section, while below TOC the ballooning force is calculated at each new depth for the pressures at this depth. In the surface casing the whole section is cemented, so a new ballooning force is calculated at each depth. The way the ballooning force is calculated affects the axial load, and thereby the axial SF as well.

After a section is cemented, it is assumed that the axial load will not change in this section as it is fixed and will not move. Buckling is therefore calculated with the initial axial load in the

cemented areas, which in the case of the surface casing covers the entire casing. There is no buckling in the initial condition, so there is no buckling during the pressure test. Figure B-17 shows the axial load included ballooning and thermal changes, which is a lot higher than the initial axial load. It is apparent from this figure how much the pressure and temperature affects the axial load. In this load the entire casing is in tension.

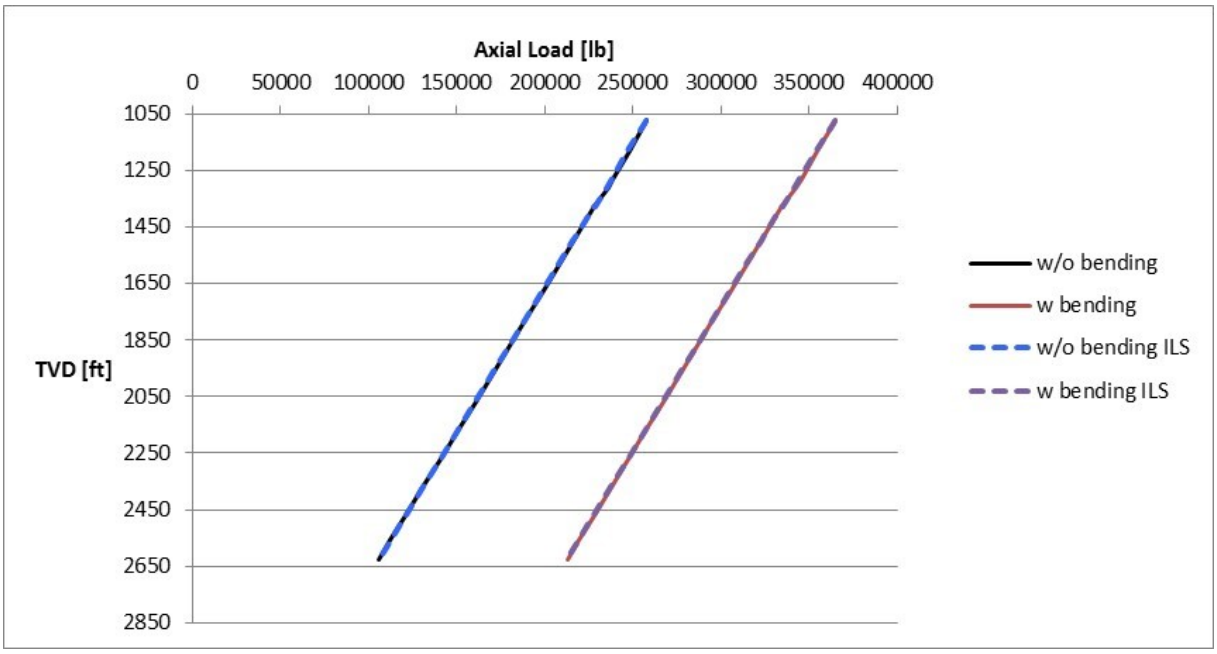

Figure B-17 Pressure test surface casing axial load

B.2.1.3 Axial Safety Factor

The pressure test has the highest pressure the well is estimated to experience during its lifetime, and so the axial load is high as seen in the previous figure. Still the axial SF is well above the DF as displayed in Figure B-18.

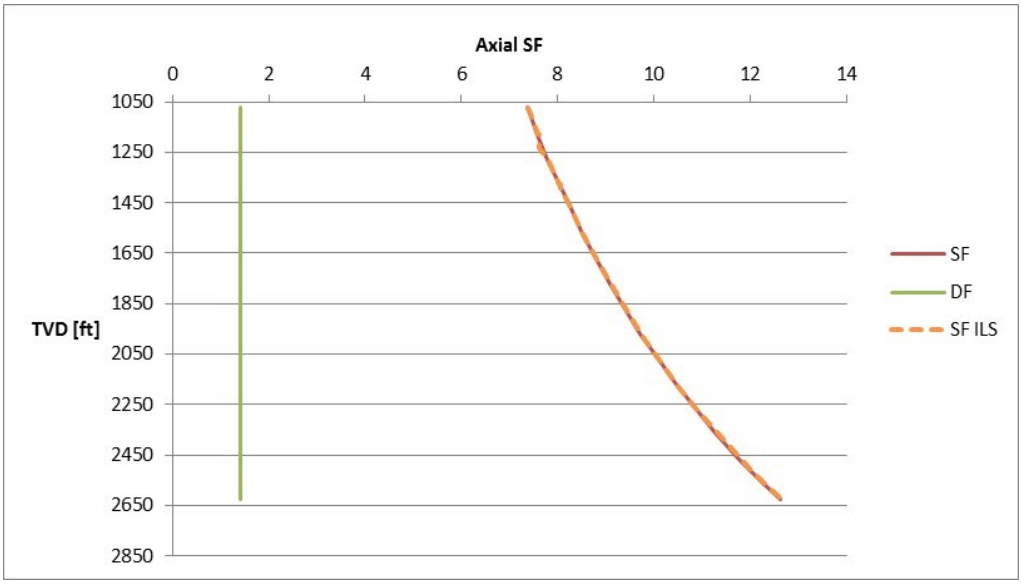

Figure B-18 Pressure test surface casing axial SF

B.2.1.4 Burst Safety Factor

The burst strength is calculated as described in chapter A.1.1, and is easier to figure out than the collapse strength. Next the burst pressure is calculated as the difference between the internal and external pressure. The burst SF is found by dividing the burst strength by the burst pressure all along the relevant section. As seen in Figure B-19 the SF is well above the DF, and matches the output from the ILS.

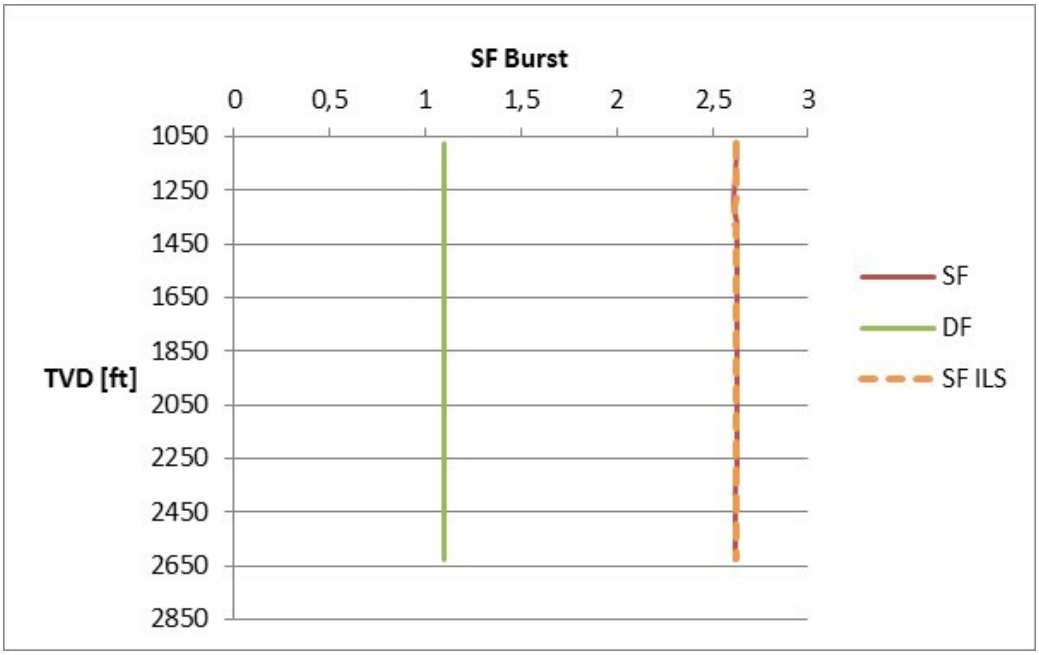

Figure B-19 Pressure test surface casing burst SF

B.2.1.5 Triaxial Safety Factor

Figure B-20 shows that the output from the ILS and the thesis model differ by about 0.4. The thesis model gives a more optimistic result. However, both models have a significant margin to the DF. The surface casing is more than strong enough to endure the pressure test; in fact,

the casing grade may be changed to a weaker grade.

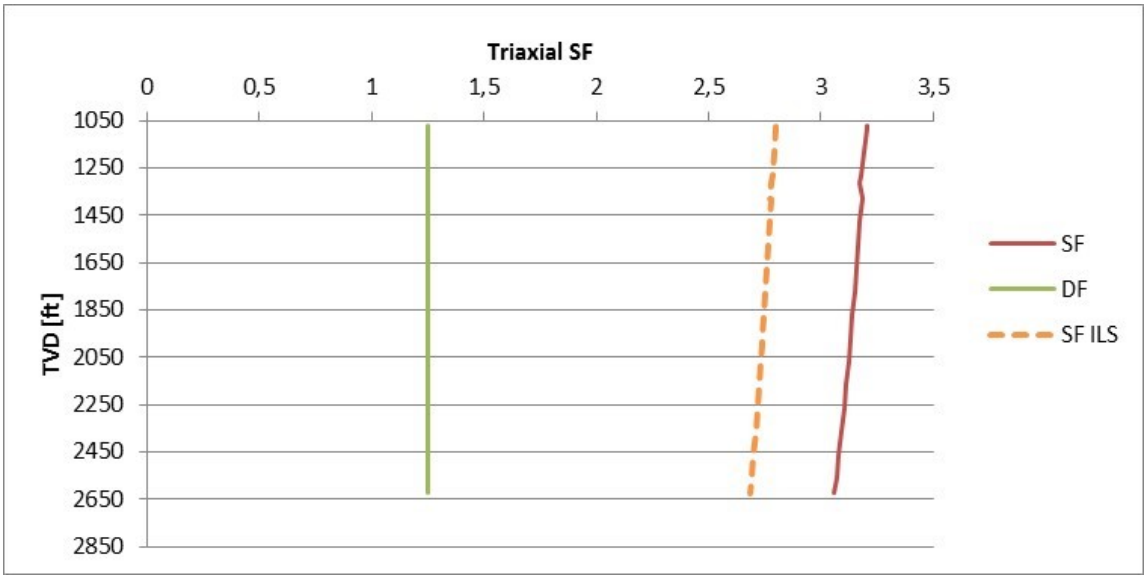

Figure B-20 Pressure test surface casing triaxial SF

B.2.2 Intermediate Casing

The effects of the temperature derated yield strength is presented in this chapter. The difference with and without this effect is evident in the figures of the safety factors.

B.2.2.1 Differential Pressure

As seen in Figure B-21, the fluid above TOC, 5,760ft, and the fluid used to pressure test is the same. This implies that the differential pressure above TOC is the same as the pump pressure at the surface. The pump pressure at surface is 4,390psi, the same as the differential pressure above TOC. Below TOC, the external pressure depends on the pore pressure, which is the reason for the behaviour in the graph below TOC. The pressures in the thesis model matches perfectly with the ILS. The differential pressure does not depend on the temperature derated yield strength.

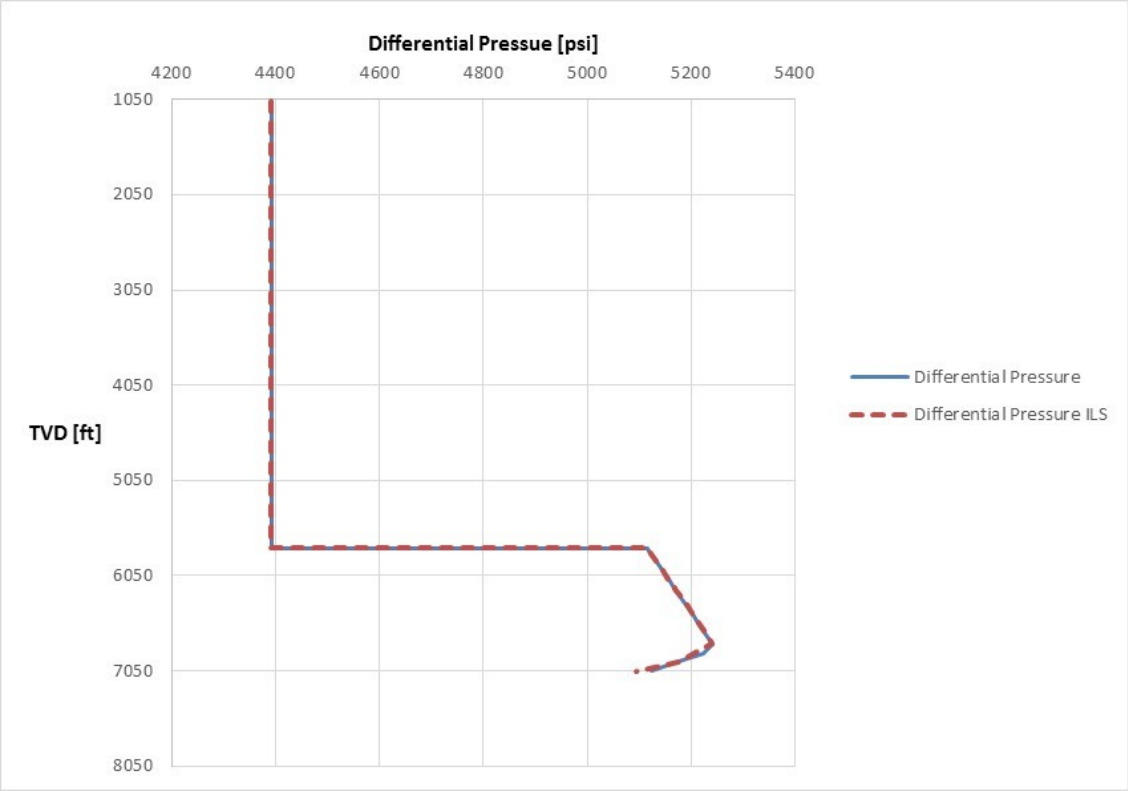

Figure B-21 Pressure test intermediate casing differential pressure

B.2.2.2 Axial Load

The axial load is calculated much the same way as for the surface casing; however in this case there is an uncemented part of casing. For the uncemented part, the ballooning force is calculated with the average pressures over this section, while below TOC it is calculated at each step. This is the reason for the kink in Figure B-22 at 5,760ft (TOC). The small discrepancy above TOC is due to a buckling force in the thesis model that is not in the ILS model. However, the difference is small and does not affect the casing design. Although the reason why there is buckling in the thesis model and not in the ILS is unknown and should be examined closer. During the pressure test, the axial load is a lot higher than in the initial conditions, and the entire casing string is in tension. The axial load is not affected by the temperature derated yield strength, however the axial safety factor depends on this effect.

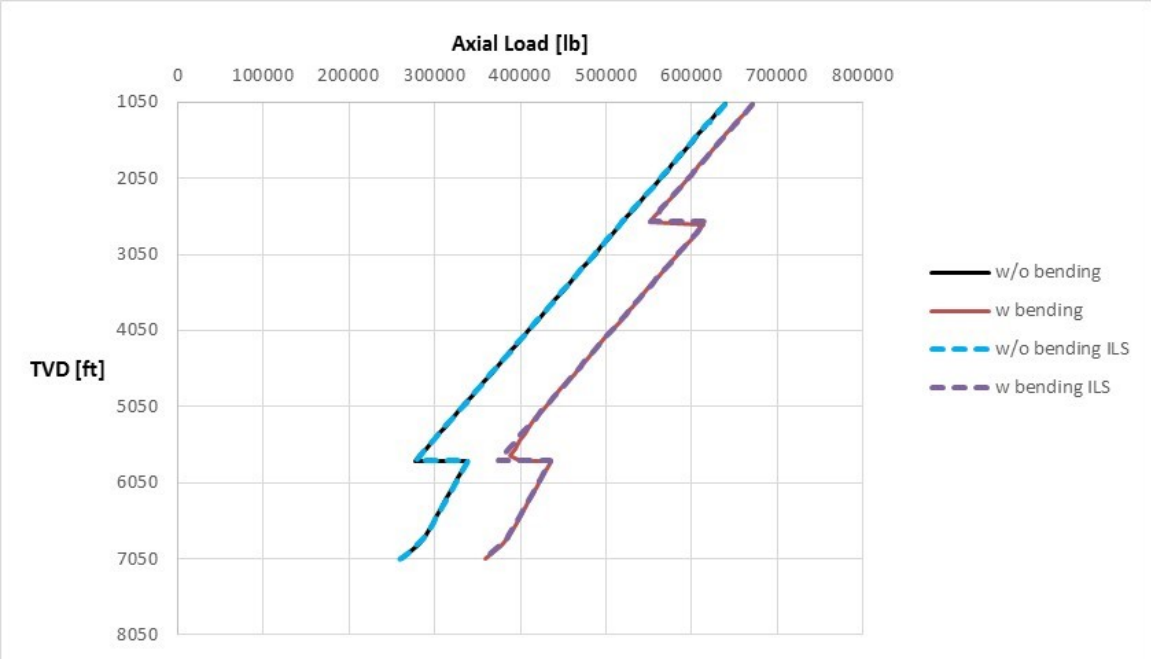

Figure B-22 Pressure test intermediate casing axial load

B.2.2.3 Axial Safety Factor

The axial SF for the thesis model is equal to the axial SF from the ILS, except for a small difference above the TOC at 5,760ft. This discrepancy is due to a small buckling as previously mentioned, but is so small that it does not affect the casing design as both the safety factors are well above the DF, especially at this point. The SF is closes to the DF at the top of the casing where the axial load is the greatest.

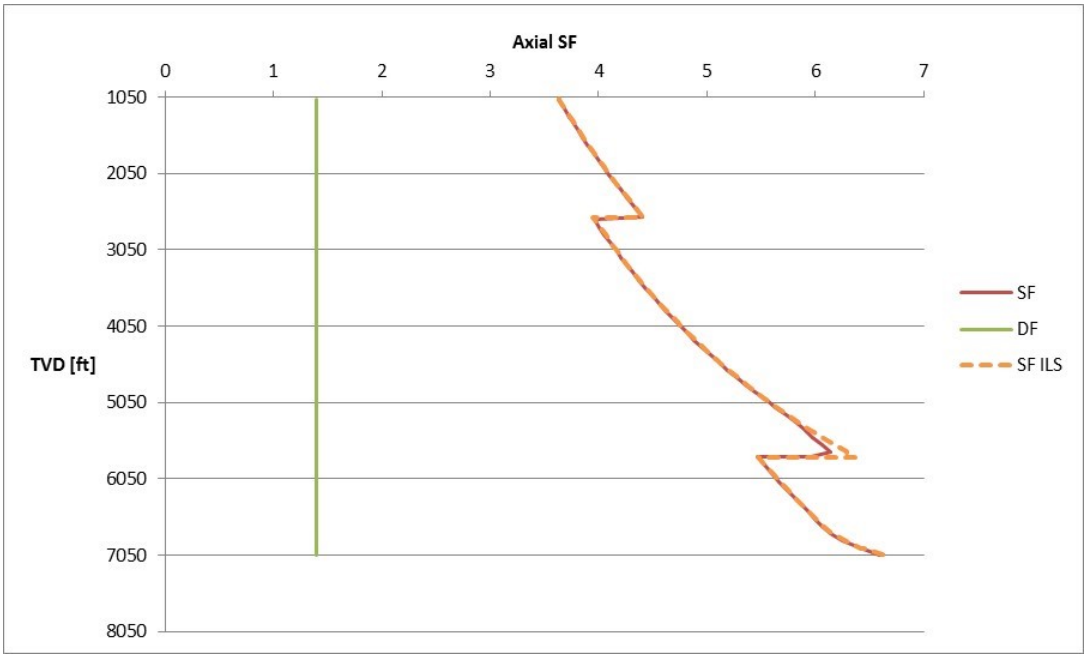

Figure B-23 Pressure test intermediate casing axial SF

The figure below shows the axial safety factor if the yield strength is not tempreature derated. As seen, the safety factors from the two models differ more and more when the depth increases as the temperature also increases with depth. The yield strength starts derating when the temperature is over 68°F, which is why the two safety factors are equal at the top. The temperature is above 68°F around 2,360ft, and so the two models starts to differ around this point. When the yield strength does not depend on the temperature, the axial SF is more optimistic.

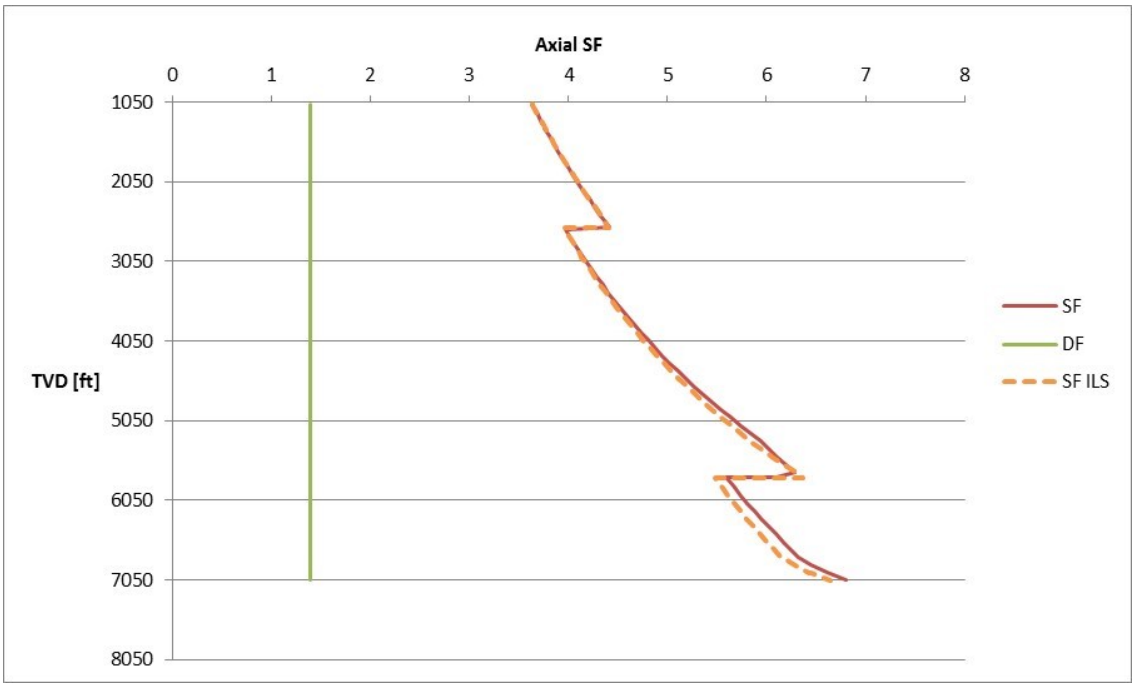

Figure B-24 Pressure test in the intermediate casing, axial SF without temperature derated yield strength

B.2.2.4 Burst Safety Factor

Figure B-25 shows that both the models give the same burst SF. The SF above the TOC would be expected to be a straight line as the fluid used to pressurise the casing is the same as the fluid behind the casing. However, as the models use a temperature derated yield strength as mentioned in the start of chapter 3, the line is a little inclined. At the TOC, the external pressure suddenly decreases because the external pressure from that point is based on the pore pressure.

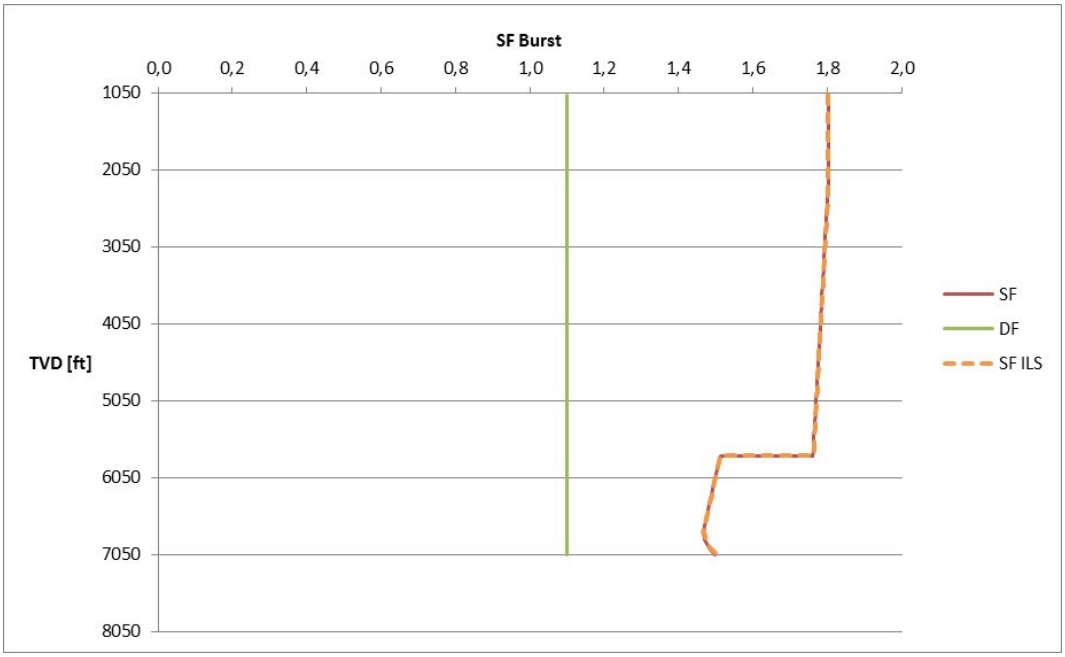

Figure B-25 Pressure test intermediate casing burst SF

The previous figure showed the burst SF when the yield strength depends on the temperature. However, when the yield strength does not depend on the temperature the burst SF is as presented in the following figure. In this case, the line above the TOC is straight as the mud used to pressurise the casing is the same as the mud behind the casing. The difference between the axial SF with and without temperature derated yield strength increases with depth as the temperature also increases with the depth.

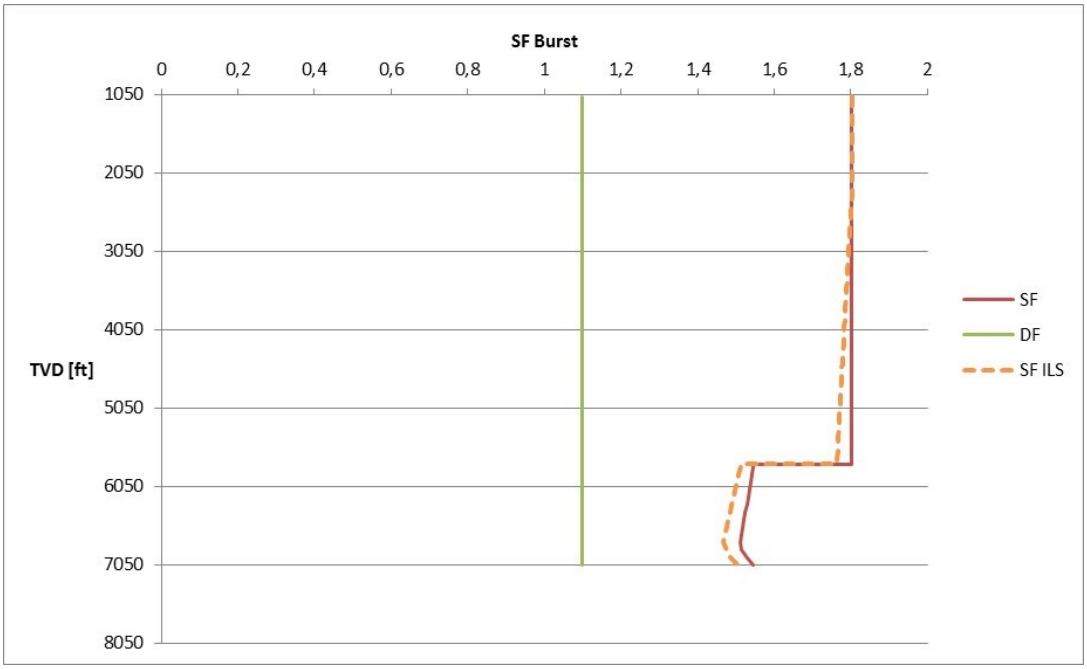

Figure B-26 Pressure test in the intermediate casing, burst SF without temperature derated yield strength

B.2.2.5 Triaxial Safety Factor

As for the surface casing, the thesis model gives a more optimistic SF than the ILS. Figure B-27 shows that the difference is about 0.3. However, the SF is above the DF for both the models, and the casing will thus tolerate the pressure test.

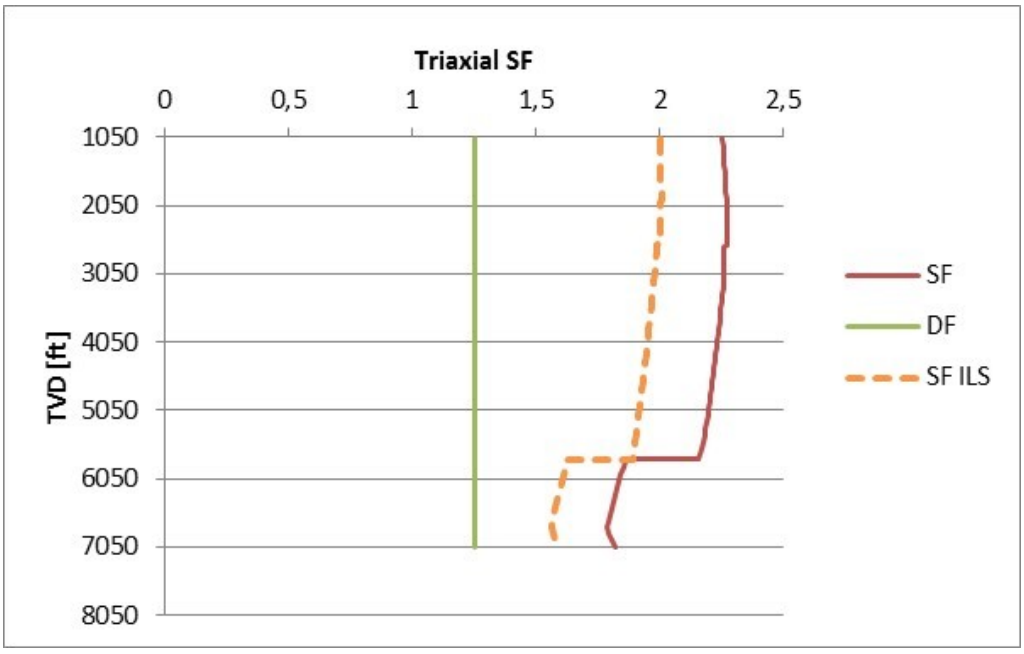

Figure B-27 Pressure test intermediate casing triaxial SF

The difference with and without temperature deration is more apparent when examining the axial and burst safety factors as the triaxial SF from the thesis model rarely matches the ILS results exactly. The triaxial SF is also affected however; the triaxial SF is more optimistic when the temperature deration is not included. In this load case whether the yield strength is derated or not does not have an impact on the casing design, however it may be in other cases and should therefore be included. If the SF is closer to the DF when the yield strength does not depend on the temperature, the SF may cross the DF when accounting for the temperature deration. This means that if the decision is based on the case without temperature deration, the casing design may fail.

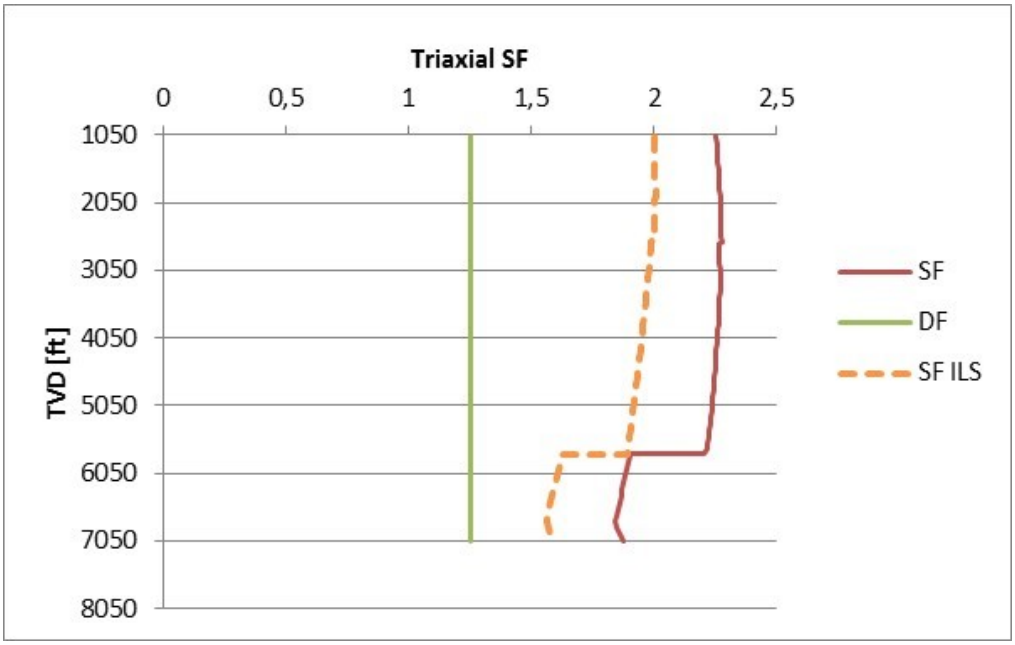

Figure B-28 Pressure test in the intermediate casing, triaxial SF without temperature derated yield strength

B.2.3 Production Casing

B.2.3.1 Differential Pressure

As for the intermediate casing, the differential pressure for the production casing is a straight line down to TOC, representing the pump pressure at surface since the fluid behind the casing and the fluid used to pressure test is the same. Below TOC the external pressure comes from the pore pressure, hence the sudden change in differential pressure. From Figure B-29 it is evident that the models match in terms of pressure.

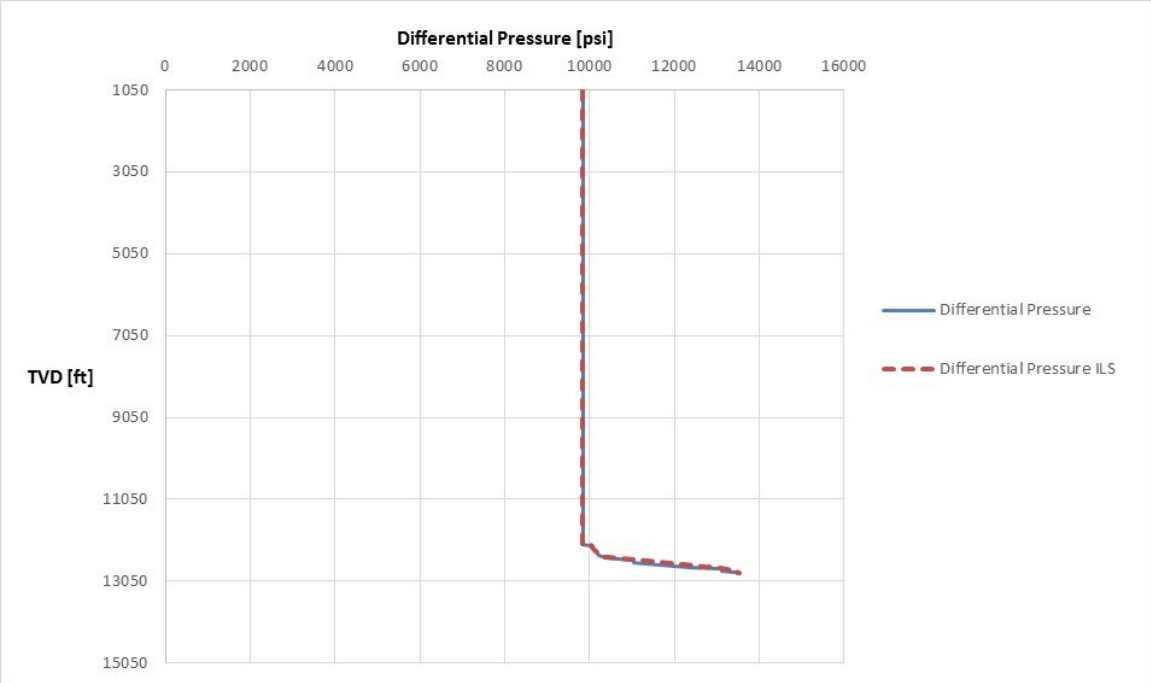

Figure B-29 Pressure test production casing differential pressure

B.2.3.2 Axial Load

Figure B-30 shows the axial load, where the ballooning force is calculated as explained in chapter B.2.1.2. The thesis model and ILS matches perfectly, and the entire casing string is in tension. Compared to the initial conditions, the axial load during the pressure test is a lot greater due to the high internal pressure.

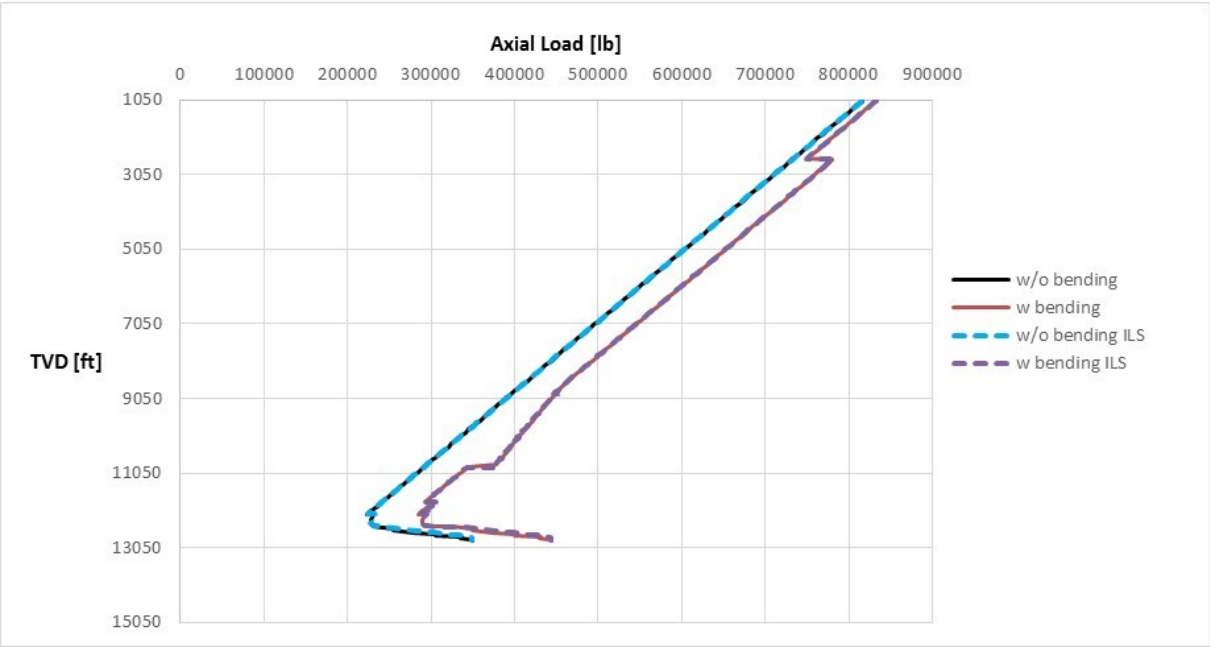

Figure B-30 Pressure test production casing axial load

B.2.3.3 Axial Safety Factor

The axial SF from the thesis model in Figure B-31 is quite accurate compared to the ILS. There is a good margin between the SF and the DF, so the casing is adequate in relation to the axial strength for the pressure test.

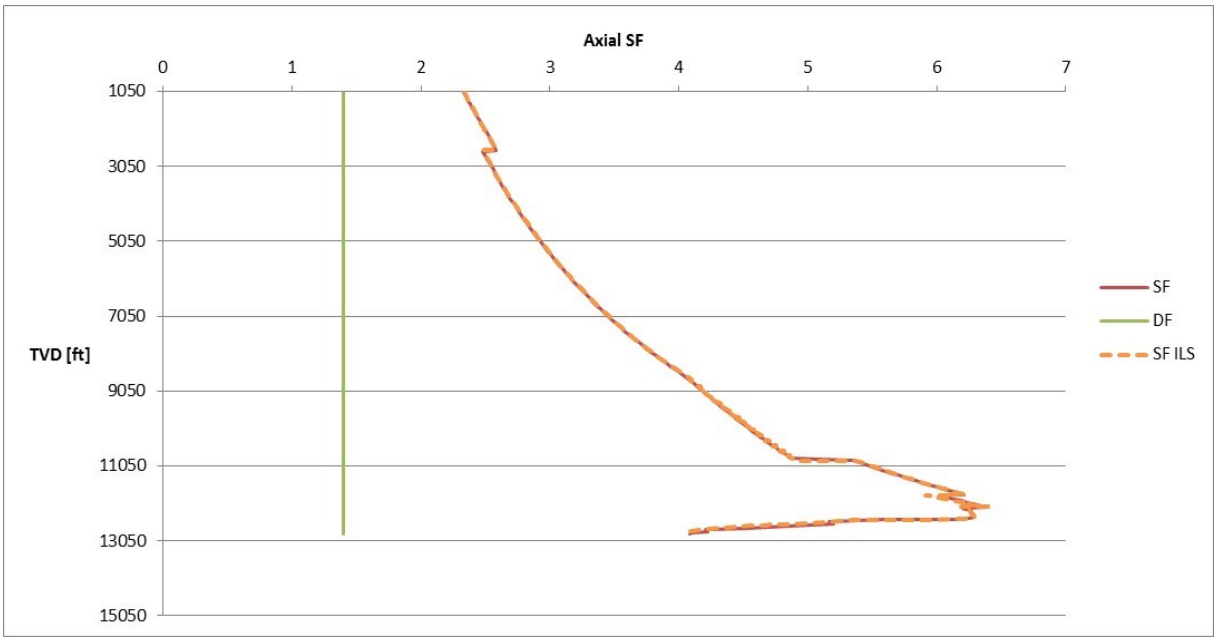

Figure B-31 Pressure test production casing axial SF

B.2.3.4 Burst Safety Factor

The burst SF from the thesis model matches the output from the ILS as displayed in Figure B-32. Above TOC, the line is slightly inclined, due to the temperature derated yield strength. As observed in the graph, the SF is lower than the DF below TOC. Normally this would mean that the casing is not strong enough to withstand the burst pressure, and should therefore be changed to a higher grade. However, as explained in chapter A.3, the cement may be assumed to give physical support if the cement job went perfectly. The safest solution would be to change the casing grade.

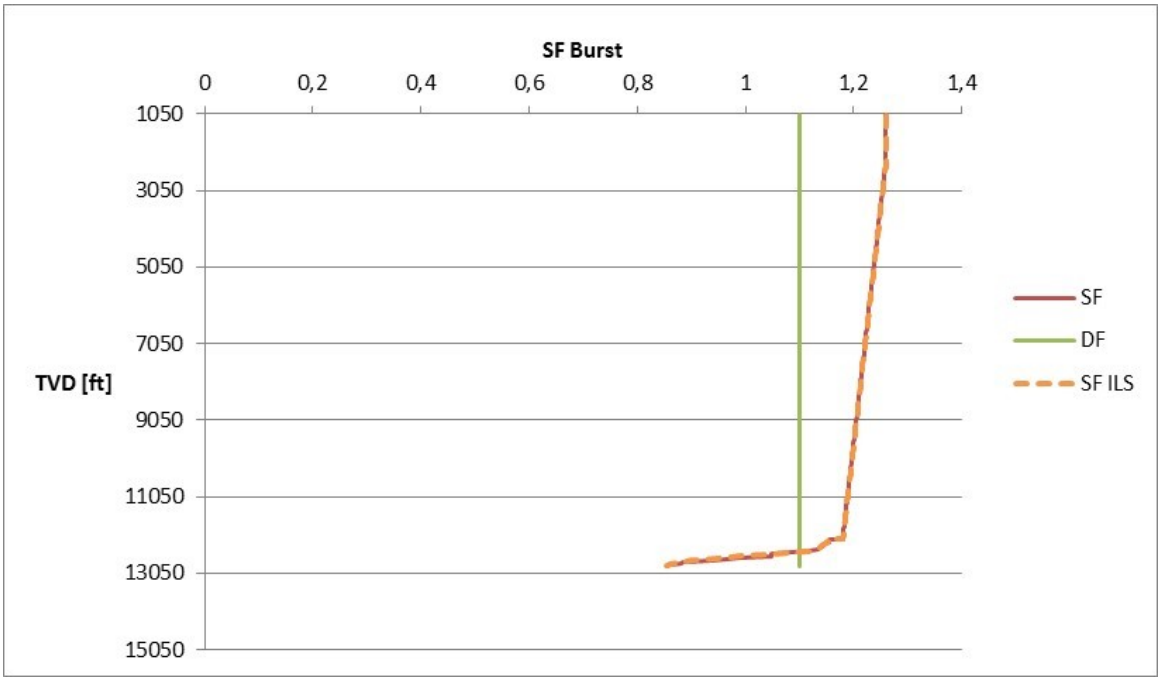

Figure B-32 Pressure test production casing burst SF

B.2.3.5 Triaxial Safety Factor

Figure B-33 displays the triaxial SF for the pressure test of the production casing. The burst SF is lower than the burst DF below TOC, and that is also the case for the triaxial SF. Even though the models differ with about 0.15, the SF of the thesis model, which is the most optimistic model, is also lower than the DF. The triaxial SF takes into account the three different stresses in the wellbore, and is therefore more accurate and trustworthy than the axial or burst SF. The SF from the ILS is dangerously close to the DF above the TOC as well due to the temperature derated yield strength. All things considered, the casing grade should be changed as a precaution.

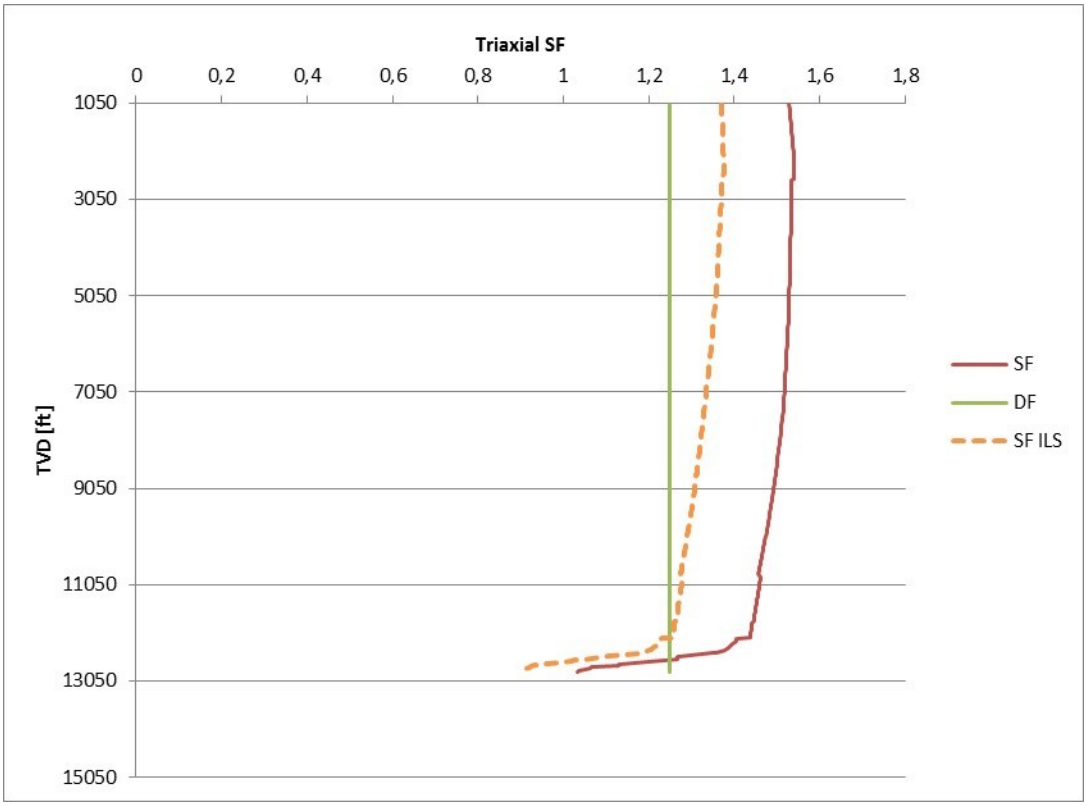

Figure B-33 Pressure test production casing triaxial SF

B.3 Lost Returns with Mud Drop

Lost returns with mud drop is a collapse load; the external pressure is higher than the external pressure. As always, the worst-case scenario is examined, which in this case means that the cement job is assumed to be poor and the external pressure is based entirely on the mud weight in which the casing was placed.

B.3.1 Surface Casing

B.3.1.1 Differential Pressure

Down to around 1,400ft, the internal pressure is zero due to mud drop because of lost returns. The mud drop level differs slightly between the two models, which is the reason for the small discrepancy seen at around 1,400ft in Figure B-34. The slope of the differential pressure down to this point is then dependent only on the external pressure, which is based on the cement weight. Below this point, the internal pressure starts to build, so the differential pressure increases. However, the external pressure is still larger than the internal as seen in the next figure.

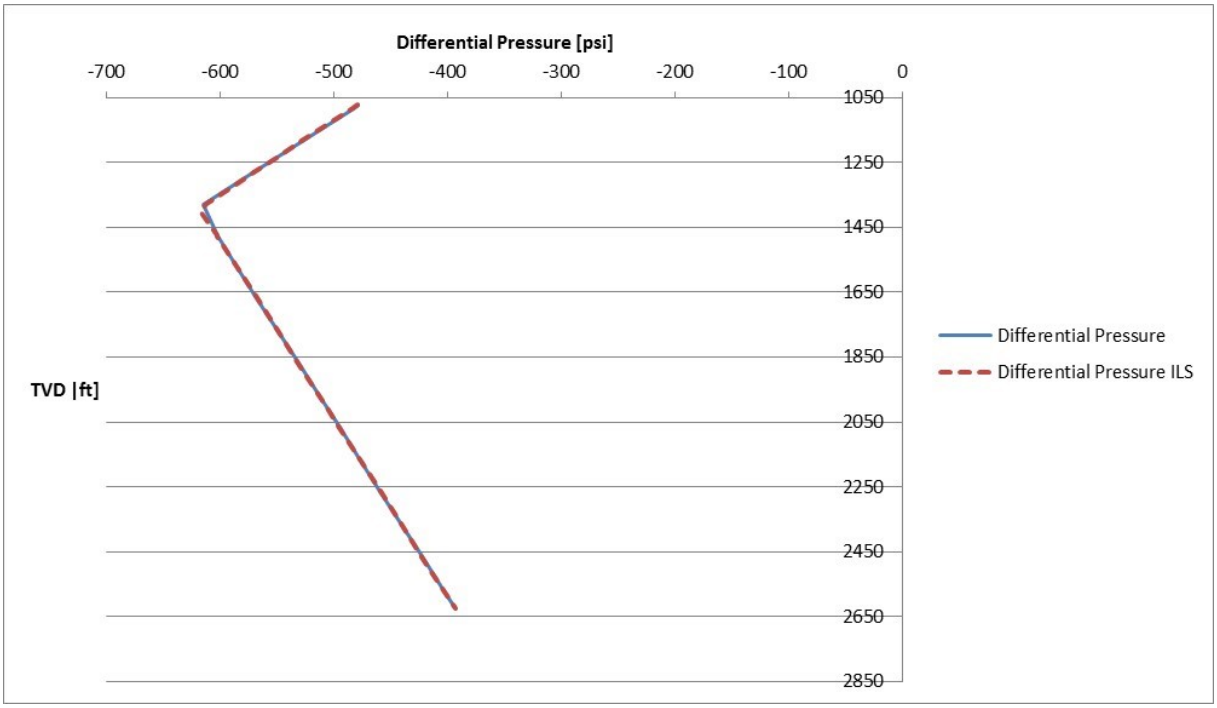

Figure B-34 Lost returns surface casing differential pressure

B.3.1.2 Axial Load

The axial load is calculated the same way as for the pressure test, and the thesis model matches the ILS as seen in Figure B-35. During this load case, the surface casing is entirely in compression as shown in the following figure, unlike the initial conditions and the pressure test.

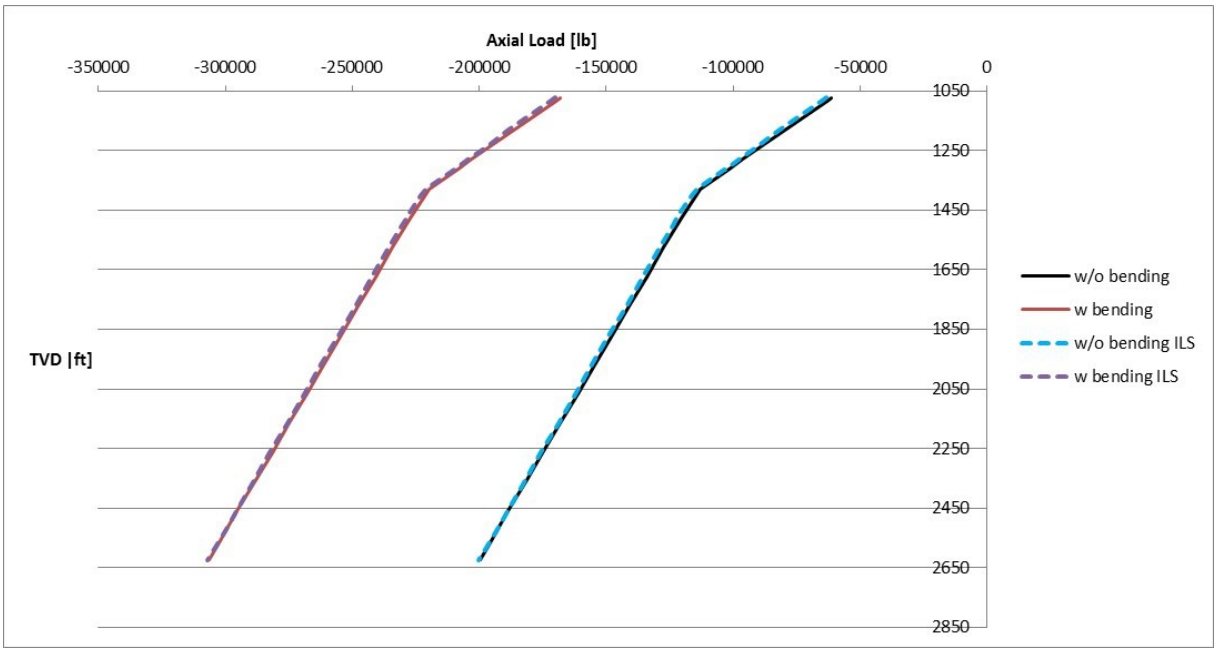

Figure B-35 Lost returns surface casing axial load

B.3.1.3 Axial Safety Factor

From Figure B-36 it is seen that the axial SF from the thesis model also matches the ILS, and is way above the DF.

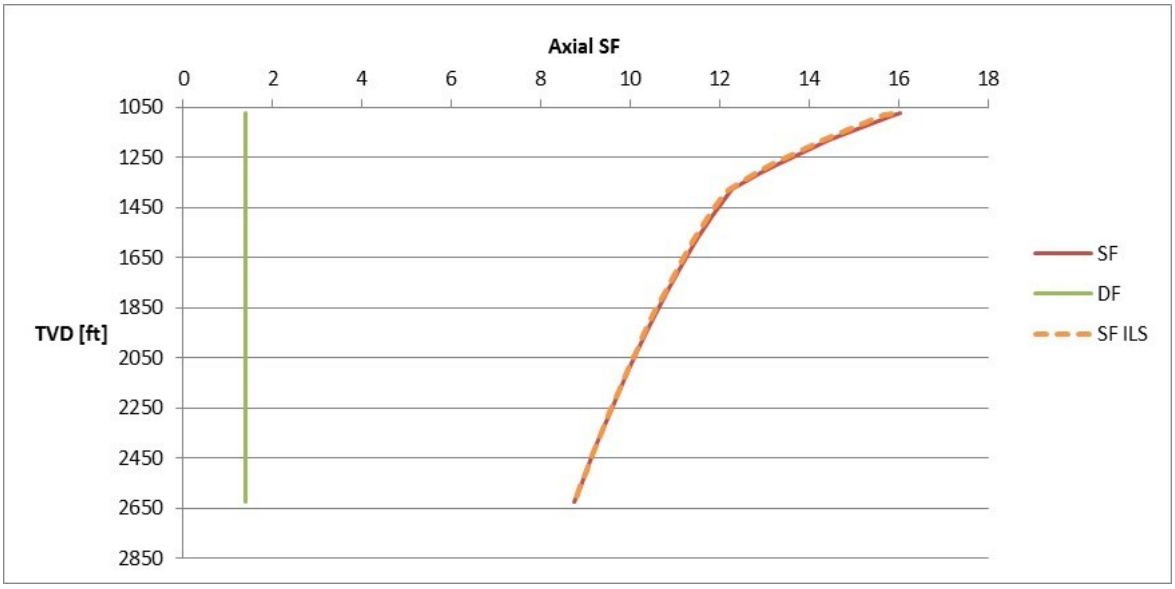

Figure B-36 Lost returns surface casing axial SF

B.3.1.4 Collapse Safety Factor

The collapse SF from the thesis is very accurate when compared to the ILS, and has a good margin down to the DF as seen in Figure B-37.

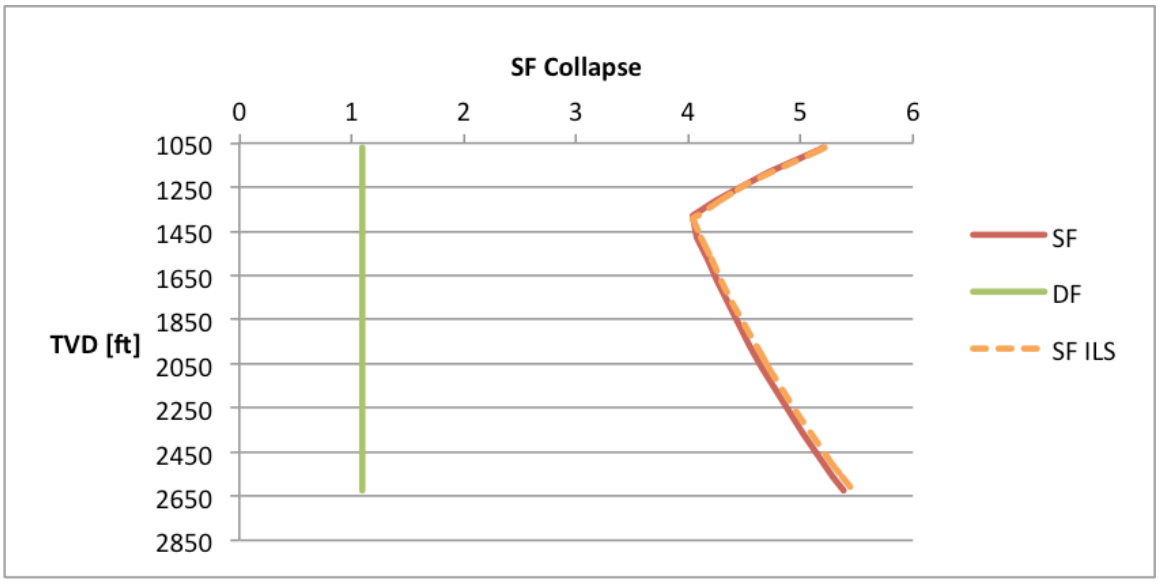

Figure B-37 Lost returns surface casing collapse SF

B.3.1.5 Triaxial Safety Factor

Figure B-38 shows that there is a difference between the thesis model and ILS when it comes to the triaxial SF. The difference is about 0.8, and once again the thesis model is the more

optimistic of the two models. However, both the safety factors are way above the DF. Since all the safety factors for the different load cases are well above the design factors for the surface casing, the chosen casing grade, K-55, is more than adequate.

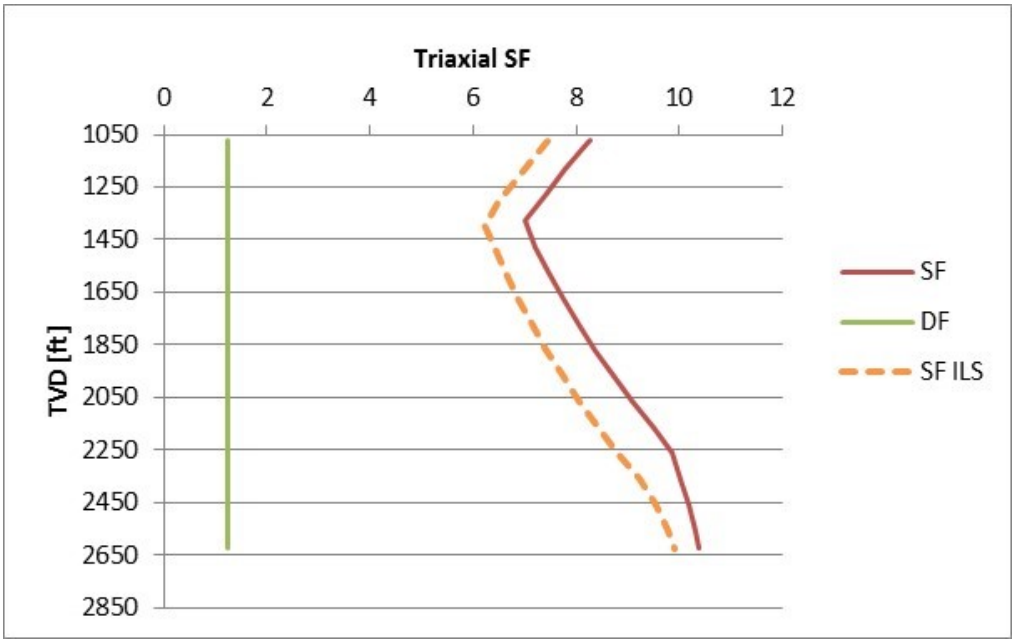

Figure B-38 Lost returns surface casing triaxial SF

B.3.2 Intermediate Casing

B.3.2.1 Differential Pressure

As for the surface casing, there is a slight difference between the thesis model and the output from the ILS for the mud drop level. It seems like the internal pressure builds up more slowly in the ILS than in the thesis model. However, this is the only difference between the two models. Figure B-39 shows that the mud drop level is around 5,000ft, which means that the mud drop is approximately 3,800ft. As explained in chapter A.3.2, this is unrealistically high, and should be modified to between 820ft and 1,500ft.

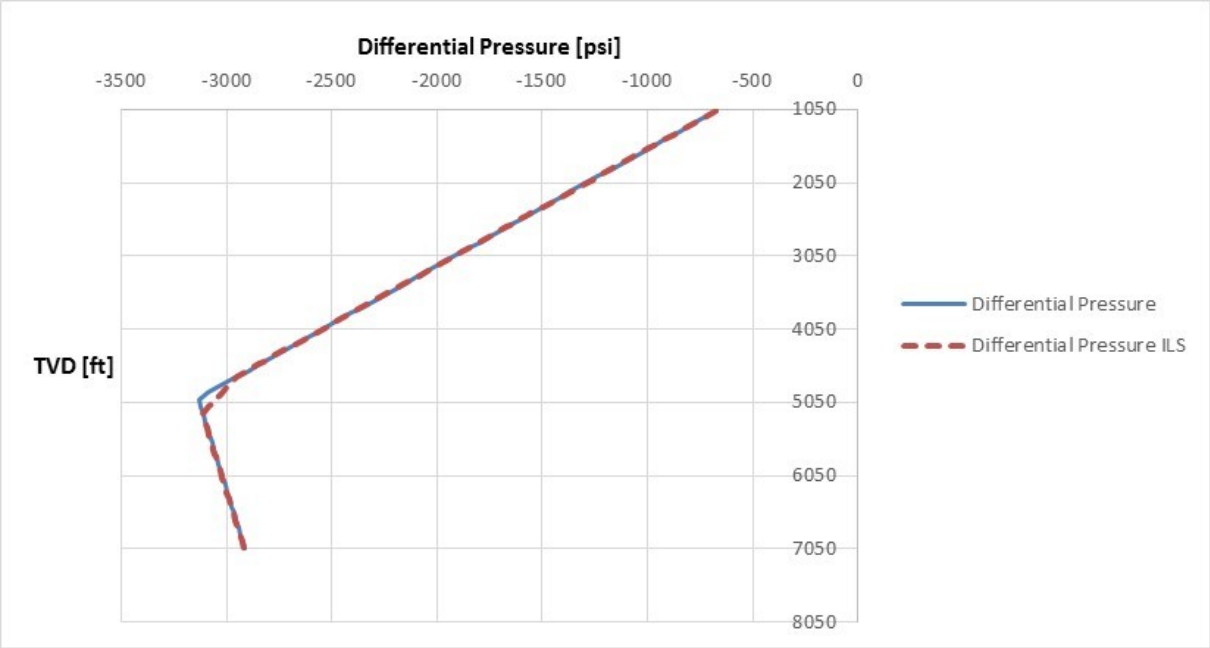

Figure B-39 Lost returns intermediate casing differential pressure

B.3.2.2 Axial Load

The thesis model and the ILS have almost the same axial load, as seen in Figure B-40. There seems to be a slight difference above TOC, which may be because there is a small difference between the differential pressures. The casing string is in tension above 3,440ft, from where it is in compression. More of the casing string is in compression in this load case than in the initial conditions as there is a more significant pressure difference in this case.

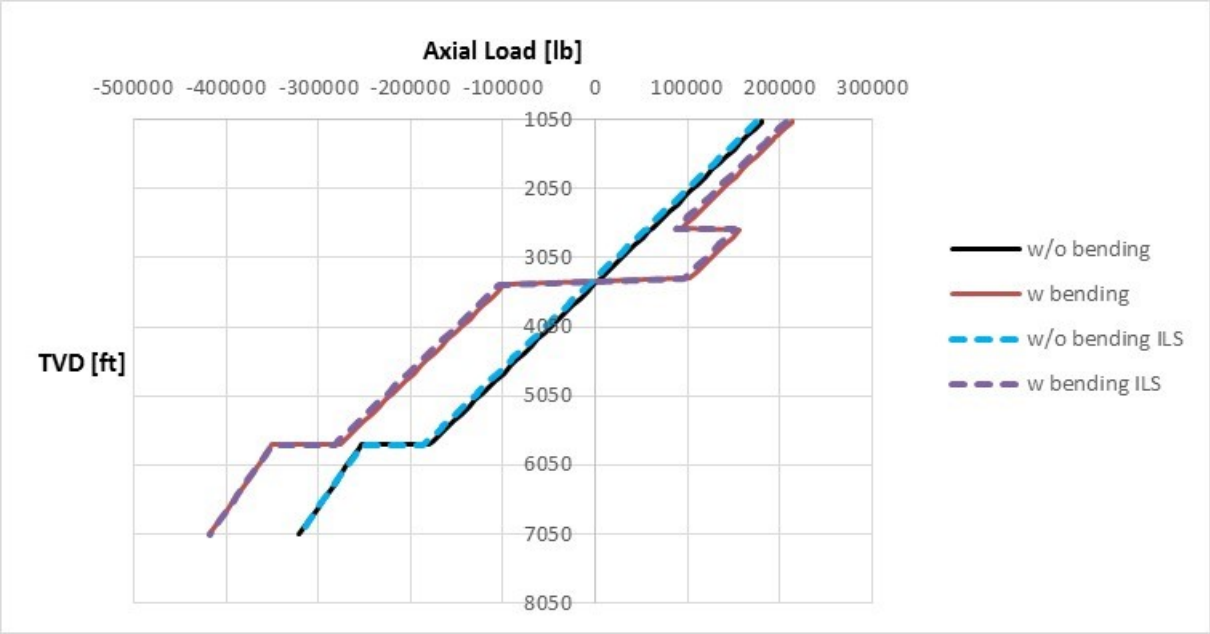

Figure B-40 Lost returns intermediate casing axial load

B.3.2.3 Axial Safety Factor

The axial safety factors from both the models match quite well, and are above the DF. There is a slight difference above the TOC as with the axial load. In this case, the axial SF is closest to the DF at the bottom of the casing, as the compression force there is more significant than the tension force at the top of the casing.

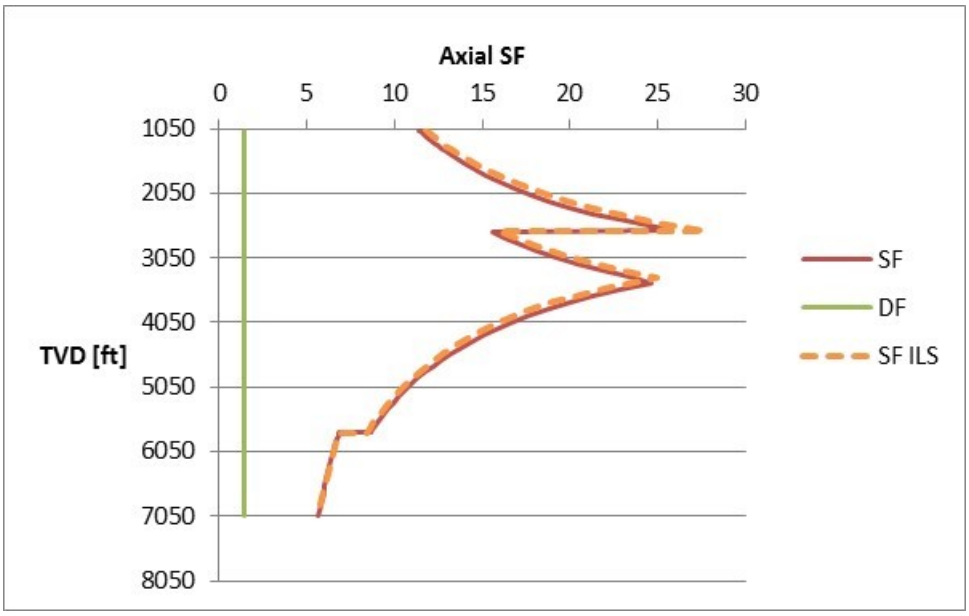

Figure B-41 Lost returns intermediate casing axial SF

B.3.2.4 Collapse Safety Factor

The collapse safety factor crosses the design factor slightly as seen in Figure B-42. However, as explained when examining the differential pressure, there is an unrealistically high mud drop in this case. This should be modified and the new SF compared to the DF before changing the casing grade. A higher casing grade is more expensive, and it is unnecessary to upgrade if the scenario is unlikely to happen. The two models match perfectly.

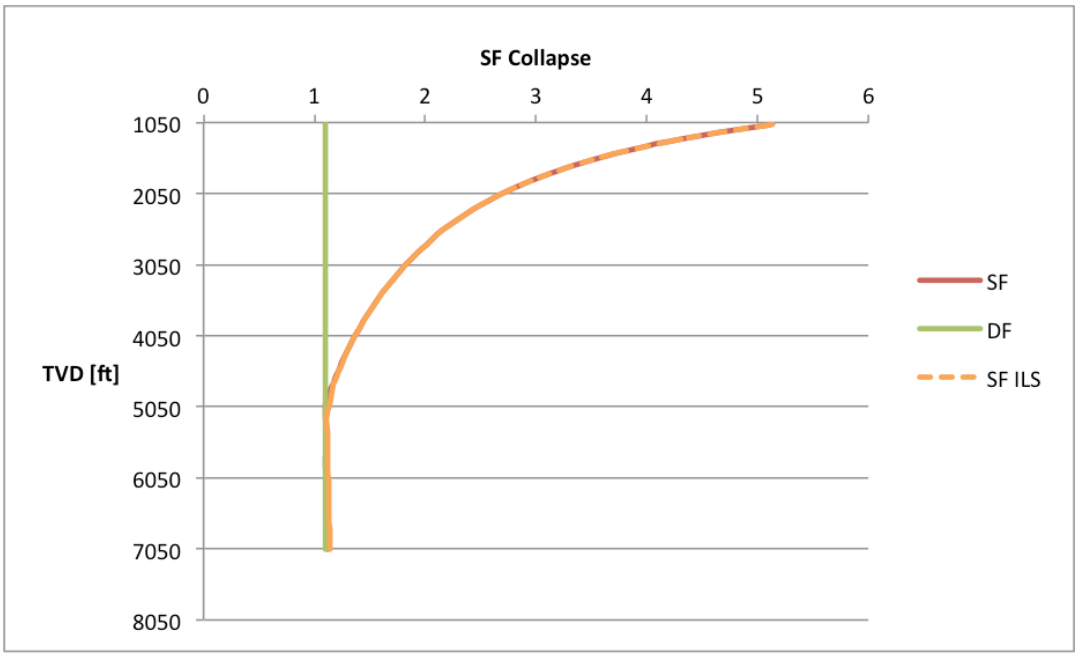

Figure B-42 Lost returns intermediate casing collapse SF

B.3.2.5 Triaxial Safety Factor

The SF in regard to collapse was not good enough for this load case. However, when examining the triaxial SF, the current casing grade is strong enough. Although the two models do not match perfectly, they are close to each other and both are above the DF with a good margin.

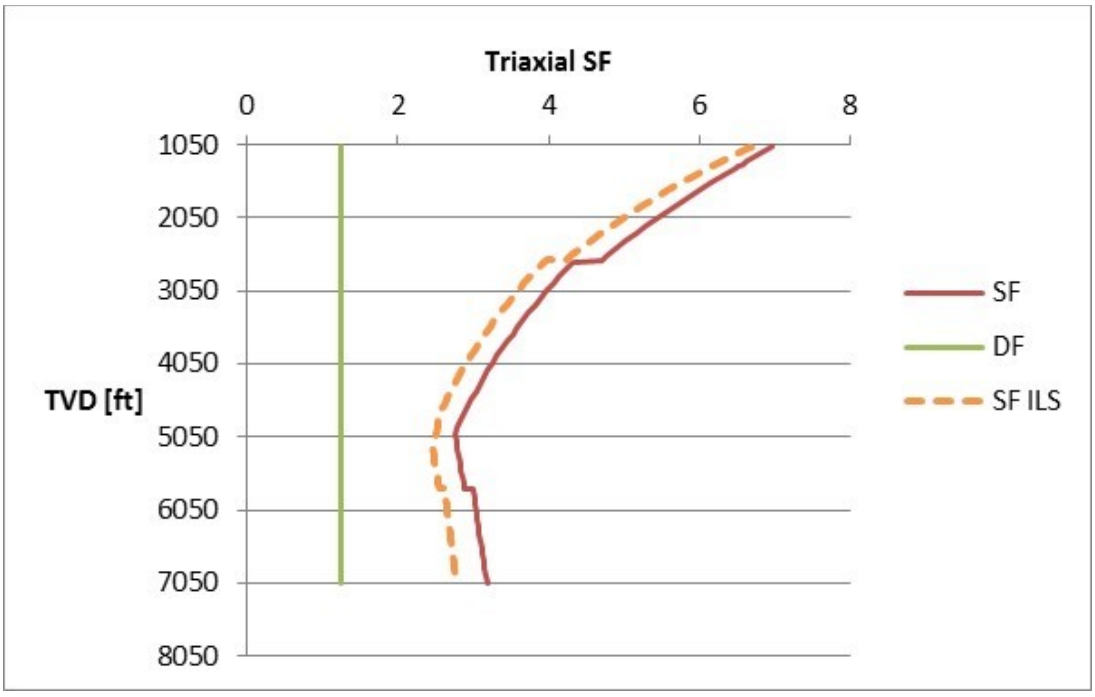

Figure B-43 Lost returns intermediate casing triaxial SF

B.3.3 Production Casing

In this chapter, the different ways of calculating the ballooning force is presented. The first way is the way the ILS calculates the ballooning force, and is also the way the ballooning force is calculated for the load cases in the thesis model.

B.3.3.1 Differential Pressure

In the production casing, the mud drop is very small and barely noticeable. The mud drop level is at about 1,380ft, which makes the mud drop around 300ft. Figure B-44 has a kink around 1,380ft; from there the slope of the line is smaller than before due to the internal pressure increasing. The mud weight the external pressure is based on is a lot larger than the pore pressure the internal pressure depends on, which is why the differential pressure does not increase below the mud drop level as it does in both the surface and intermediate casing.

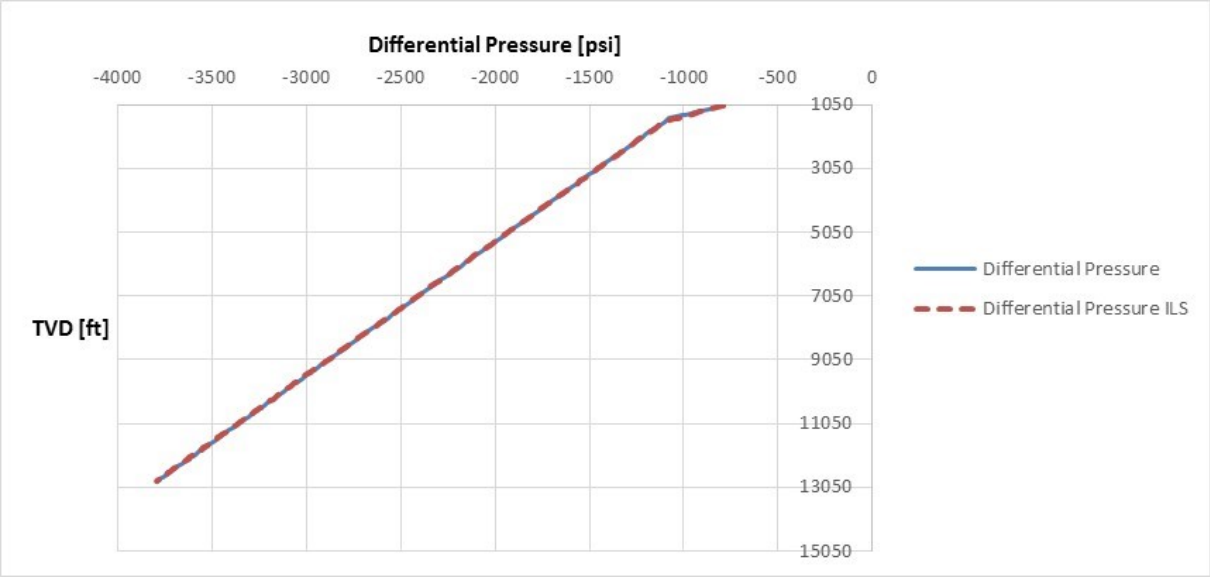

Figure B-44 Lost returns production casing differential pressure

B.3.3.2 Axial Load

The models for the axial load match perfectly in this case as well. The many kinks and changes in the bending load come from changes in the DLS as explained previously. The ballooning force is calculated with an average ballooning force above TOC, and with a new ballooning force for each new depth below TOC. This is the reason for the sudden decrease of the axial load around 12,150ft, which is the TOC. The production casing is in tension until approximately 8,480ft, from where the casing is in compression. The casing string is in compression higher up in this case than in the initial conditions because the differential pressure is less in this case.

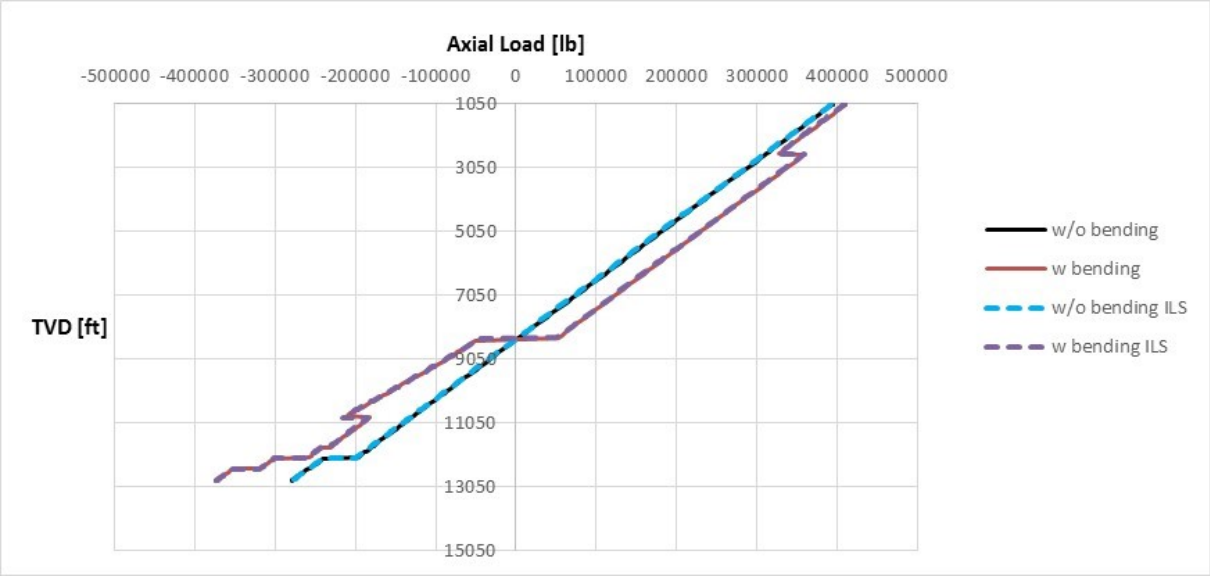

Figure B-45 Lost returns production casing axial load

B.3.3.3 Axial Safety Factor

The thesis model and the ILS match perfectly in the following figure, and there is a good margin between the SF and DF. The SF increases as the axial load decreases down to 8,480ft, from where the SF starts to decrease as the casing is now in compression. In this case, the SF is slightly smaller at the top of the casing than at the bottom of the casing.

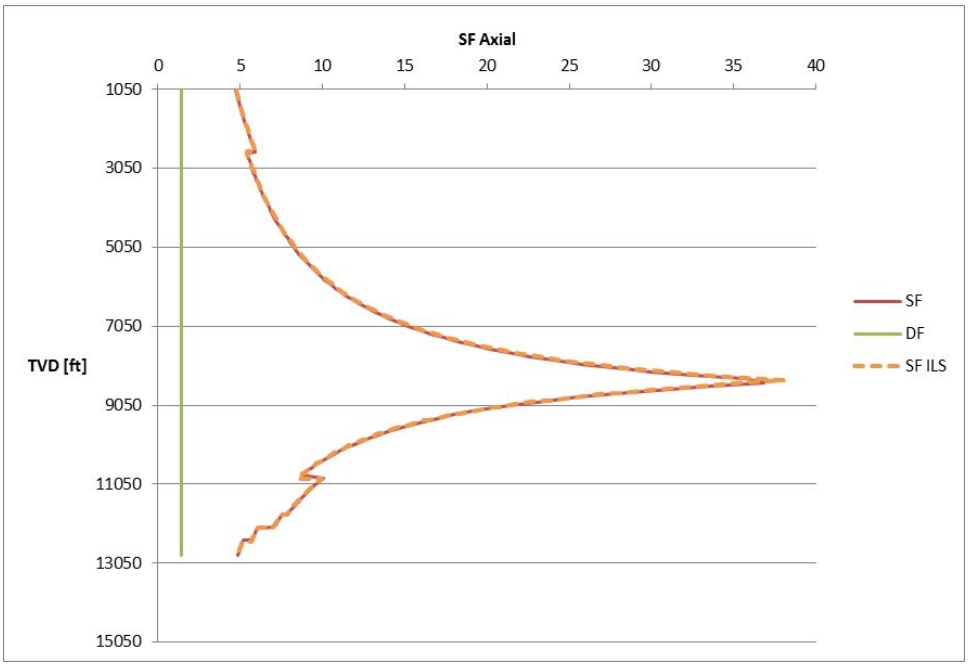

Figure B-46 Lost returns production casing axial SF

B.3.3.4 Collapse Safety Factor

Figure B-47 shows that the two models are similar considering the collapse safety factor, and both the safety factors are above the DF.

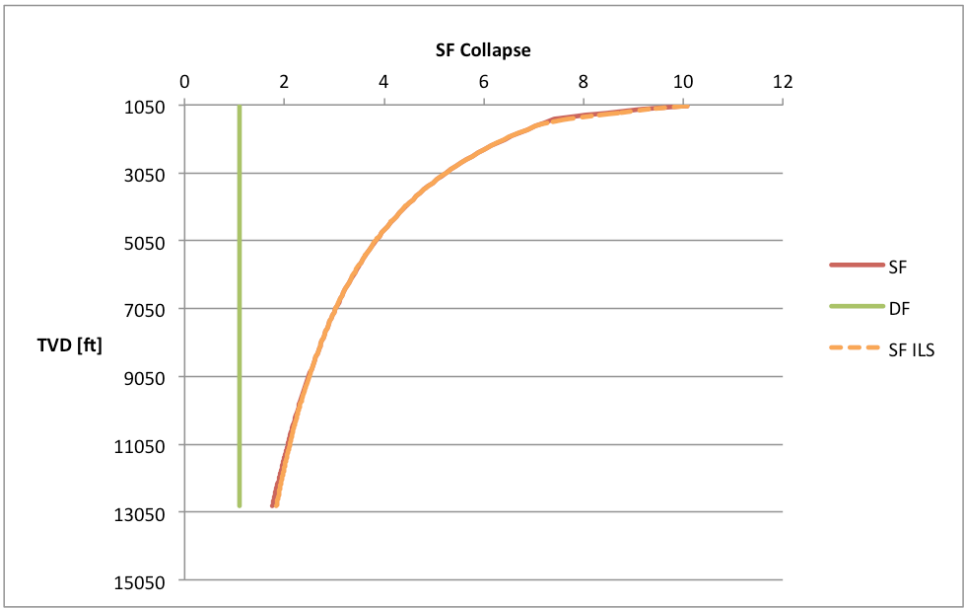

Figure B-47 Lost returns production casing collapse SF

B.3.3.5 Triaxial Safety Factor

Figure B-48 displays the result of the triaxial SF calculations. The thesis model differs slightly from the ILS, however it has the same shape although a more optimistic one. Both the safety factors are well within the limits, indicating that the casing grade chosen for this casing is more than strong enough to endure this load case.

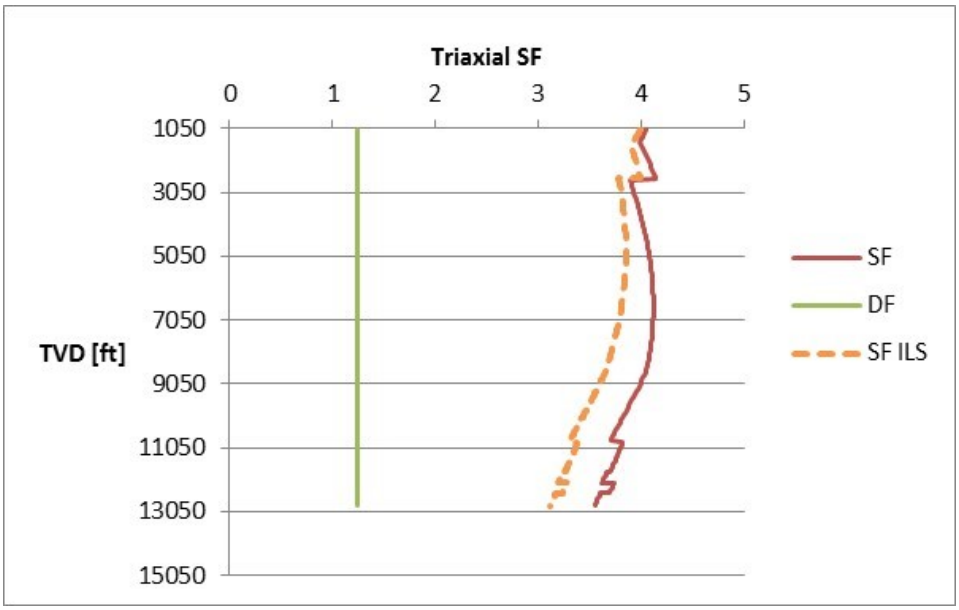

Figure B-48 Lost returns production casing triaxial SF

B.3.3.6 Ballooning Effects Calculated Three Different Ways

The ballooning force is calculated two different ways in the ILS, and therefore in the thesis model as well, depending on whether the section is cemented or not. In the cemented section

the ballooning force is calculated as a new force at each new depth with the pressures at this depth. Where there is no cement, the ballooning force is calculated as an average force over the entire section with the average pressures in this section. Both the methods use eq.(5); the difference is whether the pressure is average or specific. This chapter shows the difference between the three possible ways of calculating the ballooning effect.

The following figure shows the axial load in the load case with the ballooning force calculated in two different ways depending on the cement as is done in the ILS. The thesis model matches the ILS when the ballooning force is calculated this way. Around 12,150ft there is a sudden decrease in the axial load in this figure, due to the two different methods when calculating the ballooning force as this is the TOC.

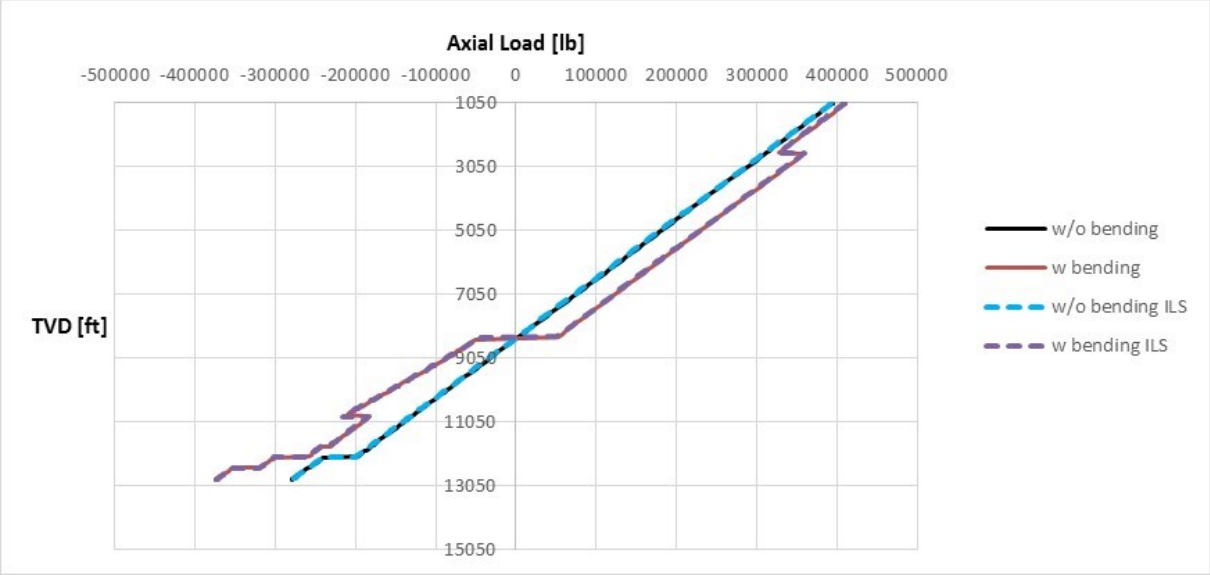

Figure B-49 Lost returns with mud drop in the production casing, axial load

The next figure shows the axial load when the ballooning force is calculated as an average force over the entire section. Above the TOC there is a small difference from the previous method due to the fact that the average pressure now includes the pressures below TOC, while below the TOC there is a more noticeable difference.

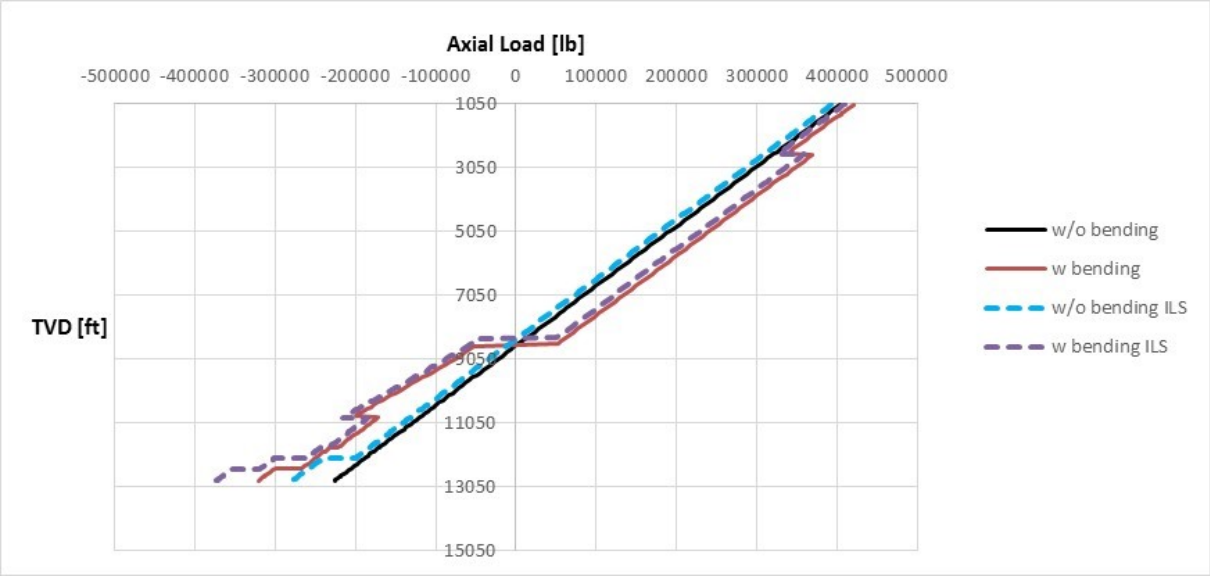

Figure B-50 Lost returns with mud drop in the production casing, axial load average ballooning force

When the ballooning force is calculated as a new force at each new depth the entire section, the result is quite different from the ILS output above TOC. The following figure shows how the axial force is shifted to more tension when the casing is in tension, and more compression when the casing is in compression. I.e. the axial load increases with this method.

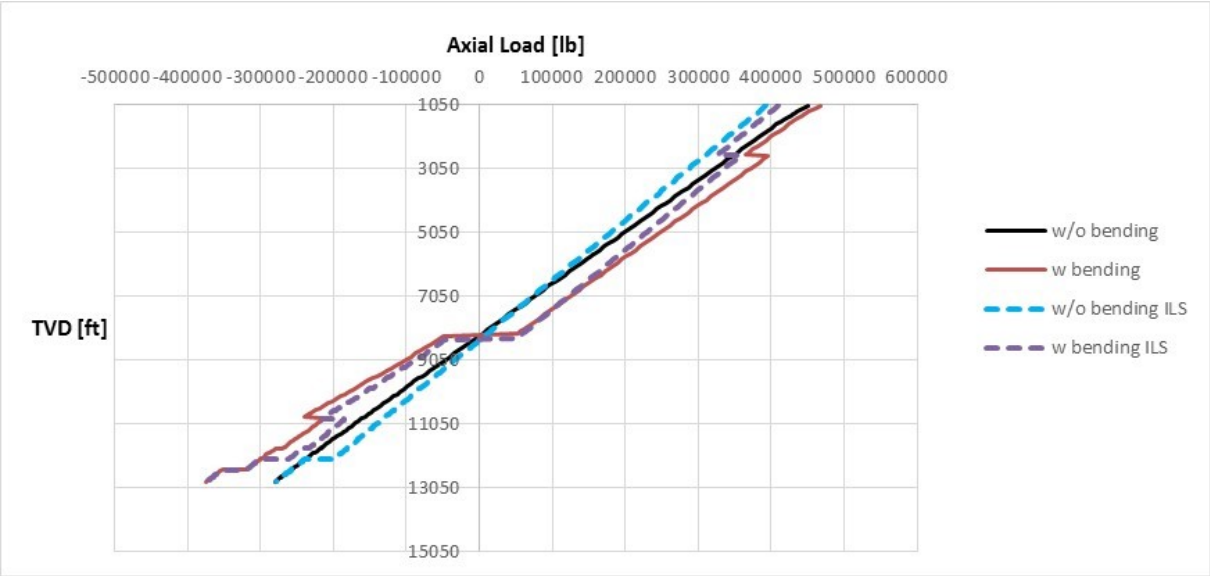

Figure B-51 Lost returns with mud drop in the production casing, axial load with new ballooning force at each step

The following figure shows the axial safety factor when the ballooning force is calculated differently above and below TOC. The two methods are in this case extactly the same, as was the case for the axial load.

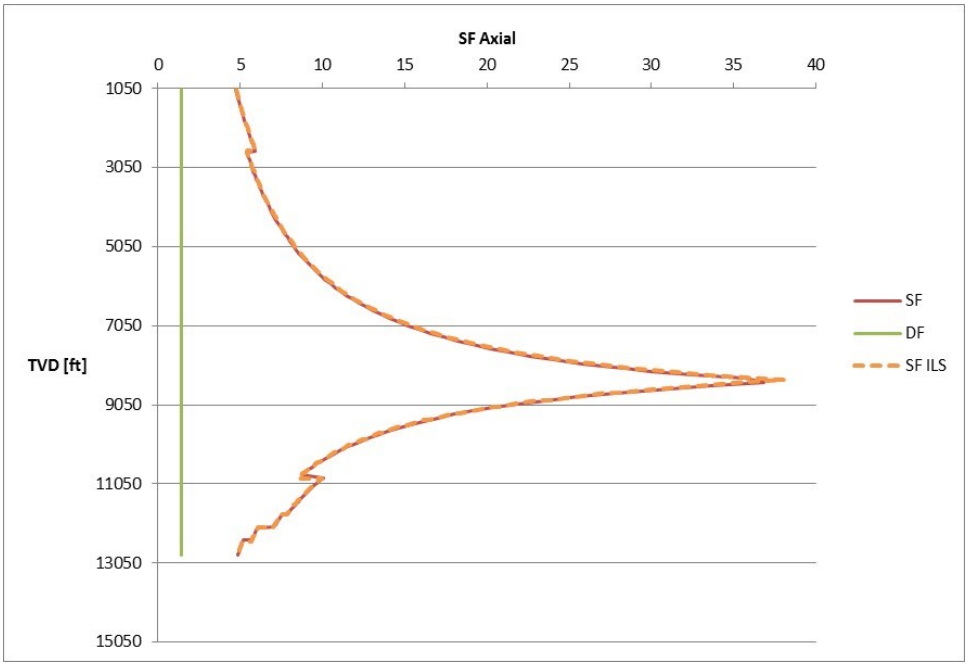

Figure B-52 Lost returns with mud drop in the production casing, axial SF

The figure below shows the axial SF when the ballooning force is calculated as an average force. There is a small difference between the two models because of the difference in calculating the ballooning force; the new SF is slightly decreased above TOC, and increased below TOC.

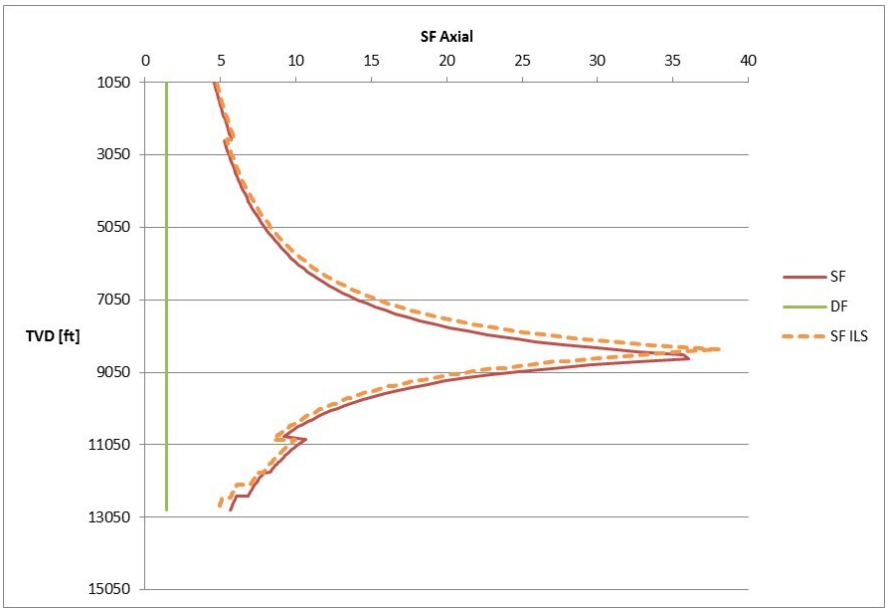

Figure B-53 Lost returns with mud drop in the production casing, axial SF average ballooning force

Calculating the ballooning force at each depth as done in the following figure makes more of a difference to the axial SF as seen below. The SF is smaller with this method of calculating.

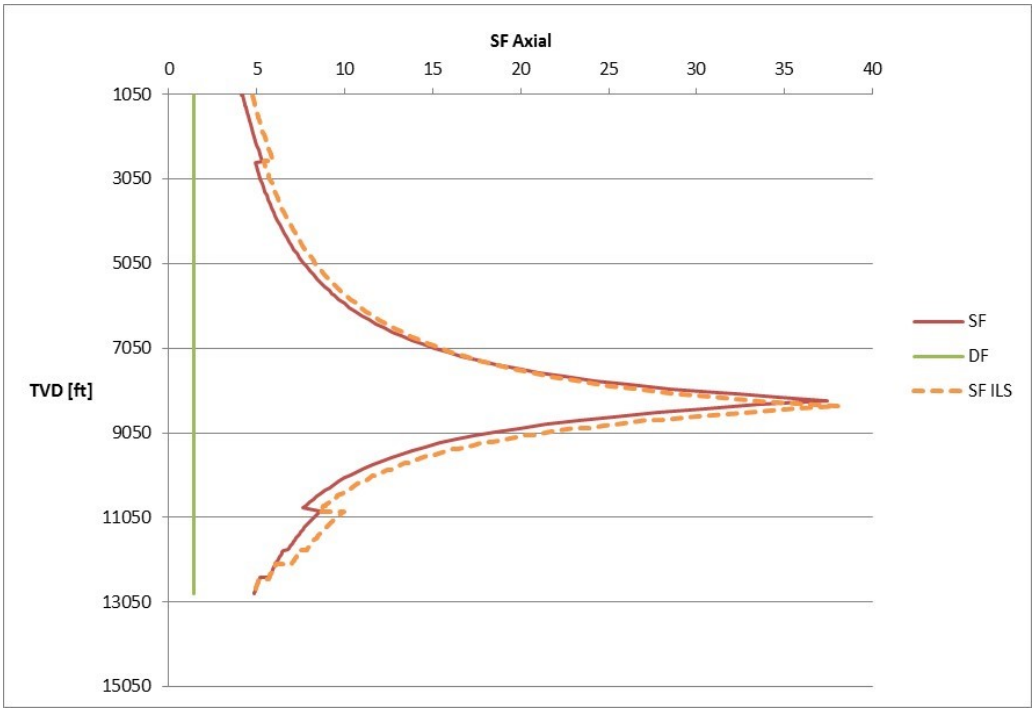

Figure B-54 Lost returns with mud drop in the production casing, axial SF with new ballooning force at each step

B.4 Tubing Leak

B.4.1 Production Casing

Tubing leak occurs during production or injection of a well, which means that the only casing affected by this load is the production casing. Therefore, the tubing leak is investigated only in the production casing.

B.4.1.1 Differential Pressure

The differential pressure in this load is quite high, which is why the pressure test of the production casing is based on this load. Both the thesis model and the ILS use deteriorated mud above TOC and pore pressure below TOC when calculating the external pressure. Figure B-55 shows that the two models get the same result for the pressure profile.

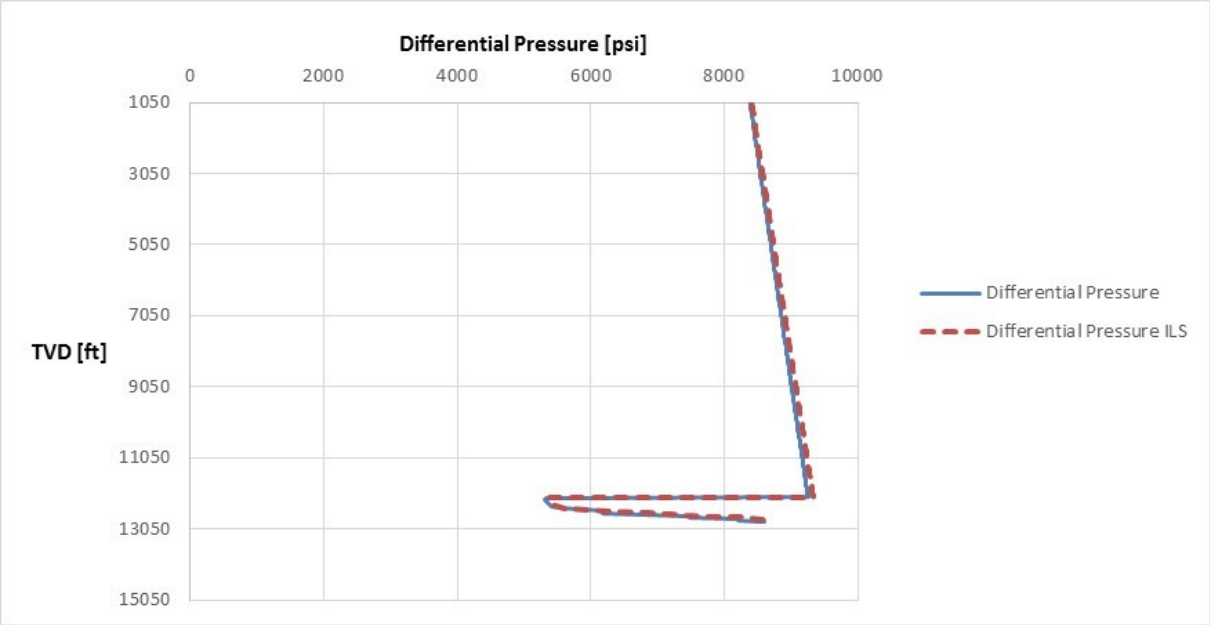

Figure B-55 Tubing leak production casing differential pressure

B.4.1.2 Axial Load

Tubing leak is the only load case examined where buckling occurs. The two models matches down to about 10,200ft where buckling occurs in the ILS model. Buckling happens later in the thesis model, around 11,400ft. There is also more buckling-induced bending force in the ILS model as seen in Figure B-56. Below TOC there is no buckling in either of the models, and so the two models are equal. The entire casing string is in tension, and the axial load is marginally smaller than the axial load during the pressure test. This is not surprising as the pressure test for the production casing is based on the tubing leak load case.

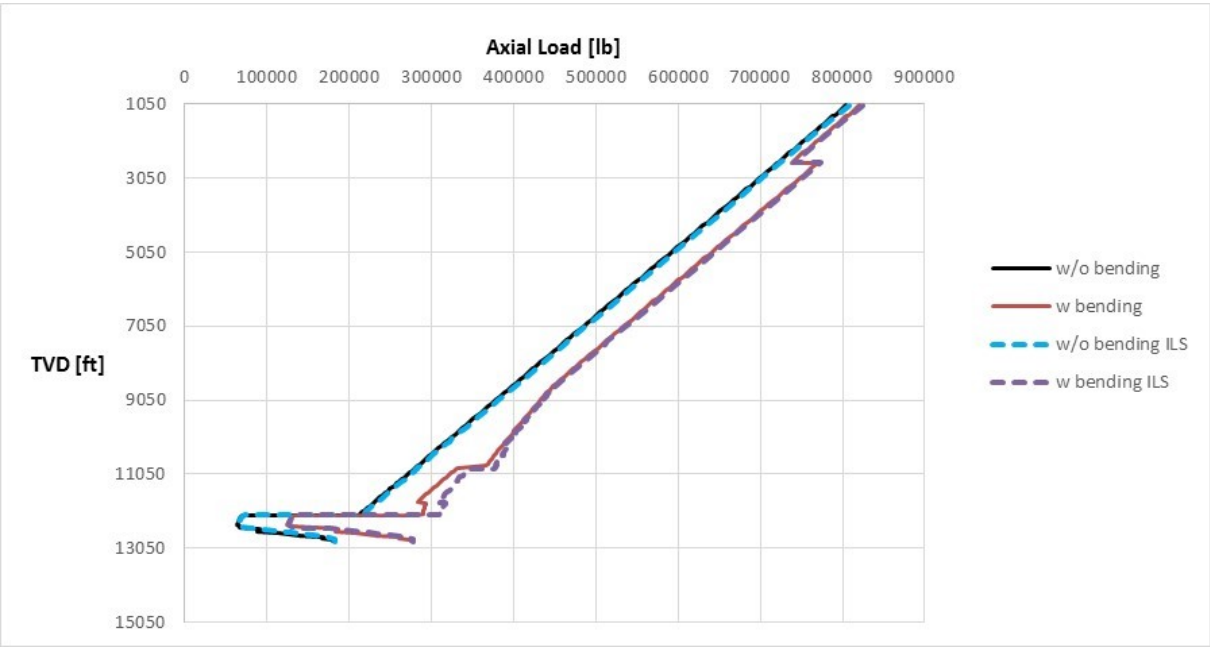

Figure B-56 Tubing leak production casing axial load

B.4.1.3 Axial Safety Factor

The axial safety factors for the two models are similar, except for the section mentioned previously, where buckling occurs earlier and stronger in the ILS. This gives a lower SF in the ILS than in the thesis model, but there is still a good clearing between both the safety factors and the DF.

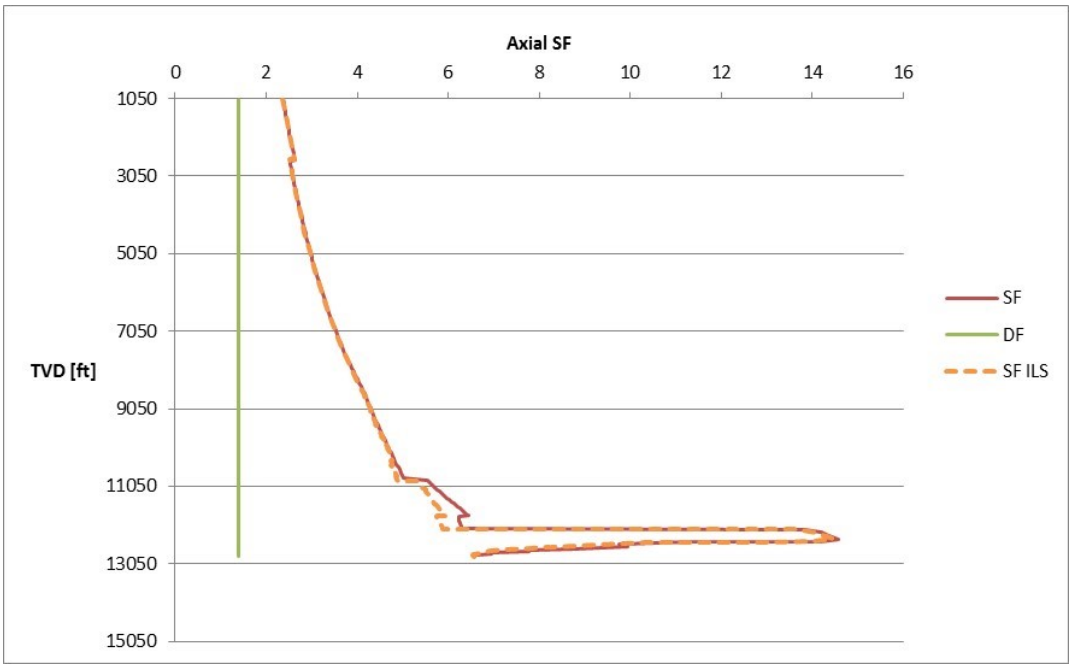

Figure B-57 Tubing leak production casing axial SF

B.4.1.4 Burst Safety Factor

The burst safety factor is not affected by buckling, only the internal and external pressure in the casing. Since the differential pressure calculated by the thesis mode was equal to the ILS, the burst SF is also the same as the ILS as seen in Figure B-58. The burst SF is closer to the DF than the axial SF was. At the closest, the difference is only about 0.23. There are two reasons why the line above TOC is not a straight line; the first reason is the deteriorated mud

behind the casing, the second is the temperature derated yield strength.

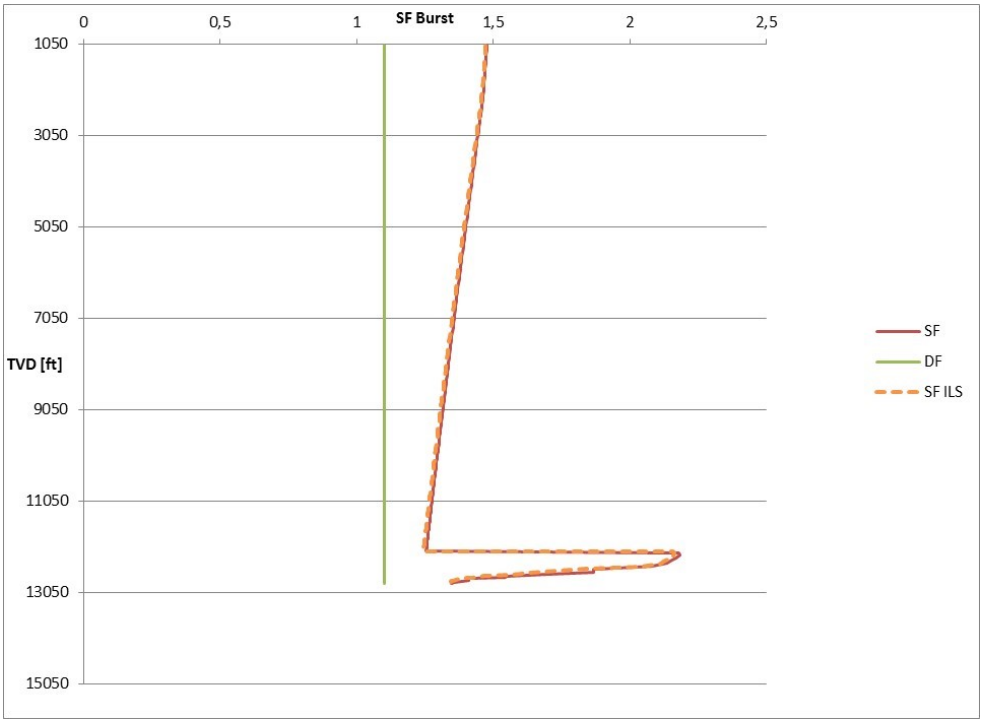

Figure B-58 Tubing leak production casing burst SF

B.4.1.5 Triaxial Safety Factor

As before, the triaxial SF from the thesis model is still slightly off compared to the ILS. The difference is about 0.17, i.e. not a lot. However, the SF from the ILS is very close to the DF, so the ILS data should be used when choosing the casing.

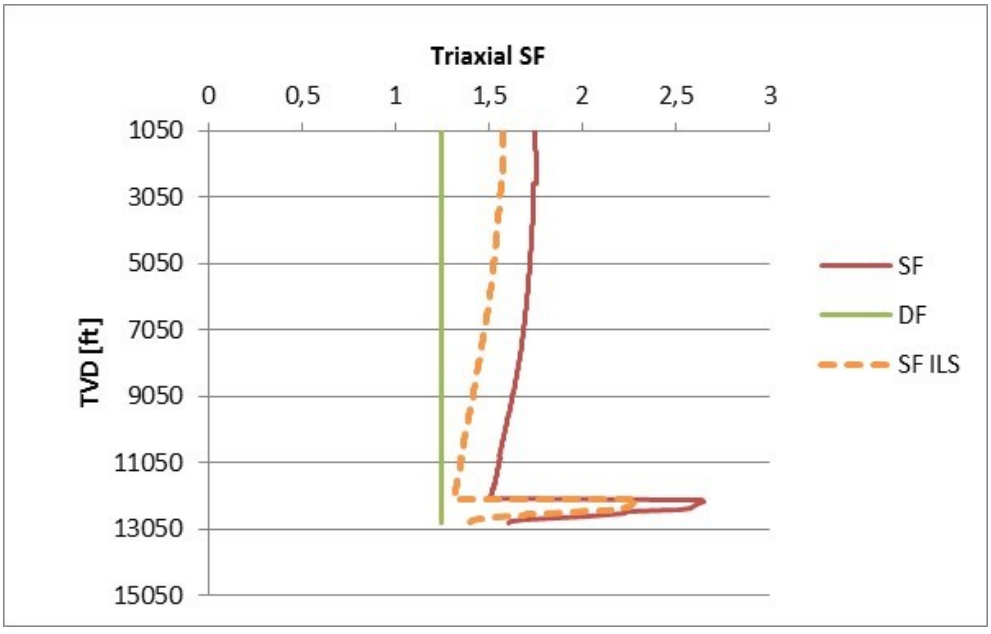

Figure B-59 Tubing leak production casing triaxial SF

Appendix C

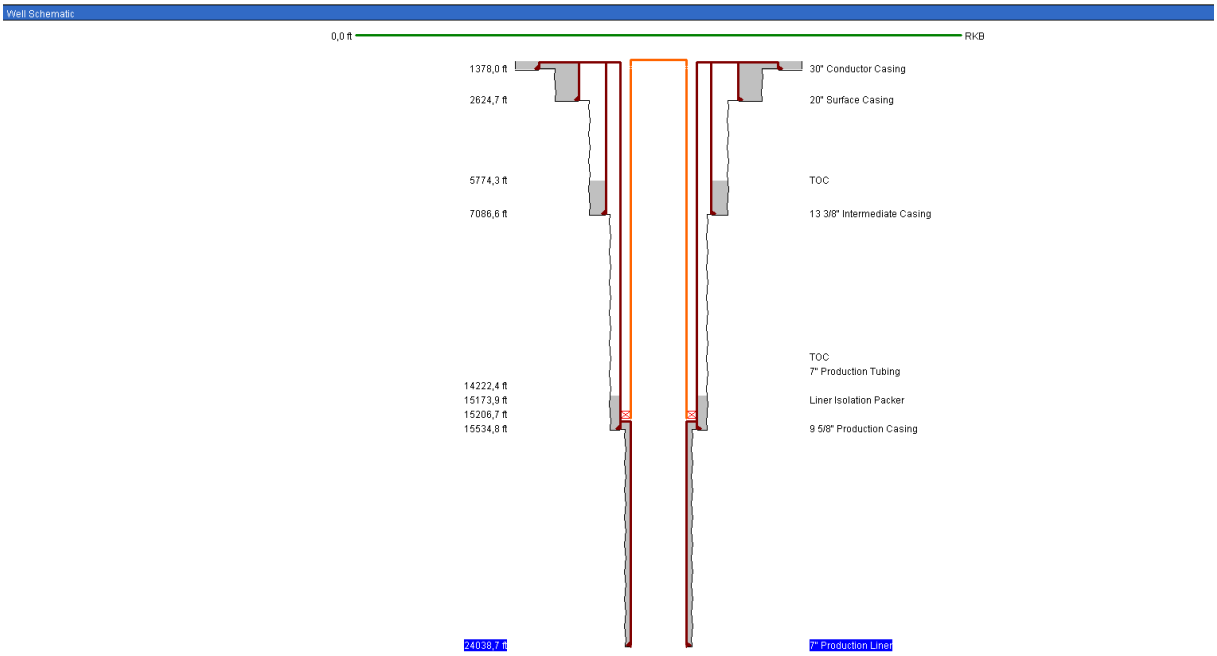

Figure C-1 Well schematic

Casing and Tubing Configuration

	Name	Type	OD (in)	MD (ft) Hanger	MD (ft) TOC	MD (ft) Base	Hole Size (in)	Annulus Fluid
1	Conductor	Casing	30.000	1072,8	1072,8	1378,0	36.000	conductor 1.030 sg
2	Surface	Casing	20.000	1072,8	1072,8	2624,7	26.000	Surface 1.030 sg
3	Intermediate	Casing	13 3/8	1072,8	5774,3	7086,6	17 1/2	Intermediate 1.450 sg
4	Production	Casing	9 5/8	1072,8	14222,4	15534,8	12 1/4	Prod csg 1.700 sg
5	Production	Liner	7.000	15206,7	15206,7	24038,7	8 1/2	Prod liner 1.150 sg
6	Production	Tubing	7.000	1000,7		15173,9		Seawater
7								

Figure C-2 Casing configuration

String Sections - 20" Surface Casing

	MD (ft) Top	MD (ft) Base	Pipe Type	Pipe OD (in)	Pipe Weight (ppf)	Pipe Grade	Connection Pipe	Connection Name	Connection Grade	Connection OD (in)	Pipe Insulation Material	Pipe Insulation Thickness
1	1072,8	2624,7		20.000	169,000	K-55		BTC	K-55	21.000	None	0,000
2												

Figure C-3 Surface casing configuration

String Sections - 13 3/8" Intermediate Casing

	MD (ft) Top	MD (ft) Base	Pipe Type	Pipe OD (in)	Pipe Weight (ppf)	Pipe Grade	Connection Pipe	Connection Name	Connection Grade	Connection OD (in)	Pipe Insulation Material	Pipe Insulation Thickness
1	1072,8	7086,6		13 3/8	77,000	P-110		Vam Top	P-110	14.299	None	0,000
2												

Figure C-4 Intermediate casing configuration

String Sections - 9 5/8" Production Casing

	MD (ft) Top	MD (ft) Base	Pipe Type	Pipe OD (in)	Pipe Weight (ppf)	Pipe Grade	Connection Pipe	Connection Name	Connection Grade	Connection OD (in)	Pipe Insulation Material	Pipe Insulation Thickness
1	1072,8	15534,8		9 5/8	53,500	Q-125		Vam Top	Q-125	10.520	None	0,000
2												

Figure C-5 Production casing configuration

Dogleg Severity Overrides

	MD (m) Top	MD (m) Base	DLS (°/100ft)
1	327,00	800,00	0,50
2	800,00	7327,00	1,50
3			

Figure C-6 Dogleg severity override input to the ILS

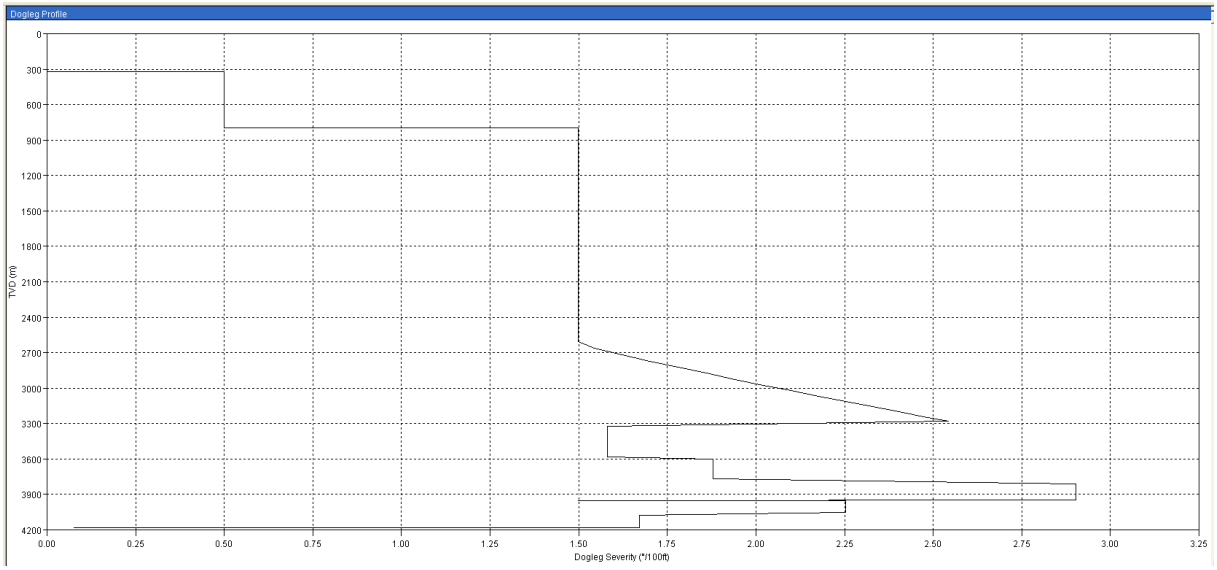

Figure C-7 Dogleg profile in the ILS